AMERICAN UNIVERSITY OF BEIRUT

RADIOSENSITIZING EFFECT OF THYMOQUINONE IN 2D AND 3D CELL CULTURE MODELS OF HUMAN COLORECTAL CANCER

by
SAMAR FADI AL BITAR

A dissertation
submitted in partial fulfillment of the requirements
for the degree of Doctor of Philosophy
to the Department of Biology
of the Faculty of Arts and Sciences
at the American University of Beirut

Beirut, Lebanon
April 28, 2022

AMERICAN UNIVERSITY OF BEIRUT

RADIOSENSITIZING EFFECT OF THYMOQUINONE IN 2D AND 3D CELL CULTURE MODELS OF HUMAN COLORECTAL CANCER

by

SAMAR FADI AL BITAR

Approved by:

Dr. Nadine Darwiche, Professor Department of Biochemistry	Chair of Committee
Dr. Hala Gali-Muhtasib, Professor Department of Biology	Advisor
Dr. Wassim Abou-Kheir, Associate Professor Department of Anatomy, Cell Biology & Physiological Sciences	Co-advisor
Dr. Rabih Talhouk, Professor Department of Biology	Member of Committee
Dr. Deborah Mukherji, Associate Professor Department of Internal Medicine	Member of Committee
Dr. Tamara Abou Antoun, Associate Professor School of Pharmacy, Lebanese American University	Member of Committee 28/04/2022
Dr. George Hilal, Associate Professor Department of Medicine, University of Sherbrooke	Member of Committee

Date of dissertation defense: April 28, 2022

AMERICAN UNIVERSITY OF BEIRUT

DISSERTATION RELEASE FORM

Student Name: _____Al Bitar_____Samar_____Fadi___
Last First Middle

I authorize the American University of Beirut, to: (a) reproduce hard or electronic copies of my dissertation; (b) include such copies in the archives and digital repositories of the University; and (c) make freely available such copies to third parties for research or educational purposes:

- ☒ As of the date of submission
- ☐ One year from the date of submission of my dissertation.
- ☐ Two years from the date of submission of my dissertation.
- ☐ Three years from the date of submission of my dissertation.

Samar May 6, 2022

Signature Date

ACKNOWLEDGEMENTS

During my PhD journey, which was challenging but full of exciting experiences, I have received support from individuals who lit up my path and whom I owe my sincere gratitude.

Firstly, I would like to express my deepest gratitude to my advisor Dr. Hala Muhtasib. Thank you Dr. Hala for your continuous support, guidance, and compassion. Your insightful and encouraging feedback pushed me to sharpen my skills and helped me immensely during this process.

I am extremely appreciative to my co-advisor Dr. Wassim for always being there for me and for being an amazing mentor. Your wise advice has helped me advance both professionally and personally. Thank you for your patience, motivation, and positive attitude and for all the opportunities you provided me with to expand my research. Your expertise was invaluable in conducting this research project. I am also extremely grateful for treating me and all your lab members like family.

I would also like to thank the committee members for their valued input and comments. Thank you for taking the time to review this dissertation. Thank you Dr. Nadine Darwiche for chairing the thesis committee.

To my friends and colleagues in the HM and WAK laboratories, I am thankful for each one of you. The positive work environment and continuous support have helped me a lot during difficult times. Thank you Drs. Farah Ballout and Alissar Monzer for being great lab partners and friends, and for your contribution to this project. Thank you Dr. Maamoun Fatftat, Amani Yehya, Kevork Wakimian, Jolie Abou Gharios, Hiba Msheik, Johnny Fawaz, and Hiam Fakhereddine for your help and assistance.

To everyone I have met during my six years at AUB, and to everyone who've listened and helped throughout, I truly appreciate each one of you and how you have helped in all your own individual ways. Special thanks to Nancy Hourani, Zeina Habli, and Rana Alaaeddine. I would like to thank the staff of the core facilities in the DTS Building, especially Vera Dermesrobian and Layal El Hajjar and the manager of the Central Research Science Laboratory, Ms. Rania Shatila for their technical help and assistance.

To my family, I dedicate this work. Thank you Rawad for being an amazing husband. You are my support system, my safety net, my best friend, and the love of my life. With your love and support, I was able to face everything. Thank you for always being there for me and for always helping me patiently. You give me strength and comfort during the hardest days, and you never fail to make me laugh.

To my beloved parents, thank you for all your unconditional love and support. Without you, I might not be the person I am today, and I am always thankful to you for everything you do and for always believing in me! My mom Najwa you are my role model and my best friend thank you for your patience and for always understanding me and cheering

me up. Your prayers have kept me going and have given me so much strength during the hardest times. Thank you, dad Fadi, for all your love, support, sacrifices, and for all what you have done for me. My dearest sisters Reem and Rana thank you for your encouragement, love, and never-ending support. I love you all so much!

I am forever grateful for my caring, patient, and supportive family-in-law who are in Australia. I miss you so much and I can't wait to see you soon. I love you all!

Lastly, the presence of the right support is a key to accomplish our dreams and goals; and I was blessed with supportive family, friends, and colleagues.

ABSTRACT

OF THE DISSERTATION OF

Samar Fadi Al Bitar for Doctor of Philosophy
Major: Cell and Molecular Biology

Title: Radiosensitizing Effect of Thymoquinone in 2D and 3D Cell Culture Models of Human Colorectal Cancer

Background: Colorectal cancer (CRC) is the third most common cancer affecting both men and women worldwide. Despite the great advances made in detecting and treating CRC cancer, it remains a major burden in many countries. Standard treatments for CRC include surgical resection, chemotherapy, radiotherapy, and ablative therapies for metastases. These treatments have increased the overall survival of patients; however, in many cases, tumor relapse occurs due to resistance of cancer stem cells (CSCs) to conventional therapies, including radiotherapy. Some natural compounds have been shown to induce radiosensitization of CSCs. Thymoquinone (TQ), the black seed extract, has shown numerous anti-cancer activities in many cancers, including CRC. In addition, a radiosensitizing effect of TQ has been documented in breast cancer, melanoma, and head and neck squamous cell carcinoma (HNSCC), yet no studies have investigated its radiosensitizing effects on CRC cells and stem cells.

Objective: The overall aim of this thesis was to investigate the radiosensitizing potential of TQ on CRC cells and stem/progenitor cells and in patient-derived organoids. Our first aim was to study the inhibitory effects of TQ and radiation on a panel of human colorectal cancer cells cultured in 2D. Our second aim was to isolate and enrich for CRC stem cells from HCT116 and HT29 cell lines using 3D sphere formation assay and study the effect/mechanism of action of TQ and radiation on self-renewal capacity of colonospheres. The third aim was to employ fresh CRC tissue specimens from treatment-naïve patients to establish 3D patient-derived organoids and study the response of the established organoids to TQ alone, radiation alone, and combinations of TQ and radiation.

Methods: We first assessed the radiosensitizing effects of TQ in 2D cultures of CRC cells (HCT116, HCT116 p53 null, HT29, and DLD1) with different mutations and sensitivity to TQ and radiation. We then tested the efficacy of the combination treatment in CRC stem/progenitor cells enriched in 3D sphere formation assay, in which single cell suspensions were plated using Matrigel as an extracellular matrix. Immunofluorescent analysis and western blot were used to determine the mechanism of radiosensitization by TQ in these 2D and 3D cultures. The effect of TQ and radiation combinations in patient-derived organoids was established using organoid forming assay and immunofluorescence staining for cancer stem cell markers CD44 and CK19. Statistical analysis was performed using Graphpad prism 6.

Results: Our results showed that TQ sensitized CRC cells to radiation and reduced cell proliferation, viability, clonogenic survival, and migration ability and was non-toxic to non-tumorigenic intestinal cells. TQ sensitizing effects were associated with G2/M arrest, DNA damage, oxidative stress, as well as changes in key signaling molecules involved in radioresistance, including p-mTOR, MEK, β-catenin, and NF-κB. Moreover, combination treatment upregulated p53 and p21 expression. Combining a low dose of TQ (3 μM) with ionizing radiation (IR) (2 Gy) resulted in complete eradication of CSC populations enriched from HCT116 and HT29 cells at generation 5 and this was associated with inhibition of survival, stemness, and DNA repair through targeting molecules involved in these processes, including CD44, CK8, CK19, CD133, β catenin, and NF-κB while upregulating γH2AX, p53, and p21. These doses also led to ~1.4- to ~3.4-fold decrease in organoid forming ability of patient-derived organoids and resulted in more than 1.3-fold decrease in stem cell markers CD44 and CK19 expression in organoids that were resistant to radiation. Our findings show that combining TQ and radiation could be a promising therapeutic strategy for eradicating CRC cells and stem/progenitor cells.

Conclusion: This study underscores the importance of 3D sphere and organoid culture assays for studying colorectal cancer stem/progenitor cell characteristics. Moreover, this study demonstrates TQ's potential as a radiosensitizing molecule against colorectal cancer cells and stem cells, in addition to patient-derived organoids that are resistant to radiation alone.

TABLE OF CONTENTS

ILLUSTRATIONS

Figure

TABLES

Table

ABBREVIATIONS

2D: Two-dimension

3D: Three-dimension

5-FU: 5-Fluorouracil

ABC: ATP-binding cassette

ACF: Aberrant crypt foci

ACNP: Aragonite calcium carbonate nanoparticles

AdDMEM: Advanced DMEM

AML: Acute myeloid leukemia

APC: Adenomatous polyposis coli

ATM: Ataxia telangiectasia mutated

ATR: ATM and Rad3-related protein

AUB: American University of Beirut

AUBMC: American University of Beirut medical center

CAFs: Cancer-associated fibroblasts

CAM: Chorioallantoic membrane

Capeox: Apecitabine and oxaliplatin

CBC: Crypt base columnar

Chk: Checkpoint kinases

CIMP: CpG island methylator phenotype

CIN: Chromosomal instability

CRC: Colorectal cancer

CSCs: Cancer stem cells

CS-NP: Chitosan-based nanoparticles

CTNNB1: Catenin-β1

DDR: DNA damage response

DHE: Dihydroethidium

DMH: 1,2-dimethyl-hydrazine

DOX: Doxorubicin

DSBs: Double strand breaks

ECM: Extracellular matrix

EGF: Epidermal growth factor

EGFR: Epidermal growth factor receptor

EMT: Epithelial to mesenchymal transition

FAM123B: Family with sequence similarity 123B

FAP: Familial adenomatous polyposis

FBS: Fetal bovine Serum

FOLFOX: 5-FU, leucovorin, and oxaliplatin

FOLFOX4: 5-FU, oxaliplatin, and leucovorin

FOLFOXIRI: 5-FU, leucovorin, oxaliplatin, and irinotecan

FZD10: Frizzled class receptor 10

G: Generation

GADD45alpha: DNA damage inducible gene

GSK-3β: Glycogen synthase kinase

H&E: Hematoxylin and Eosin

HNSCC: Head and neck squamous cell carcinoma

IBD: Inflammatory bowel disease

IR: Ionizing radiation

IRB: Institutional Review Board

ISCs: Multipotent intestinal stem cells

Lgr5: Leucine-rich repeat-containing G-protein coupled receptor 5

LOH: Loss of heterozygosity

LRP5: Low-density lipoprotein receptor-related protein 5

MAPK: Mitogen-activated protein kinase

MDR: Multiple drug resistance

MMR: DNA mismatch repair

MSI: Microsatellite instability

MTT: 3-(4, 5-dimethylthiazol-2-yl)-2, 5-diphenyltetrazolium bromide

NGS: Normal goat serum

NLC: Nano-structured lipid carriers

NPs: Nanoparticles

OD: Optical density

OFC: Organoid-forming count

PBS: Phosphate-buffered saline

PD-1: Lymphocyte exhaustion marker

PDOs: Patient-derived organoids

PE: Plating efficiency

PFA: Paraformaldehyde (PFA)

PI 3-kinase: Phosphatidyl-inositol 3-kinase

PI: Propidium iodide

PI3K: Phosphatidylinositol 3-kinase

PI3KCA: Phosphatidylinositol-4,5-bisphosphate 3-kinase catalytic subunit-α

PIKKs: Phosphatidyl-inositol 3-kinase like family of protein kinases

PSCs: Pluripotent stem cells

PTEN: Phosphatase and tensin homologue

RI: ROCK inhibitor

ROS: Reactive oxygen species

RSPO: R-spondin

SCID: Severe combined immunodeficient mice

SEM: Standard error mean

SF: Surviving fraction

SFRP: Secreted frizzled-related protein

SFU: Sphere-forming unit

SLN: Solid-lipid nanoparticle

SMAD4: SMAD family member 4

TA: Transit amplifying

TGFBR2: TGFβ _receptor 2

TGFβ: Transforming growth factor-β

TME: Tumor microenvironment

TNT: Total neoadjuvant therapy

TQ: Thymoquinone

VEGF: Vascular endothelial growth factor

VEGF1: Vascular endothelial growth factor receptor1

CHAPTER I

INTRODUCTION

A. Colorectal cancer

1. Colon structure and function

The large intestine is the final section of the digestive tract and includes the cecum, appendix, colon, rectum, and anal canal [1]. The colon consists of 4 parts: the ascending, transverse, descending, and sigmoid colon. The ascending and transverse colon constitute the proximal colon, while the descending and sigmoid colon constitute the distal colon [2]. Histologically, the small and the large intestine are composed of three tissue layers. The outer layer consists of sheets of smooth muscle that mediate, together with the enteric nervous system, the peristaltic contraction of the intestine. A supportive layer of connective tissue, known as submucosa or stroma, separates the outer layer from the innermost layer of the intestine and contains a network of blood and lymph vessels, in addition to nerves. The inner layer functions in absorption and processing and is made up of a single-epithelial cell layer known as the mucosa. Unlike the small intestine, the inner layer of the large intestine does not have villi [3]. There are four types of differentiated epithelial cells in the colon: absorptive or enterocytes, muco-secreting (also called goblet cells), enteroendocrine, and Paneth cells [4, 5].

Intestinal epithelium has a self-renewal capacity, whereby most of the gut epithelial cells are replaced every 4 to 5 days. Renewal capacity is attributed to the multipotent intestinal stem cells (ISCs) that reside at the bottom of the crypt. The immediate daughter cells that result from ISC proliferation can proliferate for infinite number of times before turning into fully differentiated cells. Undifferentiated cells in transition between stem cells and differentiated cells are called transit amplifying (TA)

cells. These cells are located directly above ISCs and are the main producers of intestinal epithelial cells [6].

Coexistence of quiescent and active normal adult ISCs has been shown in *in vivo* and *in vitro* cultures following the identification of the long-lived yet rapidly dividing intestinal crypt base columnar cells (CBCs) that specifically express leucine-rich repeat-containing G-protein coupled receptor 5 (Lgr5) [7]. These cells are capable of self-renewal and differentiation to produce all types of intestinal epithelial cells *in vivo* [3, 7]. They are now known as mitotically active ISCs and are thought to maintain the physiological homeostasis of the intestine. Interestingly, long before Lgr5 CBCs were identified, a subset of epithelial cells residing at +4 position relative to the base of the crypt were thought to represent the ISCs, as they have been observed to share some properties of adult stem cells. In fact, populations of crypt cells expressing specific markers, such as Bmi1, Hopx, mTert, Krt19, Sox9, Mex3a, or Prox1 have been identified at +4 position [8, 9]. Most of these cells are slowly dividing and can give rise to clonal lineage-tracing events at much lower frequency than Lgr5 CBCs [9]. Importantly, Wnt, bone morphogenetic protein (BMP), Notch, epidermal growth factor (EGF), and Hippo signaling have central roles in ISC regulation, intestinal homeostasis, and regeneration [8].

Self-renewal, multipotency, and plasticity of ISCs are largely controlled by intrinsic molecular processes and extrinsic signals from neighboring niche. Vital niche components include epithelial progenies of ISCs and mesenchymal cells, such as Paneth cells, fibroblasts, endothelial cells, enteric neurons, and immune cells. These niche cells secrete a variety of cytokines and growth factors to stimulate the regeneration of ISCs, in response to injury induction [8, 10].

2. Colorectal cancer epidemiology, risk factors, and subtypes

Colorectal cancer (CRC) is the third most common cause of cancer-related deaths worldwide. It is one of the most frequent malignancies in men and women worldwide. According to the American Cancer Society [11], an estimated 106,180 new cases of colon cancer and 44,850 of rectal cancer will be diagnosed in 2022 in the US, with the majority being in people older than 50 years old. Although the death rate from CRC has been dropping; however, it is expected that 52,580 deaths will result from CRC in 2022. Statistics on death from colon and rectal cancer separately are currently not available due to misconceptions in the use of the terms colon cancer and rectal cancer, which often leads to the misclassification of deaths from colon cancers as deaths from rectal cancer in almost 40% of the cases. Although the majority of CRC occur in people above 50, it was estimated that 12% of the estimated CRC deaths in 2020 was in individuals younger than age 50 [11-14].

Multiple factors are associated with an increased risk for developing CRC. Lifestyle factors including unhealthy diet, heavy alcohol consumption, lack of physical activity, and smoking contribute to half the cases of CRC in the US [11, 14]. On the other hand, people who maintain a healthy lifestyle behavior have a 27% to 52% lower risk of developing CRC, as compared to those who do not [14, 15].

Nonmodifiable factors are also among the causes of CRC. Heredity and family history contribute to 30% of CRC cases, making them a major risk factor. The risk of developing CRC increases 2 to 4 times in individuals with one or more first-degree relative who has been diagnosed with CRC. Also, the risk is higher in individuals with a personal history of adenomatous polyps or with 2 or more second-degree relatives who have been diagnosed with adenomas. Moreover, personal history of inflammatory bowel

disease (IBD) is also a condition that increases the overall risk of developing CRC by 4- to 20-fold [16].

It has been recently reported that 5% of CRC patients harbor a genetic mutation, resulting in a high-risk hereditary genetic condition, and 5% harbor a genetic variation associated with a moderate-risk condition that contributes to CRC development [17]. Lynch syndrome is an autosomal dominant genetic disease that accounts for 2-5% of all CRCs and is the most common hereditary condition associated with CRC. It is also known as hereditary non-polyposis CRC. In this disease, a germline mutation in one of several DNA mismatch repair (MMR) genes, together with the inactivation of the other normal allele, results in loss of function and microsatellite instability (MSI) [18]. Another common hereditary condition associated with CRC is familial adenomatous polyposis (FAP) that accounts for 1% of CRC cases and is caused by a mutation in the adenomatous polyposis coli (APC) gene, truncation of APC protein, and consequently loss of APC function [18]. Approximately, 75% of CRCs are sporadic, in which they occur in individuals without genetic predisposition or family history of CRC [19]. The remaining CRC cases arise through a serrated pathway that involves the activation of the MAPK pathway and the presence of CIMP [19].

3. Development of colorectal cancer

It is postulated that CRC develops as a result of sequential accumulation of mutations and epigenetic changes that drive tumor initiation and progression. Thirty-one years ago, Fearon and Vogelstein proposed a genetic model describing the transition from normal epithelia through dysplastic adenoma to cancer cells [20]. The model is illustrated in figure 1. This “classic” CRC formation model states that most CRC arise from a polyp

or an aberrant crypt, which then develops into early tubular adenoma. The adenoma then progresses into advanced adenoma, and finally CRC. This multistep process is driven by the accumulation of mutations in *APC*, *Kirsten-ras (K-ras)*, *p53*, and *SMAD Family Member 4 (SMAD4)* [20].

The homozygous inactivation of the tumor suppressor gene APC is thought to be the initiating mutation [20]. It is also responsible for FAP and approximately 85% of sporadic CRC [21]. The APC gene is located at chromosome 5q21. It encodes an 8.5-kB mRNA and a 312-kD protein. The structure of the APC protein complex is characterized by many protein/protein interaction sites that allows it to bind to and regulate the activity of key molecular players, including β-catenin [22]. APC has multiple cellular functions, such as inhibiting canonical Wnt signaling, microtubule nucleation, and RNA binding and regulation [9]. Most of the APC mutations occur in the mutation cluster region (MCR), introducing a stop codon into the APC mRNA, and resulting in deletion of the carboxyl-terminal functions of the protein, including β-catenin binding site. APC mutation provides selective growth advantage to epithelial cells and regulates their entry into the adenoma-carcinoma progression [21].

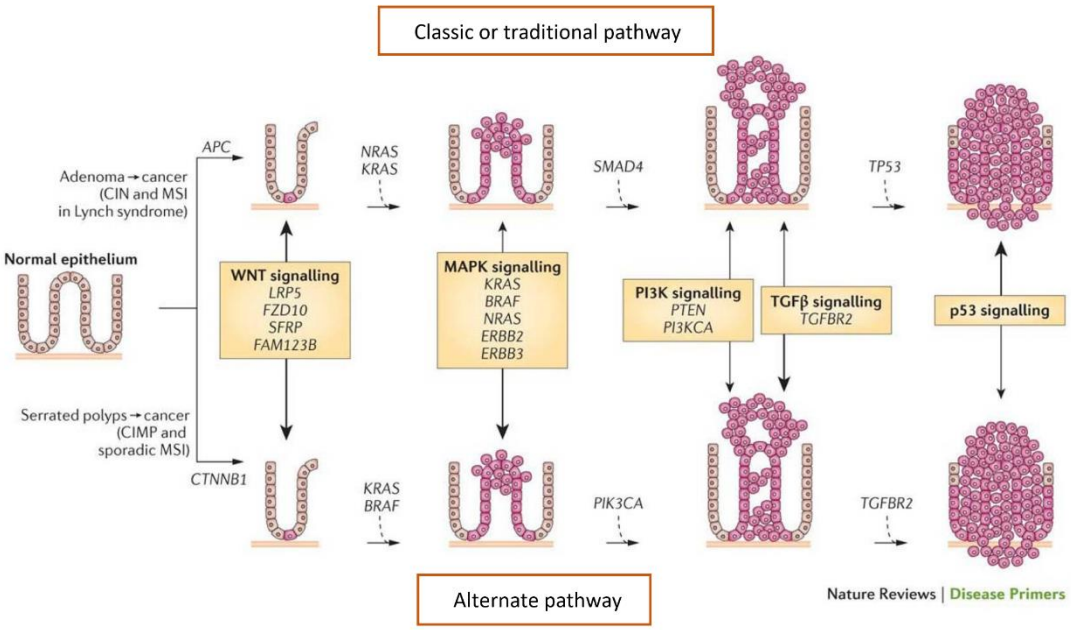

Figure 1. Mechanism of colorectal cancer progression. The 'classic' or traditional pathway (top) involves the development of tubular adenomas that can progress to adenocarcinomas. An alternate pathway (bottom) involves serrated polyps and their progression to serrated colorectal cancer. Genetically mutated or epigenetically altered genes are indicated in each pathway. The signaling pathways deregulated during cancer progression are shown, with the width of the arrow reflecting the significance of the signaling pathway in tumor formation. APC, adenomatous polyposis coli; CIN, chromosomal instability; CTNNB1, catenin-β1; FAM123B, family with sequence similarity 123B; FZD10, frizzled class receptor 10; LRP5, low-density lipoprotein receptor-related protein 5; MAPK, mitogen-activated protein kinase; MSI, microsatellite instability; PI3K, phosphatidylinositol 3-kinase; PI3KCA, phosphatidylinositol-4,5-bisphosphate 3-kinase catalytic subunit-α; PTEN, phosphatase and tensin homologue; SFRP, secreted frizzled-related protein; SMAD4, SMAD family member 4; TGFβ, transforming growth factor-β; TGFBR2, TGFβ _receptor 2. [Adapted and modified from [23]].

Mutations in p53 occur in late events during CRC development. These mutations occur in up to 70% of CRCs [24]. p53 gene is localized on the short arm of chromosome 17. p53 protein is the guardian of the genome and is also known as the gatekeeper that functions as a transcription factor to control cell cycle by interacting with a variety of proteins including p21, in response to cellular stress and DNA damage [25, 26]. Loss of

p53 activity and thereby failure to induce apoptosis is considered an important determinant of progression to a malignant tumor.

Another route to colorectal carcinogenesis has been described [27]. This route occurs through serrated polyps rather than tubular adenomas and accounts for 5-10% of all polyps. The latter arise by molecular and histological events that are distinct from adenomas described in the first model (Figure 1) [23].

Three major molecular pathways play a role in CRC development. Chromosomal instability (CIN) pathway, CpG island methylator phenotype (CIMP) pathway, and microsatellite instability (MSI) pathway. The most common pathway is the CIN pathway that accounts for more than 85% of the cases and involves the accumulation of chromosomal abnormalities [28]. Loss of heterozygosity (LOH) at tumor suppressor loci, chromosomal rearrangements, and accumulation of mutations in oncogenes (ex. K-RAS) and tumor suppressor genes (APC and p53) are characteristics of CIN CRC [29].

Microsatellite instability results from mutations and dysfunctions in DNA mismatch repair (MMR) genes. MSI is found in 15% of all sporadic CRCs [19]. The MMR system is composed of several proteins that associate with specific partners to form functional heterodimers. Silencing of MMR genes, such as *MLH1*, occurs through promotor hypermethylation. In MSI tumors, mutations in genes such as *MSH3*, *TGFBR2*, *BAX*, *CASP5*, *MSH6*, *CTNNB1*, *APC*, *IGF2*, and *E2F4* are also observed [19].

CpG island methylator phenotype also accounts for 15% of all sporadic CRCs [18]. This pathway results in genetic instability via aberrant methylation of the promotor regions, and thus the epigenetic inactivation of tumor suppressor genes, including *MLH1* [30]. CIMP-positive cancers can be further classified into CIMP-low (or CIMP-2) or CIMP-high (or CIMP-1) categories and may associate with distinct mutations [31].

4. Diagnosis and management of colorectal cancer

CRC can be classified into five stages (Figure 2). Stage 0 is defined by appearance of small tumorigenic nodules that are confined to the mucosa or inner layer of the colon (carcinoma *in situ*). Surgery is all what is required at this stage. Stage I is characterized by tumor invasion through the submucosa and muscularis propria with no spread outside these layers. Surgical resection is a standard treatment for this stage. Stage II is defined by tumor invasion through muscularis propria into pericolorectal tissues, then penetration to the surface of the visceral peritoneum [32]. Surgery is usually the only treatment needed for stage II, and the use of an adjuvant chemotherapy at this stage is still controversial. Patients with stage II CRC with high-risk features are sometimes treated with a 6-month course of adjuvant chemotherapy with one of the following regimens: 5-fluorouracil (5-FU)/leucovorin, capecitabine, or combination chemotherapy with a regimen of 5-FU, leucovorin, and oxaliplatin (FOLFOX) or capecitabine and oxaliplatin (Capeox) [33]. In stage III, the tumor invades muscularis propria and spreads outside the colon with metastases in one or more regional lymph node. Surgery is applied to remove the tumor and the affected lymph nodes (fractional colectomy). Adjuvant chemotherapy using FOLFOX and Capeox regimens are also utilized. In addition, radiation might be also applied to ensure eradication of tumor cells that remain after surgery [34]. Stage IV is characterized by tumor spread to one organ or site, such as lung, liver, ovary, or non-regional lymph node. For this stage, surgery is combined with various chemotherapy regimens to control the disease. In some cases, radiation is applied after surgery [32, 34, 35].

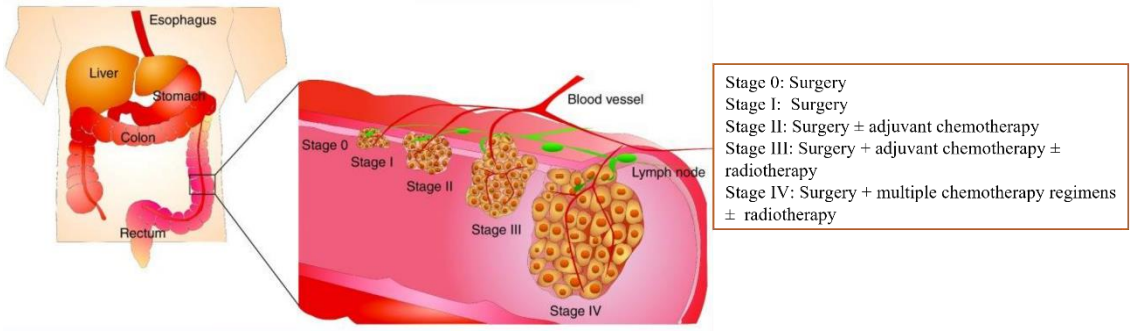

Figure 2. Colorectal cancer stages. Stage 0 is defined by appearance of small tumorigenic nodules that are confined to the mucosa or inner layer of the colon (carcinoma *in situ*). Stage I is characterized by tumor invasion through the submucosa and muscularis propria. Surgical resection is a standard treatment for stages 0 and I. Stage II is defined by tumor invasion and penetration to the surface of the visceral peritoneum. Surgery is usually the only treatment needed for stage II, and the use of an adjuvant chemotherapy at this stage is still controversial. In stage III, the tumor invades muscularis propria and spreads outside the colon with metastases in one or more regional lymph node. Surgery is applied to remove tumor and the affected lymph nodes (fractional colectomy). Adjuvant chemotherapies are also utilized. In addition, radiation might be also applied to ensure eradication of tumor cells that remain after surgery. Stage IV is characterized by tumor spread to one organ or site, such as lung, liver, ovary, or non-regional lymph node. For this stage, surgery is combined with various chemotherapy regimens to control the disease. In some cases, radiation is applied after surgery. [Adapted and modified from [32]].

B. Cancer stem cells

Cancer stem cells (CSCs) were first identified in leukemia and isolated via CD34+ and CD38− surface expression markers in the 1990s [36, 37]. Subsequently, surface markers, such as CD44, CD133, and nestin have been also identified in CSCs originating from various non-solid and solid tumors [38, 39]. CSCs develop tumors via self-renewal and multi-lineage differentiation into multiple cell types. Self-renewal capacity is one of the most known characteristics of CSCs and is essential for maintaining proliferating capacities. CSCs can symmetrically divide into two CSCs or into one CSC and one daughter cell. By expanding symmetrically, CSCs increase tumor growth, leading to tumor formation. Common signaling pathways involved in self-renewal

process include Sonic Hedgehog [40], Notch [41], and Wnt/β-catenin pathways [42]. The latter pathway is of relevance to CRC.

The ability of CSCs to differentiate into different cell types has been shown in several *in vitro* and *in vivo* studies. A study showed that CD34+/CD38− leukemia stem cells, isolated from acute myeloid leukemia (AML) patients, can differentiate, and proliferate in severe combined immunodeficient mice (SCID) [37]. Another study showed that CD133+ cells give rise to multi-lineage CD133- cells, such as astrocytes, oligodendrocytes, and neurons [43]. In CRC, CD44+/EpCAM+ [44] and CD133+ [45] subpopulation initiate tumorigenesis and differentiate into CRC cells, while also reproducing the same morphological and phenotypic heterogeneity of the original tumor they were isolated from.

Initially, CSCs were thought to originate from normal stem cells; however, several studies in mouse models showed that progenitor cells can give rise to CSCs (Figure 3). Krivtsov *et al.* [46] showed that transducing MLL-AF9 fusion protein into myeloid progenitors gives rise to leukemia stem cells, whereas Huntly *et al.* [47] reported that MOZ-TIF2 converts myeloid progenitor cells to stem cells. Notably, CSCs do not necessarily originate from normal stem cells or progenitors (Figure 3). Ectopic expression of transcription factors (e.g., TWIST1 and Snail) in epithelial cells induces stem cell-like phenotypes [48]. Oncogenic Ras or NF-κB activation induces intestinal epithelial cell dedifferentiation and acquisition of stemness state and properties [49]. Interestingly, CSCs have the ability to transdifferentiate into stromal cells, such as vascular endothelial cells and pericytes *in vitro* and *in vivo* [50]. All these findings show the plasticity of CSCs, another key characteristic of these cells.

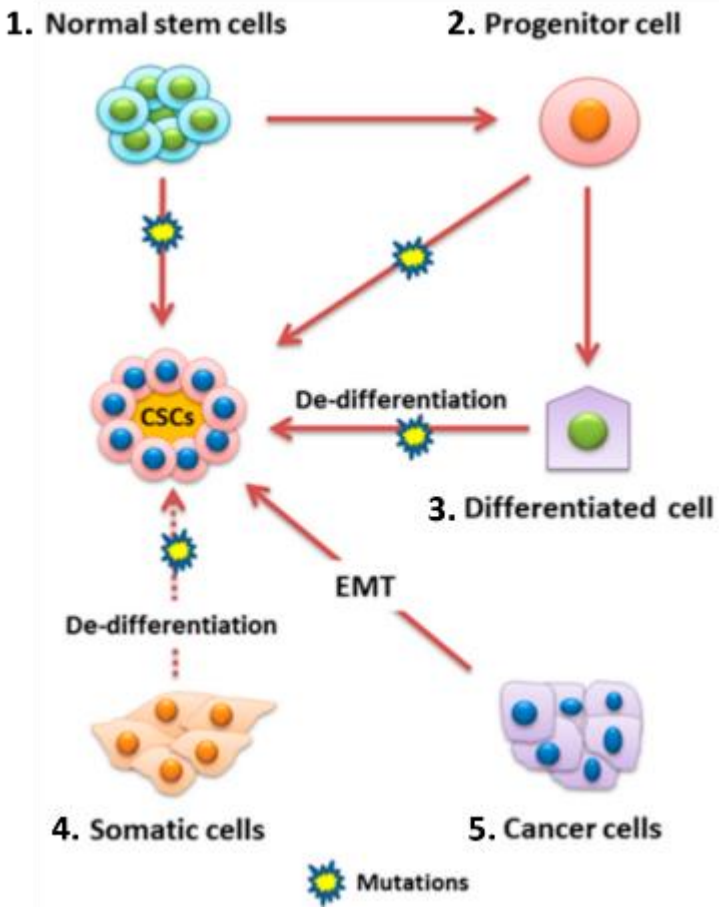

Figure 3 . Origin of cancer stem cells. Cancer stem cells may arise from (1) normal stem cells that undergo mutations, (2) progenitor cells that undergo mutations or differentiation and then de-differentiate to produce CSCs, (3) differentiated cells or (4) somatic cells that undergo de-differentiation, or from (5) cancer cells that undergo epithelial to mesenchymal transition (EMT). [Adapted and modified from [51]].

C. Colorectal cancer stem cells

1. Origin, markers, and signaling pathways

Colorectal cancer stem cells share major characteristics with stem cells from other solid tumors, including self-renewal, plasticity, multi-directional differentiation capacity, deregulation of survival and proliferation signaling pathway (Wnt, Notch, and Hedgehog), tumorigenicity, and resistance to chemo- and radiotherapy [52]. CRC stem cells also share key characteristics of normal ISCs, such as infinite division and high telomerase activity [53].

The “top-down” and “bottom-up” models have been proposed to explain the origin of CRC stem cells. The first model suggests that the differentiated (luminal) intestinal cells at the top of the crypt acquire genetic alterations, mainly at the *APC* locus, that results in stem-like properties. These cells display abnormal patterns of proliferation and form morphologically abnormal crypts by spreading laterally and downwards towards the normal crypt [54]. The “bottom-up” morphogenesis suggests that stem cells residing at the crypt base migrate to the crypt apex and expand, thereby populating the entire crypt [55].

The Wnt/β-catenin pathway activation is important for stemness maintenance and drug resistance in both models [56, 57]. The activation of this pathway is mediated through binding of Wnt ligands with Frizzled receptor complex, resulting in the activation of β-catenin, key effector and a transcription co-regulator [56]. APC/Axin/ glycogen synthase kinase (GSK-3β) complex is a negative regulator of β-catenin [58]. The multi-functional kinase GSK-3β phosphorylates β-catenin, resulting in its ubiquitination and proteasomal degradation. Upon activation of Frizzled receptor, GSK-3β is displaced from APC/Axin complex, therefore stabilizing β-catenin. β-catenin then translocates into the nucleus, binds to LEF/TCF transcription factors, and activates gene expression. Mutations in the APC/Axin/GSK-3β complex prevents degradation of β-catenin and results in its accumulation and nuclear translocation, and consequently activation of genes involved in stemness and malignancy of CRC [58].

Colorectal cancer stem cells are characterized by the expression of several cell surface markers. These include CD44, CD133, CD24, EpCAM, LGR5 and ALDH1 [44, 59]. These molecules are involved in cell adhesion, proliferation, malignant progression and metastasis, resistance to therapy, and stemness [60].

2. Resistance to therapy

Traditional treatment for CRC includes surgery, chemotherapy, and radiotherapy. Chemo-and radiotherapy kill highly proliferating non-CSCs and spare CSCs [61-64]. Mechanism of stem cell resistance is still unclear, but several potential mechanisms have been proposed (Figure 4). CSCs remain mostly in the quiescent G0 phase and do not enter cell cycle [50]. The three pathways previously described, CIN, MSI, and CIMP pathways contribute to DNA damage. Moreover, the DNA damage response (DDR), which is found in all cells, is aberrant in most cancers, including CRC [65]. DDR is initiated by damage sensors known as DDR sensors that detect DNA damage, recruit downstream transducer molecules, and trigger a cascade of phosphorylation events to eliminate deleterious damage [66]. Main transducers and regulators of DDR are ataxia telangiectasia mutated (ATM) and ATM and Rad3-related protein (ATR), which are members of the phosphatidyl-inositol 3-kinase (PI3-kinase) like family of protein kinases (PIKKs) [67]. They interact with p53 and checkpoint kinases (chk) 1 and 2 through ATM/chk2 and ATR/chk1 pathways that converge on Cdc25, a cell cycle regulator [67, 68]. An additional contributor to CSC resistance to therapy is the expression of high levels of anti-apoptotic proteins, including Bcl-2 family members and apoptotic inhibitors, which results in resistance to cell death by apoptosis [69]. Moreover, CSCs express high levels of ATP-binding cassette (ABC) transporters, which results in increased efflux of chemotherapeutic drugs from these cells [70]. Radiotherapy targets cancer cells by inducing accumulation of reactive oxygen species (ROS) and DNA damage, thereby leading to cell death. Resistance to radiotherapy is conferred mainly by the upregulation of anti-apoptotic proteins, activation of an enhanced DDR, and activation of survival pathways. Moreover, radiotherapy may induce cancer cells to

acquire phenotype and functions of CSCs, in addition to epithelial to mesenchymal transition (EMT), resulting in stemness and resistance to therapy [71].

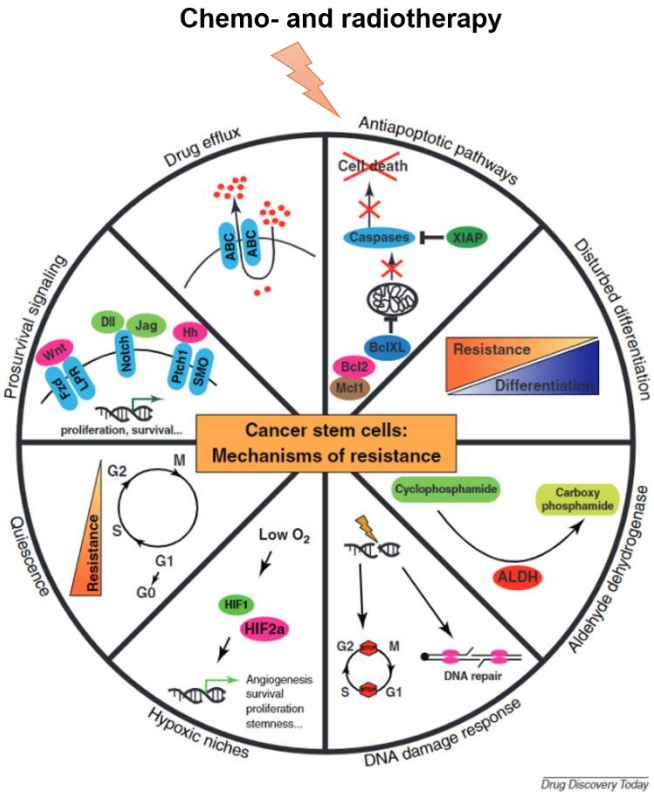

Figure 4. Mechanisms of CSC resistance to therapy. Multiple mechanisms of CSC resistance have been identified and studied: Activation of apoptotic pathways through upregulation of Bcl2 family of proteins, dysregulation in differentiation, increased ALDH activity, enhanced DNA damage response, presence of hypoxic niche that stimulates resistance (through regulating angiogenesis, survival, proliferation, and stemness), quiescence, and activation of prosurvival pathways (Wnt, Notch, and Hedgehog pathways). [Adapted and modified from [72]].

3. Enrichment of colorectal cancer stem cells

Three-dimensional (3D) models of CRC have emerged as useful tools for a better simulation of *in vivo* tumors, as compared to their 2D counterparts. Although 2D cultures have been widely used to study CRC, they do not truly represent the complexity and

interactions that take place between cancer cells and tumor microenvironment (TME), such as the extracellular matrix (ECM).

a. 3D colonosphere cultures

Sphere cultures or tumorospheroids are major 3D *in vitro* models used for enrichment of CSCs, including CRC stem cells [73]. In these models, cells are grown as aggregates in suspension or on a reconstituted basement membrane (BD Matrigel matrix). They maintain cell-cell and cell-matrix interaction and allow for evaluation of CSC characteristics, such as self-renewal capacity and differentiation potential [74].

3D spheroids are composed of different cell layers [75]. The external layer consists of highly proliferating cells, the middle layer harbors senescent cells, while the inner core consists of hypoxic and necrotic cells, similar to tumors *in vivo*, which is basically due to limitations in nutrients and oxygen supply to the center of the tumor [75]. This important feature makes spheroids good models for evaluating drug resistance, and they are usually more resistant to chemo- and radiotherapy compared to cells grown in 2D monolayers [76].

In our study, we adopted a sphere formation assay to isolate and enrich CRC stem cells from different CRC cell lines, whereby single cells are resuspended in serum-free media and Matrigel. The latter is a semi-solid basement membrane majorly composed of collagen IV, laminin, heparin sulfate proteoglycans, entactin, nidogen, and growth factors, mimicking TME *in vivo* [77]. Upon propagation of spheres, progenitors are capable of self-renewal up to 2-3 generations, due to their limited self-renewal capacity. On the other hand, the continuously self-renewing stem cells continue to form spheres up to generation 10.

b. Patient-derived organoids

Organoids have emerged as advantageous disease models that bridge the gap between 2D cultures and *in vivo* models and have improved basic and clinical cancer research. The term organoids signifies “resembling an organ”, whereby organoids are capable of self-organization into 3D structures that mimic the structure and characteristics of the original tissue [78]. Organoids can be derived from either pluripotent stem cells (PSCs) or organ-specific adult stem cells [79]. These novel models are being used in multiple fields and for various purposes. They have been used to model several diseases including cancer, infectious diseases, and inheritable genetic disorders [80].

Intestinal organoids from either postnatal or adult intestinal epithelium [81] or from a single adult ISC [82] were cultured in media supplemented with EGF, noggin, and Wnt agonist R-spondin (RSPO). Mouse- and human-colonic stem cells have been also used to establish organoids using slightly different media compositions [83]. Sato *et al.* [83] succeeded in expanding single crypts and stem cells derived from mouse and human intestine using long-term culture conditions and the resulting organoids displayed major hallmarks of small intestinal epithelium, including cell type composition and self-renewal capacity.

Multiple organoids have been established from gastric [84, 85], colorectal [86, 87], pancreatic [88], liver [89], bladder [90], esophagus [91], brain [92], lung [93] and endometrial [94] cancers. This has enabled the study and validation of personalized therapy and prediction of treatment response [95]. Co-culturing organoids with immune cells enabled the progress of cancer immunotherapy research, while co-culturing organoids with other stromal cells, such as cancer-associated fibroblasts (CAFs) allowed the understanding of TME contribution to carcinogenesis [95, 96].

The development of patient-derived organoids (PDOs) has enabled disease modeling with precision, which opened new opportunities in biomedical applications, translational medicine, and personalized therapy [95]. In the context of CRC, organoids from patients with primary, metastatic or recurrent disease were used to evaluate the response to standard-of-care chemotherapy, radiotherapy [97], and neoadjuvant chemoradiation [98]. Ganesh *et al.* [97] reported that *ex vivo* organoid responses to chemotherapy (5-FU alone or FOLFOX) or radiotherapy (single dose, 0-8Gy) correlated with clinical responses in patients' tumors. Interestingly, radioresistance was observed in organoids derived from patients who received radiotherapy or who have shown no to minimal clinical response. Results from another recent study showed that PDOs treated with neoadjuvant chemoradiation (5-FU and irinotecan) reported promising predictive value for clinical response, with 78% sensitivity and ~92% specificity [98]. Several studies also used PDOs to screen for effective targeted therapies based on specific genetic variants detected within organoids and that could serve as potential targets for therapy [99-101]. This approach was implemented using colon and CRC organoids, among other tumor tissue-derived organoids, to identify patient subsets with vulnerability to targeted agents, such as Plocabulin, EZH2 inhibitors, and EGF receptor (EGFR) inhibitors [99-101]. A more than additive combination effect was demonstrated in patient-derived CRC organoids treated with second-generation TRAIL receptor agonist (APG-880) in combination with radiation, suggesting the potential use of AG880 as a radiosensitizer for treating CRC [102].

We have succeeded in generating PDOs from fresh rectal and colon cancer tissues. These preclinical models were used to model CRC disease, validate our 2D and 3D spheroid results, and predict treatment response.

4. Targeting colorectal cancer stem cells

CRC stem cells are resistant to traditional chemo- and radiotherapy, resulting in disease recurrence and decreased survival [103, 104]. Notably, therapeutic approaches have been devised to overcome resistance to radiation and chemotherapy in CSCs. 5-FU is a pyrimidine analog that disrupts DNA, thus inhibiting DNA replication and leading to cell death. It is the standard treatment for metastatic CRC. Other chemotherapeutic drugs have been also implemented in clinical practices including irinotecan, oxaliplatin, and capecitabine [105]. These drugs have become standard treatments for patients with CRC; however, their efficacy is limited by the intrinsic and acquired resistance to these therapies, limiting overall survival. The effective use of multidrug chemotherapy regimens such as 5-FU, leucovorin, and irinotecan (FOLFIRI), 5-FU, leucovorin, oxaliplatin, and irinotecan (FOLFOXIRI), and 5-FU, oxaliplatin, and leucovorin (FOLFOX4) has been evaluated in randomized clinical trials [106, 107]. These combination therapies have led to superior therapeutic results and significantly improved survival of patients with advanced CRC. CSCs can be directly targeted by inhibiting pathways involved in self-renewal capacity, such as Wnt, Notch, and Hedgehog pathways [108]. Frank *et al.* [109] summarized current approved and investigational therapies targeting CRC stem cells (Figure 5). These include the administration of small molecule inhibitors of MEK, mutant BRAF, c-Met, and STAT3 and monoclonal antibodies against epidermal growth factor receptor (EGFR) and vascular endothelial growth factor receptor1 (VEGFR1). Additional approaches include selective CSC killing through targeting Lgr5 and CXCR4 cell surface molecules, differentiation therapy through administration of BMP4, and reversal of multiple drug resistance (MDR) by blocking ABCB5 transporters. The application of these therapies has generally further improved

overall survival [106, 107, 109]. In addition, immune checkpoint therapy has also shown promising results in patients with metastatic CRC [110]. Interestingly, there is a growing interest in the use of natural compounds, such as phytochemicals, for sensitizing CSCs to conventional therapies. These compounds are generally safe, available, cost effective, and potent when used as complementary treatments for therapies implemented in the clinic [111].

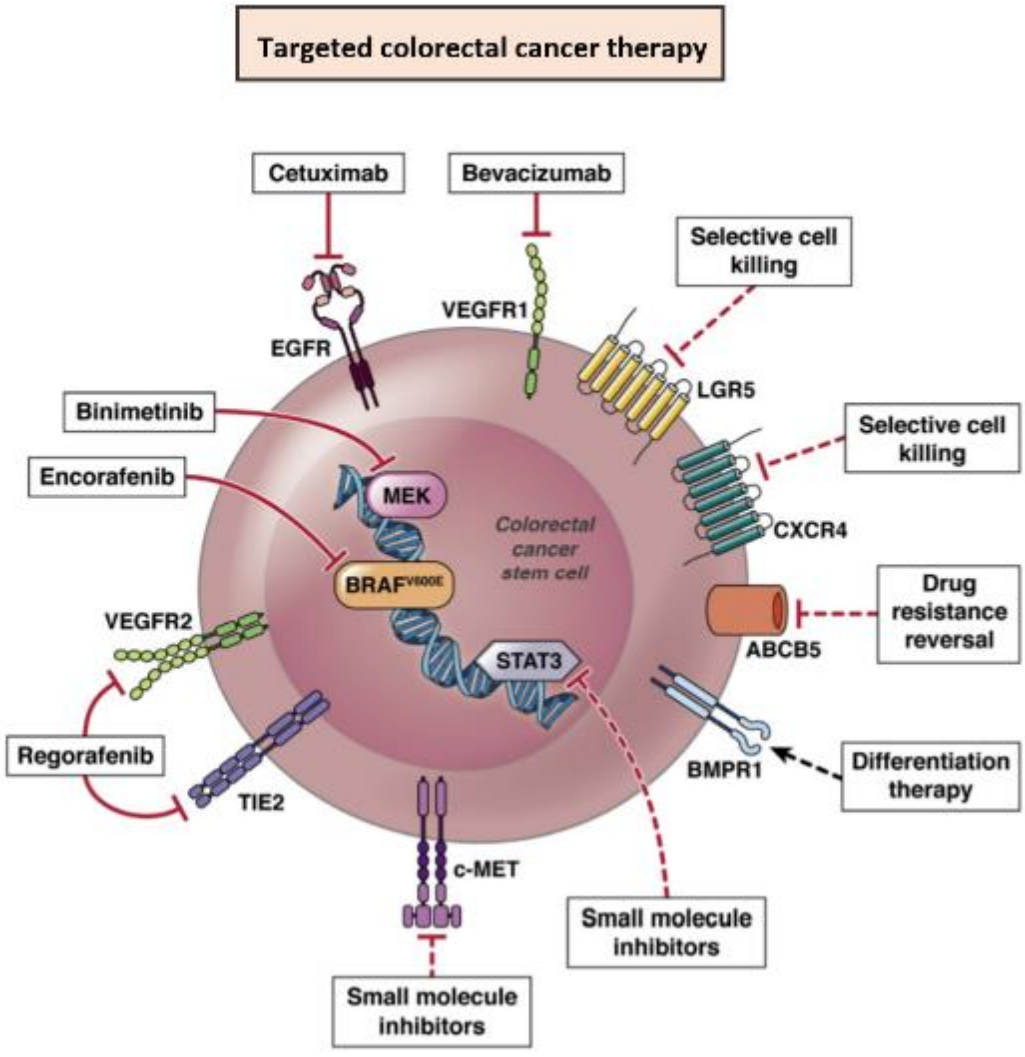

Figure 5. Targeted therapies against colorectal cancer stem cells. Clinically approved therapies that target CRC stem cells include small molecule inhibitors of MEK, mutant BRAF, c-Met, and STAT3 and administration of monoclonal antibodies against EGFR and VEGFR1. Additional approaches include selective CSC killing through targeting Lgr5 and CXCR4 cell surface molecules, differentiation therapy through administration

of BMP4, and reversal of multiple drug resistance (MDR) by blocking ABCB5 transporters. [Adapted and modified from [109]].

D. Thymoquinone

Thymoquinone (TQ) (2-isopropyl-5-methyl-1,4-benzoquinone) is the bioactive phytochemical constituent of the oil of Nigella sativa L. black seed [112]. *Nigella sativa*, also known as black cumin, fennel flower, or nutmeg flower, is a common medicinal herb with well-known properties that help contain and treat several diseases. It was traditionally believed to be useful for all diseases except death (Prophetic hadith) [113]. TQ has a basic quinone structure consisting of a para substituted dione conjugated to a benzene ring in which the hydrogens at positions 2 and 5 are replaced by methyl and isopropyl groups, respectively (Figure 6) [114].

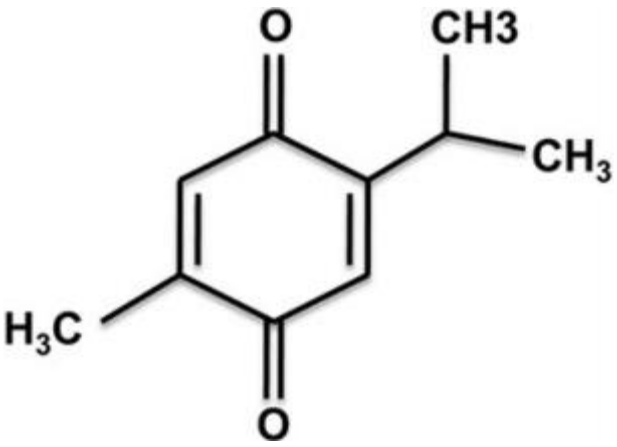

Figure 6. Chemical structure of Thymoquinone. [Adapted from [115]].

TQ exhibits anti-oxidant [116], hypoglycemic [117], anti-inflammatory [118], anti-cancer [112], neuro- [119], cardio- [120], nephro- [121] and hepato-protective [122] activities, in addition to its immune-modulating property [123]. It has also shown anti-proliferative, anti-oxidant, anti-inflammatory, and apoptotic activities in multiple cancer

types, including colorectal [124-127], gastric [128], prostate [129], bladder [130], breast [131], lung [132], and osteosarcoma [133].

TQ has shown promising anti-cancer effects in *in vitro* and *in vivo* models of CRC, alone and in combination with chemotherapeutic compounds [124, 127, 134-138]. In human LOVO colon adenocarcinoma cell line, TQ was reported to reduce the expression levels of cancer-promoting molecules such as p-PI3K, p-Akt, p-GSK3β, and β-catenin, thereby reducing Cox-2 levels and modulating cellular proliferation and migration. The anti-metastatic effect of TQ was further confirmed in a highly aggressive human LOVO cancer cell xenograft nude mouse model [134]. In another study, TQ decreased the viability of COLO205 and HCT116 cells and sensitized these cells to cisplatin by inhibiting NF-κB activation. Molecular analysis showed that TQ decreased the levels of phosphorylated p65 in the nucleus. It also reduced the levels of VEGF, c-Myc, and Bcl-2 [124]. By inhibiting NF-κB through activation of JNK and p38, TQ also inhibited metastasis in Irinotecan-resistant (CPT-11-R) LOVO cells [135]. Another study showed that TQ induces apoptosis in HCT116 cells through enhancing the activity of caspase 3 and cleavage of caspase-9, -7, and -3, and PARP. It also reduced the expressions of Bcl-2 and Bcl-xl [136]. The inhibition of EGFR, JAK2, and Src kinase phosphorylation by TQ inhibited STAT3 activation [136]. TQ mediates p53-dependent chk1 inhibition and consequently, apoptosis induction in HCT116 [137]. TQ reduced tumor multiplicity and aberrant crypt foci (ACF) and inhibited tumor growth while inducing apoptosis in HCT116 xenograft [127]. TQ inhibited 1,2-dimethyl-hydrazine (DMH)-induced colon carcinogenesis in Wistar rats through modulating ROS and lipid peroxidation levels and reducing dysplasia degree [138]. It has been reported that TQ derivatives inhibit the proliferation by increasing p21cip1/waf1 mRNA levels and

reducing cyclin E levels in HCT116 cells [139]. Recently, combining TQ and 5-FU or using a novel 5-FU/TQ hybrid were shown to be more effective than 5-FU in targeting resistant CRC stem cells by inhibiting self-renewal capacity through targeting Wnt/ß-Catenin and PI3K/Akt signaling pathways *in vitro*. *In vivo*, 5-FU/TQ hybrid was effective in reducing the growth of chick chorioallantoic membrane (CAM) xenograft [140].

In addition to its anti-cancer role, TQ has been shown to have radio-potentiating role in several types of cancer with limited toxicity to normal cells and thus, might be an ideal adjuvant to radiotherapy in CRC. Studies have shown that TQ enhances apoptosis and cell cycle arrest when combined with radiation in breast cancer cells [141]. Another study showed that TQ enhances radiosensitivity, alone or in combination with paclitaxel, of breast cancer cells. Further investigation showed that it mediates sensitivity and inhibits radiation-induced migration and invasion and EMT via restoring high levels of E-cadherin and decreasing TGF-β, integrin αV, MMP9, and MMP2 expression [142]. Moreover, it was shown that TQ modulates pathways involved in radiotherapy resistance, including PI3K/Akt/mTOR signaling pathway [143]. TQ also demonstrated synergistic effects when combined with radiation in head and neck squamous cell carcinoma (HNSCC) cells through inhibition of proliferation [144]. It also enhanced the effect of gamma knife on apoptosis and DNA damage in B16-F10 melanoma cells by modulating the JAK2/STAT3 pathway [24].

On the other hand, *in vivo* studies have shown that TQ has a radio-protective effect by reducing radiation-induced oxidative [145] and nitrosative stress in brain tissues [146]. Moreover, TQ protected T cells from apoptosis and exhaustion, in gamma radiation-exposed rats, through modulating the expression of apoptosis-related proteins (Bcl-2, Bax, and caspase-3), pro-inflammatory cytokines (TNF-α and IL-6), and T

lymphocyte exhaustion marker (PD-1) [147]. TQ mediates its radio-protective activity mainly by acting as a free radical and superoxide radical scavenger through activating anti-oxidant enzymes in healthy cells [148], while inducing ROS, and thus oxidative stress in cancer cells [138, 148].

Few studies investigated the pharmacokinetic and pharmacodynamic characteristics of TQ [149, 150]. It was shown that TQ is reduced by catalyzing liver enzyme into hydroquinone [149]. Upon oral administration, TQ was detected in the plasma of rats up to 12 hours [150]. Despite the promising anti-cancer effects of TQ, its use in clinical practice is hindered by its limited bioavailability, hydrophobicity, and high capacity to bind plasma proteins [151]. For this reason, encapsulation of TQ in nanoparticles (NPs) is being extensively studied and has shown promising results so far for better TQ bioavailability, delivery, and targeting against cancer cells. Examples include the use of polymeric TQ nanoparticles (PLGA, PHA–mPEG, and PEGylated), lipid-based (Nano-structured lipid carriers (NLC), liposomes, and solid-lipid nanoparticle (SLN)), and chitosan-based (Chitosan (CS-NP)) [151].

As for the safety and effectiveness of TQ administration, a recent phase I study reported that TQ reduced potentially malignant oral lesions in patients at a dose of 100/200 mg [152]. In a phase I trial, TQ was found non-toxic in patients up to 10 mg/kg/day; however, no significant anti-cancer effect was achieved at this dose [153].

E. Aim of the study

Colorectal cancer is still one of the leading causes of death worldwide. Despite the great advances made in detecting and treating CRC, it remains a major burden in many countries. This is due to some limitations in using traditional chemotherapy and

radiotherapy alone for cancer treatment. Many chemotherapeutic drugs are nonspecific to cancer cells and cytotoxic to normal cells. Additionally, multidrug resistance may occur during treatment, resulting in recurrence and metastasis [154]. It is believed that cancer stem cells (CSCs), which are a subpopulation within the tumor characterized by stemness and self-renewal capacity, are responsible for resistance and aggression of the disease.

There is a growing interest in developing combination therapy for effective and significant targeting of CSCs. Natural compounds are attractive candidates in combination therapy due to their multitargeting, safety, and cost-effectiveness [111].

Thymoquinone, the major bioactive compound found in *Nigella sativa*, exhibits several cytotoxic activities against many cancer types, including CRC, through the modulation of multiple hallmarks of cancer. Notably, TQ can sensitize chemo- and radio-resistant cancer cells by modulating several survival and DNA repair pathways involved in resistance [155]. Although multiple investigators explored the effect of TQ on cancer, no studies have investigated the anti-tumor effect of TQ in combination with radiation on CSCs.

In this study, we aim to investigate a novel approach to the inhibition of CRC cells and CRC stem cells using a novel combination therapy with promising possibilities for clinical translation. Panels of CRC cell lines (HCT116, HCT116 p53 null, HT29, and DLD1) with different mutations and sensitivity were used to study the effects of TQ and ionizing radiation (IR). 3D spheroid cultures derived from HCT116 and HT29 cells were used to enrich for stem/progenitor cells and study effects of TQ and IR on CSCs self-renewal capacity. Patient-derived organoids from fresh rectal and colon cancer tissues were successfully established and propagated to investigate the anti-cancer potential of

TQ alone and in combination with IR. These models were used to validate the radiosensitizing effect of TQ.

CHAPTER II
MATERIALS & METHODS

Based on my manuscript that was published in *Cancers* journal [156], below is the methods:

A. Cell culture conditions

Human non-tumorigenic intestinal epithelial FHs74Int cells and CRC cell lines HCT116, HCT116 p53 null, HT29, and DLD1 were purchased from ATCC (ATCC, USA). HCT116, HT29, and DLD1 cells were cultured and maintained in RPMI 1640 (Sigma-Aldrich, Germany) with 20 mM HEPES and L-Glutamine. HCT116 p53 null cells were cultured in DMEM 4.5 g/L Glucose with L-Glutamine (LONZA). FHs74Int cells were cultured in DMEM 4.5 g/L Glucose with L-Glutamine (LONZA) supplemented with 10 µg/mL insulin and 1% sodium pyruvate. Media was supplemented with antibiotics [1% Penicillin-Streptomycin (100 U/mL)] and 10% heat-inactivated fetal bovine serum (FBS) (Sigma-Aldrich, Germany). Cells were incubated at 37ºC in a humidified incubator containing 5% CO2 and 95% air. All cells were mycoplasma free.

B. TQ preparation and treatment

Directly before use, fresh stocks of the purified synthetic compound TQ (Sigma-Aldrich: CAS: 490-91-5; 99.5% purity) reconstituted in methanol were prepared as per manufacturer's instructions. Intermediate concentrations were prepared in appropriate media by serial dilutions from stock.

C. Irradiation

Irradiation of 2D and 3D cultures was performed using the 225 kV biological X-ray Irradiator. Following treatment with TQ for 24 hrs, 2D cells were irradiated with 2 Gy once and incubated for another 24 and/or 48 hrs, unless indicated otherwise. For MTT assay, cells were irradiated with different IR doses (1, 2, or 4 Gy). For 3D assays, spheres/organoids were irradiated with 2 Gy once at each generation.

D. MTT cell proliferation assay

Cell proliferation was determined by MTT ([3-(4, 5-dimethylthiazol-2-yl)-2, 5-diphenyltetrazolium bromide]) (Sigma-Aldrich) assay according to the manufacturer's instructions. Non-tumorigenic and CRC cells were plated in 100 µL complete medium in 96-well culture plates and then treated at 50% confluency in triplicates with various TQ concentrations or IR doses or with TQ followed by irradiation. TQ treatment was replenished every day. At specific time points, 10 µL of MTT (5mg/mL in DMSO) was added to each well and incubated at 37°C for 4 hrs, after which 100 µl isopropanol was used to dissolve violet crystals. Consequently, MTT optical density (OD) was measured at a wavelength of 595 nm using ELISA reader (Multiskan Ex). Cell proliferation was expressed as a percentage of the control. The percentage of proliferating cells was calculated as: % proliferation= OD of treated cells/OD of untreated cells x 100.

E. Trypan blue exclusion assay

Non-tumorigenic and CRC cells were seeded in 24-well plates and treated with TQ, IR, or TQ+IR for 48 and 72 hrs. TQ treatment was replenished every day. Each experiment was repeated three times and in duplicate measurements. Following treatment

attached live cells were harvested by trypsin/EDTA and the cell pellet was re-suspended in media. 50 µl of cell suspension was mixed with 50 µL of trypan blue and live cells were counted using a hemocytometer.

F. Clonogenic survival assay

1. 2D clonogenic survival assay

Non-tumorigenic and CRC cells were seeded in 12-well plates and treated at 50% confluency with TQ alone, radiation alone, or combinations for 48 hrs. Cells were then trypsinized, counted, and plated at low density (2000-3500 cells) in 100-mm tissue culture dishes and left for 8-10 days in the incubator. Subsequently, cells were washed with PBS, fixed with 95% ethanol, and stained with 1 mL of aqueous 0.5% solution of crystal violet. Colonies having more than 50 cells were counted. The plating efficiency (PE), defined as the ability of control cells to survive and grow into colonies, was calculated as: PE = colonies counted in control/plating density of control. Surviving fraction (SF) for each treatment was calculated as: SF = colonies counted/[cells plated × (PE/100)]. The SF value of each treatment was then plotted.

2. 3D clonogenic survival assay

3D clonogenic survival assay was done as described above; however following trypsinization, cells were re-suspended in serum free media, counted, and single cell suspensions (1000 cells/well) were mixed with growth factor-reduced Matrigel™ (1:1) in a total of 10 µL. The solution was then plated gently around the rim of individual wells of 96-well culture plates (10 µL per well). Each experimental condition was performed in duplicate. The Matrigel™ (Corning Life Sciences) was allowed to solidify for 1 hr at

37°C in a humidified incubator, after which 200 µL/well of complete media (+5% FBS), without treatment, was gently added to the center of each well and regularly changed every 3 days. Sphere counts were performed at day 10-12 of culture. The sphere-forming unit (SFU) was calculated as the ratio of the number of spheres formed/ number of cells originally seeded x100. Bright field images of the spheres were obtained using Axiovert microscope from Zeiss at 10X magnification.

G. Wound healing assay

Cells were seeded in 6-well plates and allowed to adhere in the respective medium. When cells reached 90-100% confluency, 2 µg/mL of mitomycin C (Sigma-Aldrich) was added to each well for 20 mins to block cellular proliferation. The media was discarded, and the monolayer was scraped to make a scratch in the middle of each well using a 200 µL micropipette tip. Wells were then washed twice using phosphate-buffered saline (PBS) to remove the detached cells. The medium alone or with TQ alone, or radiation, or combinations was added to the cells. Photos were taken directly after treatment at different intervals. The percentage of the wound width was calculated: (wound width at specific time point)/(control wound width at 0 h) × 100.

H. Cell cycle analysis

Cells were seeded in 6-well plates at appropriate densities and treated at 50% confluency with TQ alone, radiation alone or combinations. Dead and live cells were then collected, washed, and incubated in 70% cold ethanol for 30 mins. Cells were then incubated for 30 mins at 37 °C with 100 µL of propidium iodide (PI) solution [6 µL RNase, 30 µL PI (1 mg/mL) in PBS]. Cell cycle analysis was performed by flow

cytometry using Guava EasyCyte8 Flow Cytometer-Millipore. GuavaSoft™ 2.7 Software was used to analyze the distribution of cells in the different phases of the cell cycle.

I. ROS detection by DHE stain

The level of oxidative stress was assessed by Dihydroethidium (DHE) staining of cells treated with TQ, IR or combinations. DHE is a cell-permeant reagent that intercalates with the cell's DNA, staining its nucleus a bright fluorescent red when it is oxidized by ROS. Briefly, HCT116 and HT29 cells were seeded on coverslips in 12 well plate. After 48 hrs of treatment with TQ, IR, or combination, cells were washed gently with PBS twice and then incubated in 10 mM DHE at 37°C for 45 mins in a dark environment. Cells were then washed with PBS twice to remove DHE that did not combine with nucleus and were incubated with DAPI for 15 mins. Cells were mounted and images were directly taken using confocal microscope. Analysis of DHE intensity was done using Zen 2012.

J. Sphere formation assay

The sphere formation assay was used as previously reported by our laboratory [157]. In brief, single cell suspensions (2000 cells/well) of non-tumorigenic and CRC cells were seeded in cold growth factor-reduced Matrigel™/ serum-free media (1:1) in a total volume of 50 μL. The solution was then plated gently around the rim of individual wells of 24-well culture plates. Each experimental condition was performed in duplicate. The Matrigel™ (Corning Life Sciences) was allowed to solidify for 1 hr at 37°C in a humidified incubator. Wells were randomly assigned to control and treatment conditions,

and 1 mL/well of complete media (+5% FBS), with or without treatment, was gently added to the center of each well and changed regularly every 2 to 3 days. Irradiation (2 Gy) was performed at day 4 of sphere culture. Sphere counts were performed at day 10-12 of culture. SFU was calculated as the ratio of the number of spheres formed/ number of cells originally seeded x100. Bright field images of the spheres were obtained using Axiovert microscope from Zeiss at 10X magnification.

K. Propagation assay

To enrich for CSCs, the media was aspirated from the well and the Matrigel™ -containing spheres was collected using ice-cold media. The resulting sphere suspension was centrifuged, and the pellet resuspended with Trypsin/EDTA at 37°C for 2-2.5 mins. Single cells resulting from the dissociation of spheres were counted and re-plated at the same density of 2000 cells/well in 24-well plates as previously described.

L. Patient-derived organoids

1. Study design and ethical considerations

Human colon/rectal tissues were obtained from the American University of Beirut medical center (AUBMC) after obtaining informed consent forms from patients prior to sample acquisition. The study was conducted under the Institutional Review Board (IRB) approvals of the American University of Beirut (AUB) and AUBMC. The work was carried out in accordance with relevant guidelines and regulations, and in agreement with all ethical considerations of the IRB. Tumor tissues and unaffected adjacent tissues were isolated from resected colorectal/rectal segments from patients diagnosed with colorectal/rectal cancer and undergoing colectomy at AUBMC.

2. Establishment and propagation of patient-derived colorectal cancer organoids

Tissues were processed using protocols described by Boehnke K. *et al.* (Figure 7) [158]. Tissues from patients were rinsed with Hank's Balanced Salt Solution (Gibco), minced using sterile scalpels, and digested in advanced DMEM/F12 (adDMEM/F12) (Gibco) supplemented with dihydrochloride kinase inhibitor, Y-27632, 1% P/S, collagenase IV (Sigma-Aldrich), and amphotericin B (Sigma-Aldrich) at 37 °C for 60 mins. During incubation, tissue fragments were mechanically dissociated by repetitive pipetting. The suspension was filtered through a 40 µm cell strainer (Corning) to remove undigested fragments. Isolated single cells were seeded in 24-well plates with Matrigel in a 9:1 ratio at a cell density of 20,000 cells/well. A volume of 20 µL volume was plated in the middle of the well. Plates were placed upside down in the incubator for 30 mins to allow Matrigel to solidify. Cells were cultured with adDMEM/F12 with various factors added to maintain tumor's biological traits and growth activity. Medium (supplemented with Y-27632) without treatment was changed every 2-3 days. Organoids were propagated at day 10-12. Ice cold adDMEM/F12 medium without factors was added to detach and collect Matrigel with organoids. Organoids were then pelleted and dissociated enzymatically using TrypLE on a shaking platform for 5 mins at 37°C. TrypLE was inactivated by adding adDMEM/F12 containing 5% FBS. Following centrifugation, cells were resuspended in adDMEM/F12 and centrifuged again. Finally, pellet was resuspended in Matrigel and cells plated as described above. Medium with or without TQ was refreshed every 2-3 days and organoids were irradiated at day 4. Organoids were counted at day 10-12 of passage under inverted microscope at 10X magnification. Images were taken and analyzed by Carl Zeiss Zen 2012 image software to determine size. Organoid-forming count (OFC) was reported as the number of organoids counted.

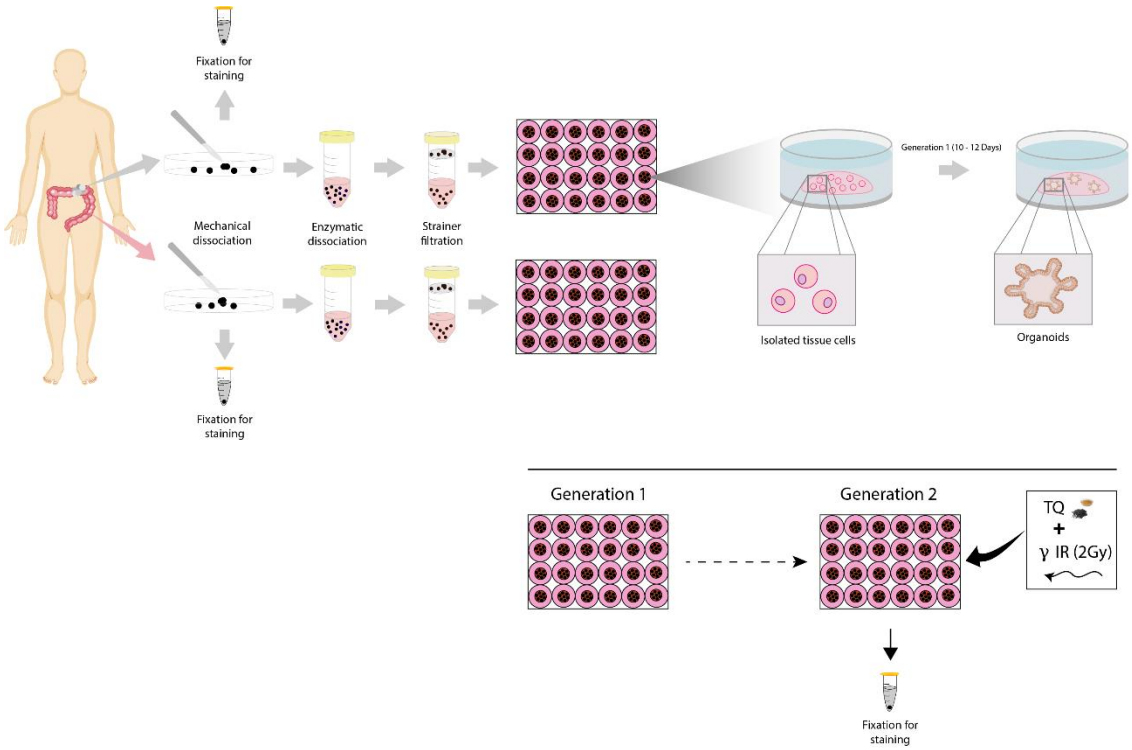

Figure 7. Schematic diagram summarizing the experimental plan adapted for establishing patient-derived organoids. Fresh unaffected and tumor colon/rectal tissue fragments were minced before being digested in 5 mg/mL collagenase type II in Advanced DMEM/F12 medium with RI (ROCK inhibitor). After 1 hr, tissue pellet was subjected to strain filtration and the resulting cell suspension was counted and plated in droplets of 90% Matrigel™ and supplemented with serum-free human colon growth medium. After 10-12 days, organoids were propagated into generation 2 (G2), after which organoids were treated with TQ, IR, or combinations. After 10-12 days, organoids were counted, and images taken before collection for fixation and staining. Fragments of tissue specimens were also fixed in 4% PFA.

M. Cell line-derived organoids

The organoid formation assay was used as previously reported by our laboratory [157] and as described above with minor modifications. In brief, single cell suspensions (5000 cells/well) seeded in cold growth factor-reduced Matrigel™/serum-free adDMEM/F12 (Gibco) in a 9:1 ratio in a total volume of 5 µL in the middle of individual wells of 96-well culture plates. Each experimental condition was performed in duplicate. The Matrigel™ (Corning Life Sciences) was allowed to solidify for 1 hr at 37°C in a

humidified incubator. Wells were randomly assigned to control and treatment conditions, and 200 µL/well of adDMEM/F12 media with several factors, with or without treatment, was gently added to each well and changed regularly every 2 to 3 days. Irradiation (2 Gy) was performed at day 4 of organoid culture. Organoids were counted at day 10-12 of culture. The organoid-forming count (OFC) was calculated as the ratio of the number of organoids formed/ number of organoids in untreated group x100. Bright field images of the spheres were obtained using Axiovert microscope from Zeiss at 10X magnification.

N. Immunofluorescent Analysis

1. 2D cultures

Immunofluorescent staining was performed to assess the mechanisms of TQ radiosensitization on DNA repair markers and pathways involved in radioresistance in 2D cells. Cells were grown on glass coverslips and treated at 50% confluency with TQ and then exposed to 0 Gy (no IR) or 2 Gy. At the specific time point, media was removed, and cells were washed with 1x PBS. Cells were then fixed with 4% paraformaldehyde (PFA) in PBS for 20 mins and permeabilized with 0.5% Triton X-100 in PBS for 30 mins at room temperature. Cells were blocked with blocking buffer (0.1% BSA, 0.2% Triton X-100, 0.05% Tween-20, and 10% normal goat serum (NGS) in PBS) for 1 hr at room temperature. Cells were incubated overnight with γH2AX, p-ATM, ATR, MEK, and p-mTOR primary antibodies (Table 1). Cells were washed with PBS containing 0.1% Tween-20 and incubated with fluorophore-conjugated secondary antibody for 1 hr at room temperature. After washing, cells were mounted with the anti-fade Fluoro-gel II with DAPI. γH2AX foci were visualized and counted using confocal microscope. For the other molecules, fluorescent signals were captured using a Zeiss LSM 710 laser scanning

confocal microscope (Zeiss, Germany), and images were acquired and analyzed using the Zeiss ZEN image software.

Table 1: List of primary and secondary antibodies used in immunofluorescent /immunohistochemical staining

Antibody name	Species	Dilution	Catalog number	Company
Primary antibodies				
γH2AX	Rabbit	1:250	# 9718S	Cell signaling
p-ATM	Mouse	1:200	Sc-47739	Santa Cruz
p-ATR	Rabbit	1:200	sc-109912	Santa Cruz
p-mTOR	Rabbit	1:200	# 2971S	Cell signaling
MEK	Rabbit	1:200	# 9126S	Cell signaling
CD44	Mouse	1:100	sc-7297	Santa Cruz
CK8	Mouse	1:200	904801	Biolegend
CK19	Rabbit	1:200	Ab15463	Abcam
Ki67	Mouse	1:50	sc-23900	Santa Cruz
Secondary antibodies				
Alexa fluoro 488	Goat anti-mouse	1:400	A-28175	Invitrogen
Alexa fluoro 568	Goat anti-rabbit	1:200	A-11011	Invitrogen
Phalloidin		1:200	R415	Invitrogen

2. 3D cultures

Immunostaining was performed according to a protocol described previously by our laboratory [159]. Spheres and organoids were grown then collected with cold media and centrifuged to washout all Matrigel debris. After centrifugation, spheres and organoids were fixed in 4% PFA. After washing, spheres and organoids were permeabilized with 0.5% Triton X-100 and blocked with sphere blocking buffer (0.1% BSA, 0.2% Triton X-100, 0.05% Tween-20, and 10% NGS in PBS) for 2 hrs at room

temperature. Spheres were then incubated overnight at 4°C with various primary antibodies (CD44, γH2AX, CK8, and CK19; Table 1) prepared in blocking solution. Organoids were stained for CD44 and CK19. Spheres and organoids were then washed and incubated with secondary antibody for 1 hr at room temperature. Finally, spheres and organoids were washed and mounted using 5-7 µL anti-fade reagent Fluoro-gel II with DAPI (Abcam, Cambridge, UK). Fluorescent signals were captured using a Zeiss LSM 710 laser scanning confocal microscope (Zeiss, Germany), and images were acquired and analyzed using the Zeiss ZEN image software.

3. Immunofluorescence of embedded tumor tissues

Fresh tissues were fixed in 4% PFA at room temperature for 30 mins. Immunofluorescence staining was performed against CRC markers β-catenin, CK8, CK19, and CD44. Slides were dried, dewaxed in xylene and rehydrated using a decreasing alcohol series. Antigen retrieval was performed in 10 mM citrate buffer pH 6 followed by blocking with blocking buffer (10% NGS, 0.1%Triton-X, 3% BSA in PBS). Sections were incubated with primary antibody at 4°C overnight in antibody solution (2% NGS, 0.1% Triton-X, 3%BSA in PBS). After washing, tissue sections were incubated for 2 hrs with secondary antibodies diluted in PBS containing 2% NGS and 0.1% Triton-X. Mounting was performed using mounting media with DAPI, after which cells were left to dry and then imaged using Zeiss LSM 710 laser scanning confocal microscope (Zeiss, Germany) at 10X.

O. Histology and Immunohistochemical Analysis

Serial tissue sections (4μm) were H&E stained and analyzed by an expert who was blinded for the treatment groups. Immunohistochemical staining was performed on paraffin-embedded tissues spheres using Ki67 antibody. Slides were dried, dewaxed in xylene and rehydrated using a decreasing alcohol series. After blocking of endogenous peroxidase with H2O2, antigen retrieval was performed in 10 mM citrate buffer, pH 6. Subsequently, slides were blocked with Protein Block (Novolink Polymer Detection Kit, RE7150-K, Leica). Primary antibody was incubated at 4°C overnight, followed by Post Primary and Novolink™ Polymer (Novolink Polymer Detection Kit, RE7150-K, Leica). Staining was visualized using 3,3-diaminobenzidine (DAB), and nuclear counterstaining was performed using hematoxylin (Novolink Polymer Detection Kit, RE7150-K, Leica Biosystems, Germany). Slides were dehydrated and embedded in Histofluid (6900002; Marienfeld, Lauda Koenigshofen, Germany). Images were recorded at 20X magnification using an Olympus BH-2 microscope and an Olympus E330 digital camera.

P. Western blot analysis

Cells were plated in 100-mm tissue culture dishes and treated with TQ, IR, or combinations and then collected. Spheres were grown with or without treatment in 24-well plates then collected at G1 with cold media and centrifuged to wash out all Matrigel debris. Cellular protein extracts were prepared using RIPA lysis buffer (sc-24948, Santa Cruz, CA, USA). Protein extracts were quantified using the DC Bio-Rad Protein Assay (Bio-Rad Laboratories, USA) according to the manufacturer's protocol. Protein samples were mixed with 5% β-mercaptoethanol and 2X Laemmli Sample Buffer (Bio-Rad, CA, USA) for gel electrophoresis. An equal amount of protein lysate was separated on 8%,

10%, or 12% SDS–PAGE for 2 hrs at 90 V then transferred onto 0.45 μm nitrocellulose membrane (Bio-Rad, CA, USA) in transfer buffer for 2 hrs at 220 mA at 4°C. Membranes were blocked with 5% skim milk in tris-buffered saline with 0.1% tween 20 (TBST) for 1 hr and then incubated overnight at 4°C with different primary antibodies (Table 2). Membranes were then washed and incubated with the diluted secondary antibody for 1 hr at room temperature. Hybridization with GAPDH-HRP (6C5) (1:10,000–20,000, Abnova, #MAB5476) coupled antibody was performed for 30 mins at room temperature as housekeeping gene. Target proteins were detected using the ECL system (Bio-Rad, CA, USA). Images were generated and quantified using ChemiDoc™ Imaging Systems (Bio-Rad, CA, USA).

Table 2: List of primary and secondary antibodies used in western blot experiments

Antibody name	Species	Dilution	Catalog number	Company
Primary antibodies				
β catenin	Mouse	1:200	sc-7963	Santa Cruz
CD133	Rabbit	1:500	# 64326S	Cell signaling
NF-κB p65	Rabbit	1:50	sc-372	Santa Cruz
p53	Rabbit	1:50	sc-6243	Santa Cruz
p21	Mouse	1:50	sc-6246	Santa Cruz
GAPDH-HRP (6C5)	Mouse	1:20,000	#MAB5476	Abnova
Secondary antibodies				
Goat anti-mouse	Goat	1:1000	sc-516102	Santa Cruz
Mouse anti-rabbit	Mouse	1:1000	sc-2357	Santa Cruz

Q. Statistical analysis

Statistical analysis was performed using GraphPad Prism 6 Software version 6.0.1. Experimental values are expressed as mean ± SEM. Student's t-test was employed for significance and values of $p<0.05$ was considered significant (* $P<0.05$; ** $P<0.01$; *** $P<0.001$, **** $P<0.0001$).

CHAPTER III
RESULTS

A. Effect of TQ and radiation on proliferation of colorectal cancer cells

Our first objective was to investigate the effects of TQ, IR, and combinations on CRC cell lines (HCT116, HCT116 p53 null, HT29, and DLD1), along with human non-tumorigenic intestinal cells (FHs74Int), using MTT (Figures 8–12). The CRC cell lines have different mutations [160] and sensitivity to TQ [126, 161]. Treatment with individual or combination treatment induced a time- and dose-dependent reduction in proliferation of these cells. IC50 of TQ at 24 hrs was highest (112 µM) in HT29 cells (Figure 10) and lowest (61 µM) in DLD1 cells (Figure 11). IR doses of 1 Gy and 2 Gy reduced the proliferation of HCT116 at 48 hrs (Figure 8). IR dose of 2 Gy reduced the proliferation of HCT116 p53 null at 24 hrs (Figure 9), while all IR doses were toxic to DLD1 cells at 24 hrs (Figure 11). However, the effect of IR was reversible at 48 and 72 hrs in these cell lines. None of the IR doses applied to HT29 induced a significant reduction in proliferation at the studied time points. Treatment with TQ (40 µM or 60 µM) followed by irradiation significantly reduced the proliferation of HCT116 cells at 48 hrs; however, this effect was comparable to TQ alone (Figure 8). A similar effect was observed in HCT116 p53 null (Figure 9). In DLD1 (Figure 11) and HT29 (Figure 10) cells, combining TQ and IR reduced proliferation in comparison to IR alone at TQ concentrations of 60 µM and 120 µM, respectively. Interestingly, TQ was non-toxic to FHs74Int human non-tumorigenic intestinal cells at doses up to 60 µM at 24 hrs (Figure 12). High IR dose (4 Gy) reduced the proliferation of FHs74Int cells at 24 hrs, while lower IR doses (1, 2, and 4 Gy) were toxic to these cells at 48 hrs; however, this effect

was reversible at 72 hrs. TQ and IR combination treatment had similar inhibitory effect to TQ alone.

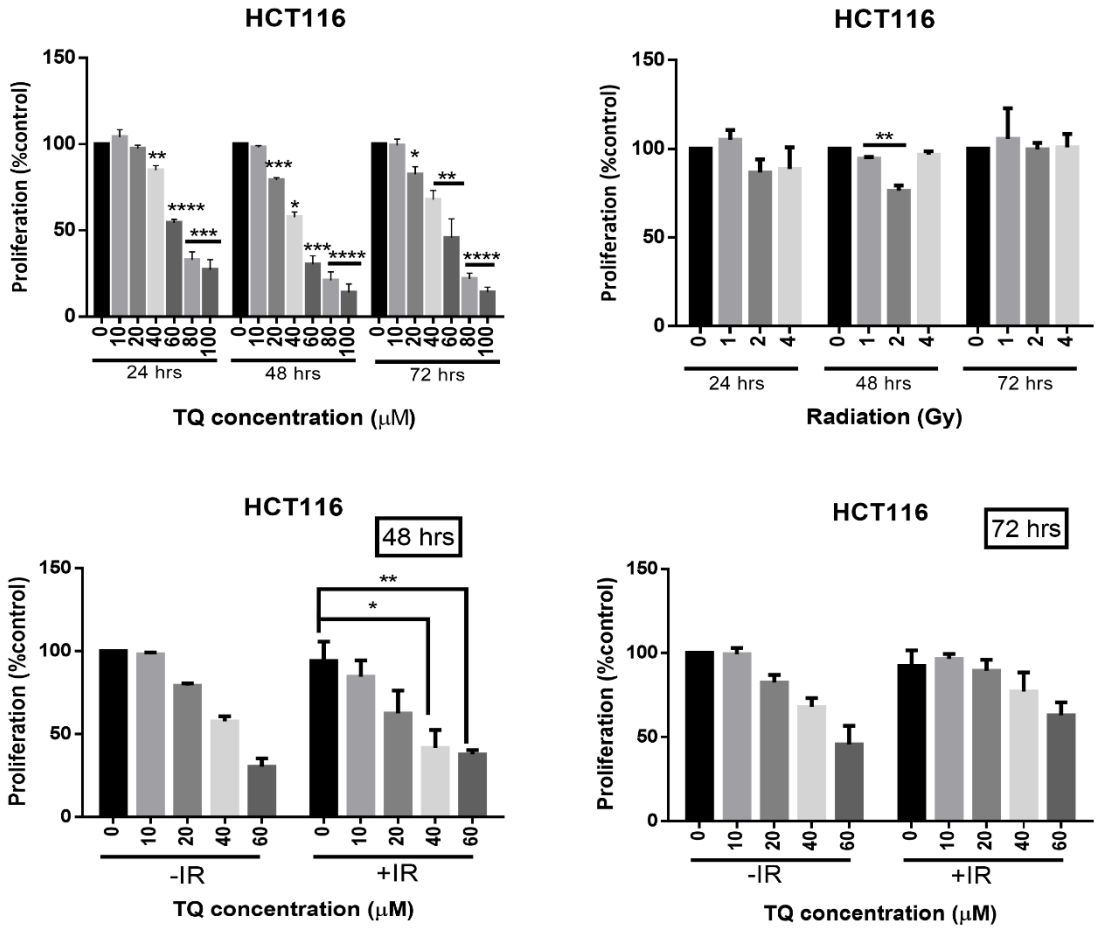

Figure 8. Effect of TQ and IR on HCT116 cell proliferation. HCT116 cells were either left untreated or were incubated with TQ alone, IR alone (2 Gy), or combinations for 24, 48, or 72 hrs. Cell proliferation was determined using MTT. Results are expressed as percentage of the studied group as compared to its control. Data represent an average of three independent experiments. The data are reported as mean ± SEM (* $P<0.05$; ** $P<0.01$; *** $P<0.001$, **** $P<0.0001$).

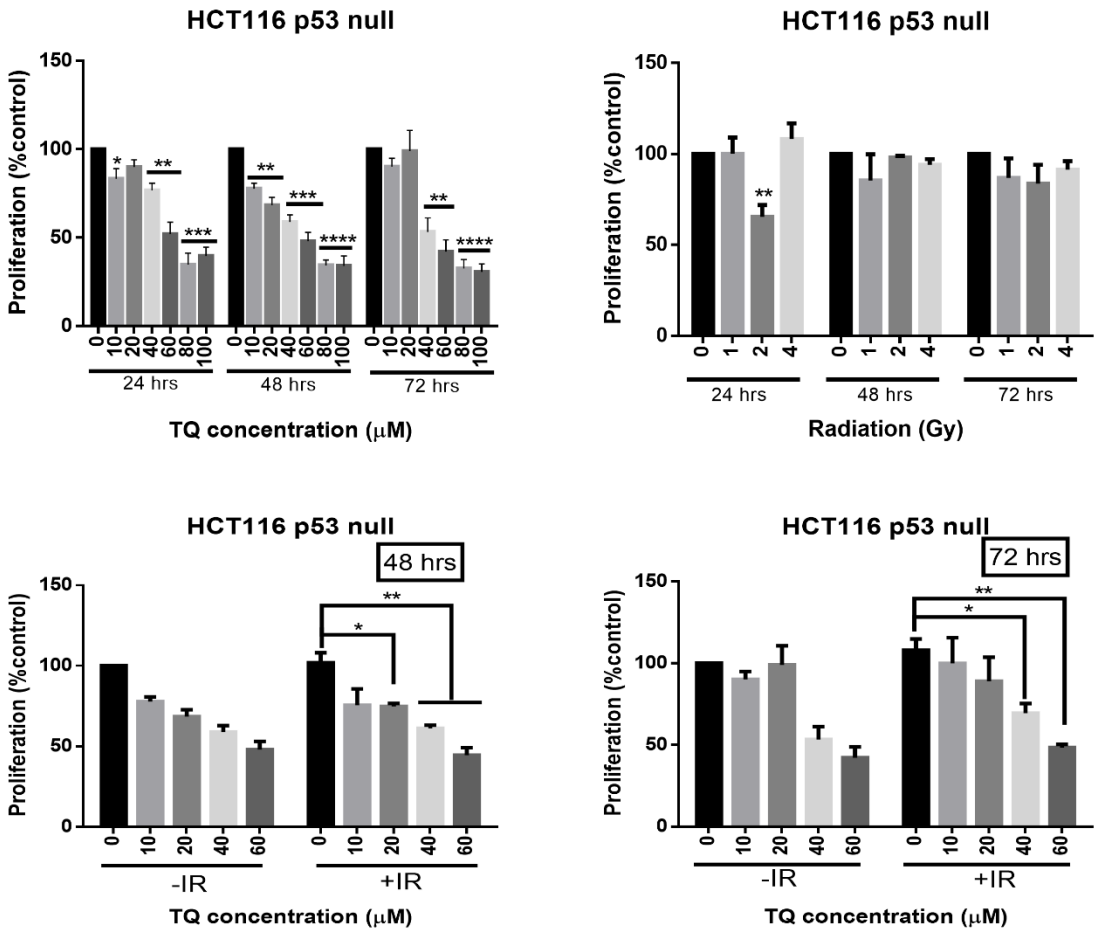

Figure 9. Effect of TQ and IR on HCT116 p53 null cell proliferation. HCT116 p53 null cells were either left untreated or were incubated with TQ alone, IR alone (2 Gy), or combinations for 24, 48, or 72 hrs. Cell proliferation was determined using MTT. Results are expressed as percentage of the studied group as compared to its control. Data represent an average of three independent experiments. The data are reported as mean ± SEM (* P<0.05; ** P<0.01; *** P<0.001, **** P<0.0001).

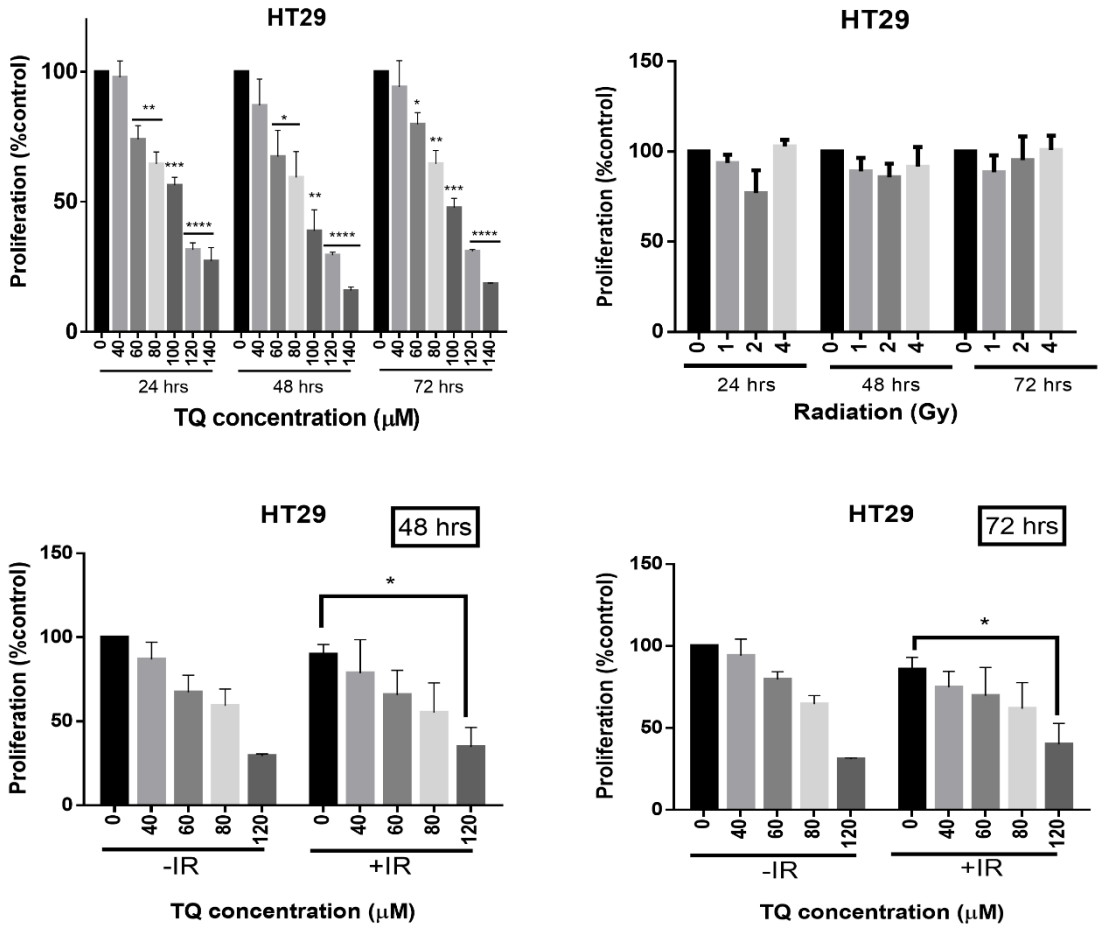

Figure 10. Effect of TQ and IR on HT29 cell proliferation. HT29 cells were either left untreated or were incubated with TQ alone, IR alone (2 Gy), or combinations for 24, 48, or 72 hrs. Cell proliferation was determined using MTT. Results are expressed as percentage of the studied group as compared to its control. Data represent an average of three independent experiments. The data are reported as mean ± SEM (* P<0.05; ** P<0.01; *** P<0.001, **** P<0.0001).

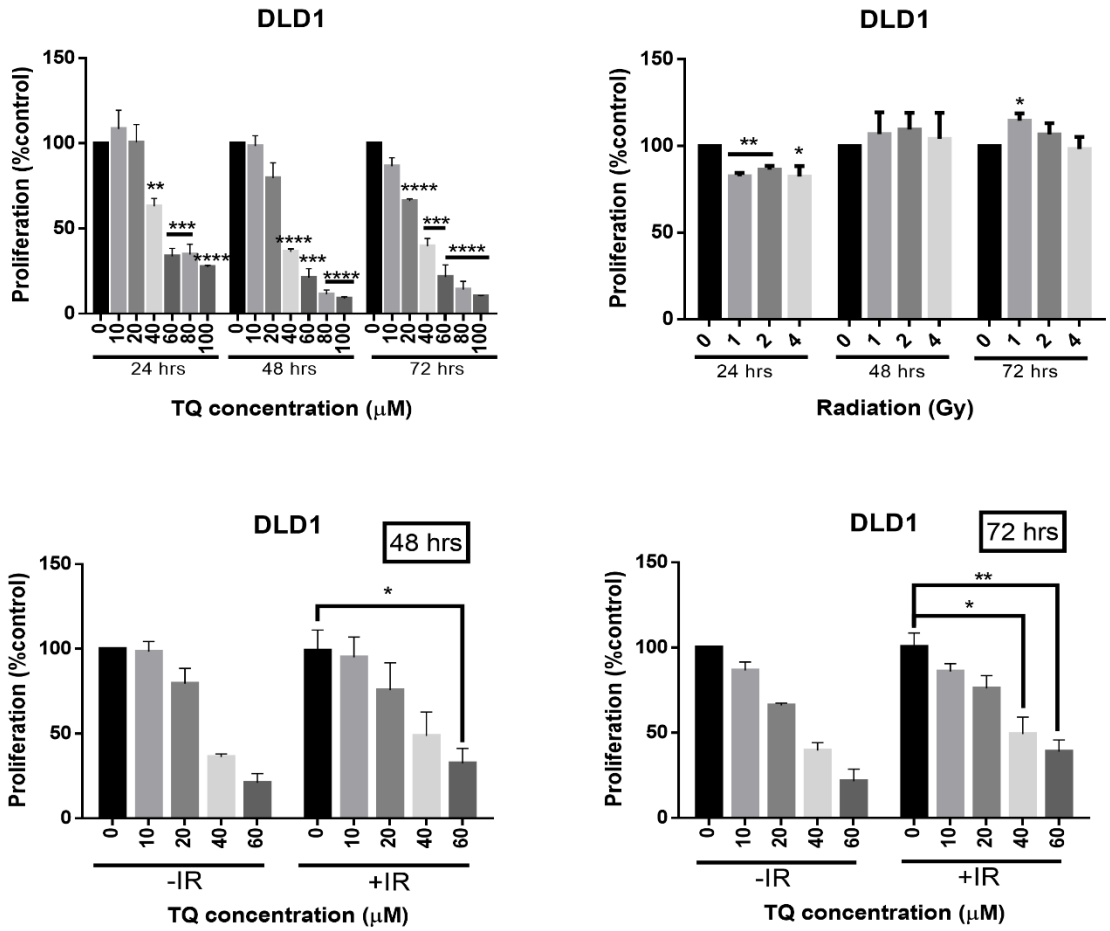

Figure 11. Effect of TQ and IR on DLD1 cell proliferation. DLD1 cells were either left untreated or were incubated with TQ alone, IR alone (2 Gy), or combinations for 24, 48, or 72 hrs. Cell proliferation was determined using MTT. Results are expressed as percentage of the studied group as compared to its control. Data represent an average of three independent experiments. The data are reported as mean ± SEM (* P<0.05; ** P<0.01; *** P<0.001, **** P<0.0001).

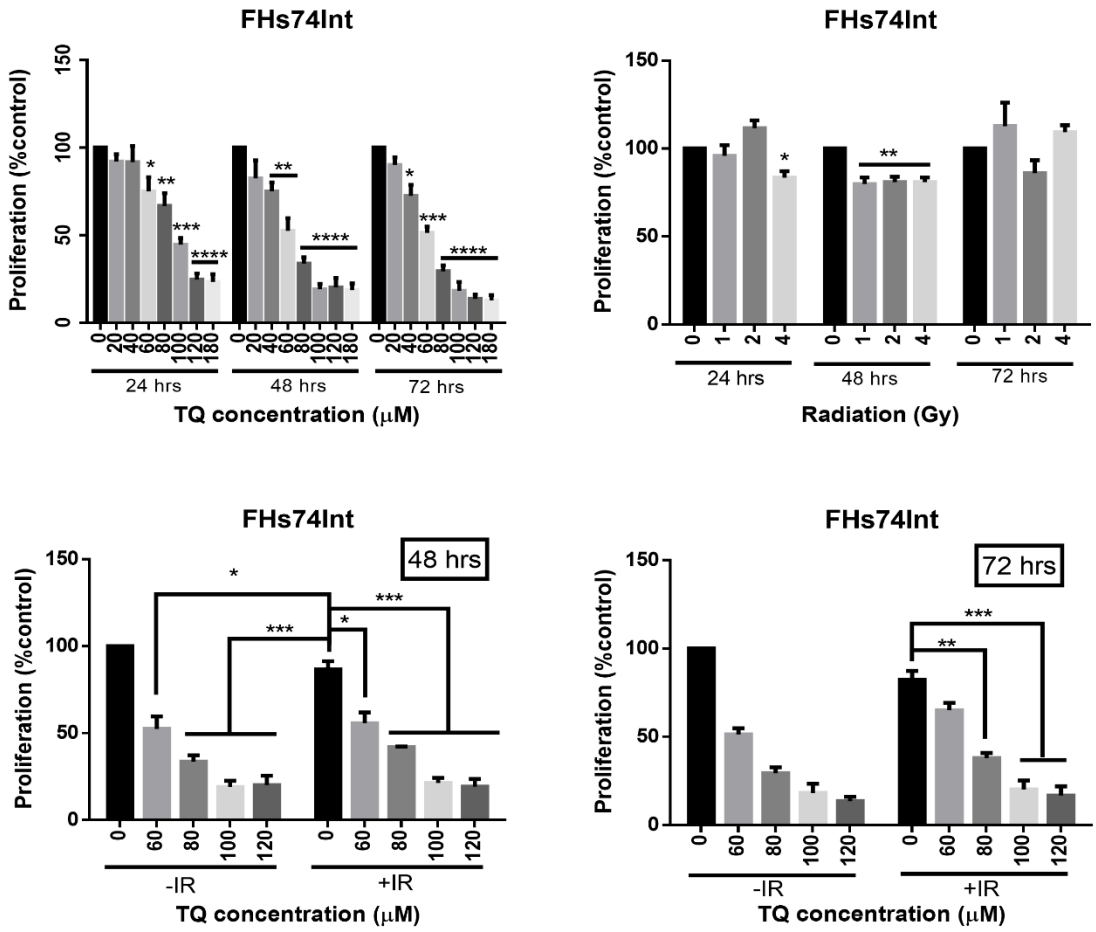

Figure 12. TQ and IR combination is non-toxic to non-tumorigenic intestinal cells. FHs74Int cells were untreated or were incubated with TQ alone, IR alone (2 Gy), or combinations for 24, 48, or 72 hrs. Cell proliferation was determined using MTT assay. Results are expressed as percentage of the studied group as compared to its control. Data represent an average of three independent experiments. The data are reported as mean ± SEM (* P<0.05; **P<0.01; ***P<0.001, **** P<0.0001).

B. Effect of TQ and radiation on colorectal cancer cell viability

We then studied the effect of TQ, IR (2 Gy), and combinations on the viability of CRC and non-tumorigenic cells using Trypan blue exclusion assay (Figures 13 & 14). While treatment of CRC cells with 10 μM TQ alone did not inhibit cell viability at 48 and 72 hrs, combining the same doses of TQ and IR significantly inhibited cell viability when compared to TQ alone (Figure 13). Combining 10 μM TQ with 2 Gy IR led to a 30%,

31%, 26%, and 21% inhibition of HCT116, HCT116 p53 null, HT29, and DLD1 cell viability at 48 hrs, respectively. A combination of TQ (30 µM or 60 µM) and 2 Gy IR led to a significant reduction in the viability of all CRC cells at 48 hrs, when compared to IR alone (Figure 13). In HT29 cells, combining 60 µM TQ and IR caused a significant ~60% reduction in cell viability compared to either treatment alone (Figure 13C). In FHs74Int cells, TQ alone was non-toxic at doses up to 60 µM at 48 hrs and 72 hrs, and IR alone reduced the viability of these cells at 48 hrs (Figure 14). The effect of TQ and IR combination was comparable to the individual treatments at both time points.

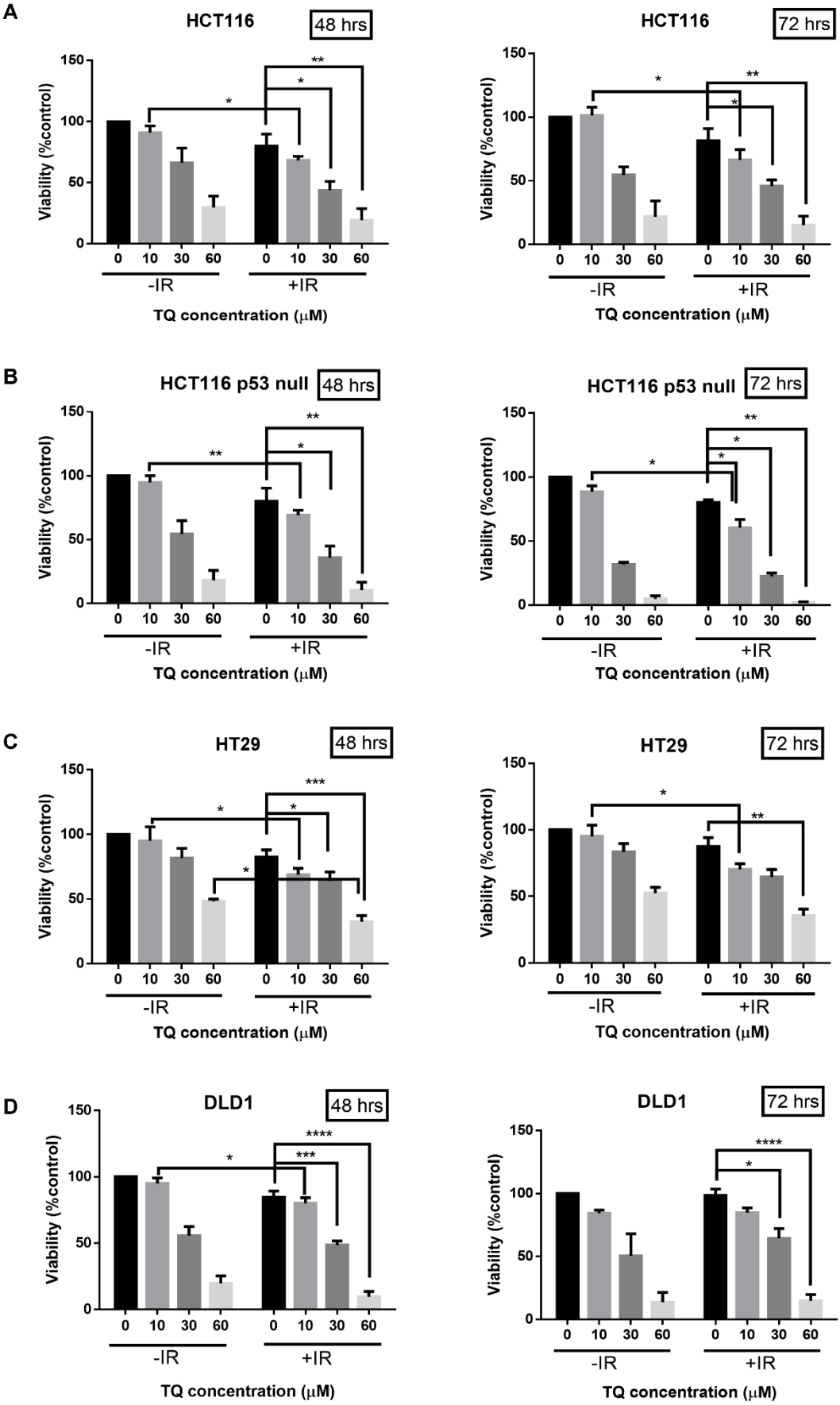
A
HCT116
48 hrs
HCT116
72 hrs
B
HCT116 p53 null
48 hrs
HCT116 p53 null
72 hrs
C
HT29
48 hrs
HT29
72 hrs
D
DLD1
48 hrs
DLD1
72 hrs
Viability (%control)
150
100
50
0
0 10 30 60 0 10 30 60
-IR
+IR
TQ concentration (μM)

Figure 13. TQ sensitizes colorectal cancer cells to IR that leads to reduction in their cell viability. HCT116 (A), HCT116 p53 null (B), HT29 (C), and DLD1 (D) colorectal cancer cells were either left untreated or were incubated with TQ alone, IR alone (2 Gy) or combinations for 24, 48, or 72 hrs. At the specific time point, cell viability was determined using trypan blue exclusion assay. Results are expressed as percentage of the studied group as compared to its control. Data represent an average of three independent experiments. The data are reported as mean ± SEM (* P<0.05; **P<0.01; ***P<0.001, **** P<0.0001).

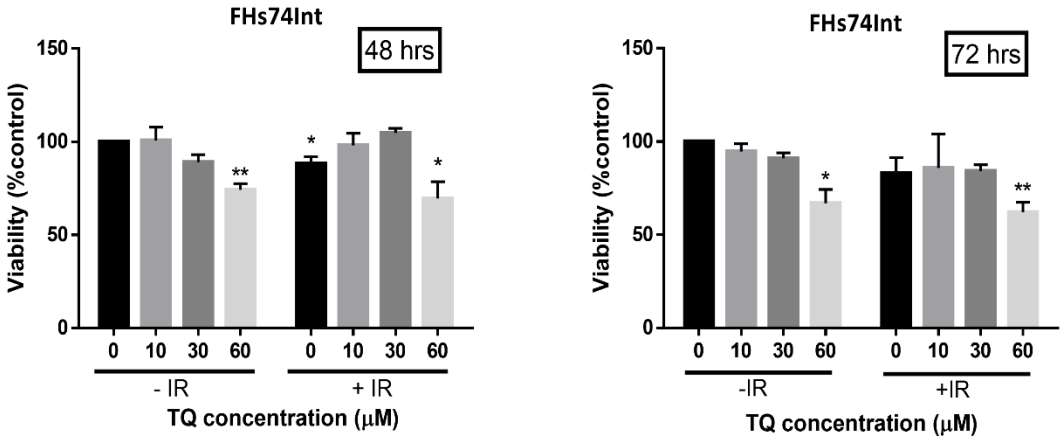

Figure 14. Effect of TQ and IR on non-tumorigenic intestinal cells viability. FHs74Int cells were either left untreated or were incubated with TQ alone, IR alone (2 Gy) or combinations for 24, 48, or 72 hrs. At the specific time point, cell viability was determined using trypan blue exclusion assay. Results are expressed as percentage of the studied group as compared to its control. Data represent an average of three independent experiments. The data are reported as mean ± SEM (* P<0.05; **P<0.01).

C. Effect of TQ and radiation on colony and sphere-forming ability of previously treated cells

1. 2D clonogenic survival assay

We next studied the effect of TQ and IR on colony formation ability (long-term survival) of CRC and non-tumorigenic FHs74Int cells using 2D clonogenic survival assay. Cells were treated with TQ alone, IR (2 Gy) alone, or combinations for 48 hrs, after which they were collected, seeded at low densities (2000-3500 cells), allowed to form colonies for 7–10 days, and stained with crystal violet. Combining low TQ concentration (10 μM) with 2 Gy IR had a more pronounced inhibitory effect, when

compared to TQ alone in all CRC cell lines (Figure 15). In DLD1 cells, 10 µM TQ and IR led to a significant inhibition when compared to TQ or IR alone (Figure 15D). Combining 30 µM and IR resulted in more than 64% reduction in long-term survival of HCT116 (Figure 15A) and HCT116 p53 null (Figure 15B), when compared to TQ alone. Combining 60 µM TQ and IR led to 77% and 69% reduction in HCT116 (Figure 15A) and HT29 (Figure 15C) colony formation, respectively, an inhibition that was greater than the effect of either treatment alone. The combination of TQ and IR inhibited HT29 long-term survival by 54.85%, 69%, and 72.56% at 10 µM, 60 µM, and 120 µM TQ, respectively (Figure 15C). Similar to MTT and Trypan results, clonogenic survival assay showed an inhibitory effect on the survival of non-tumorigenic FHs74Int cells at high TQ concentration (60µM) (Figure 16). IR alone inhibited the long-term survival of these cells, and this inhibition was comparable to combination treatment. Interestingly, combining low (10 µM) or high (60 µM) TQ dose and IR did not increase cytotoxicity in comparison to individual treatments.

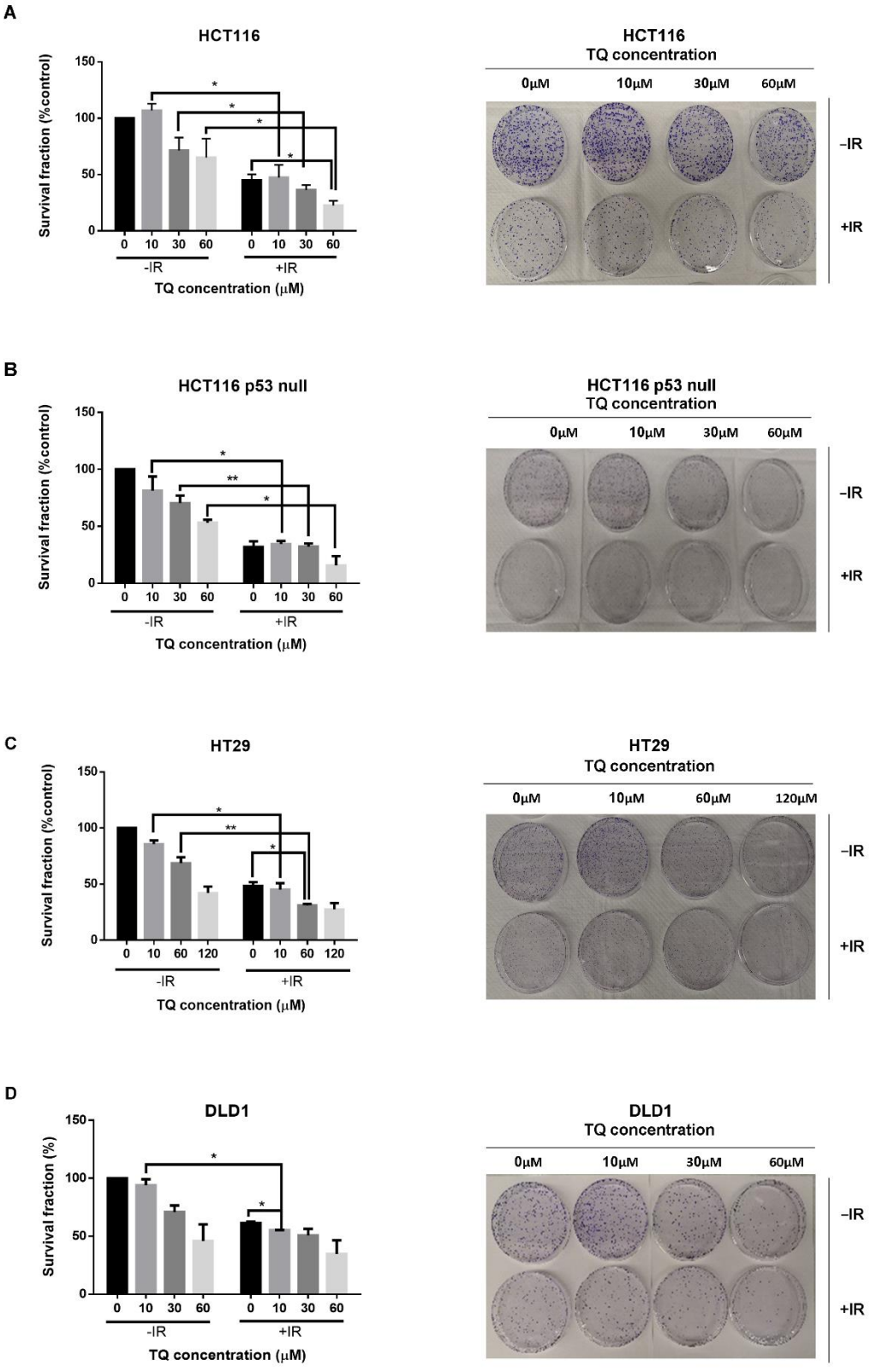

Figure 15. TQ sensitizes colorectal cancer cells to IR that leads to reduction in their colony forming ability. (A-D) Colony formation assay was used to determine the effect

of TQ and IR on the long-term survival of HCT116 (A), HCT116 p53 null (B), HT29 (C), and DLD1 (D) colorectal cancer cells. Cells were treated with TQ, IR, or combinations, after which they were collected and seeded in treatment-free media at low density (2000-3500 cells). After 7-10 days, the resulting colonies were fixed, stained with 0.5% crystal violet and counted. Representative images of colonies are shown. Results are expressed as percentage of the studied group as compared to its control. Data represent an average of three independent experiments. The data are reported as mean ± SEM (* P<0.05; **P<0.01).

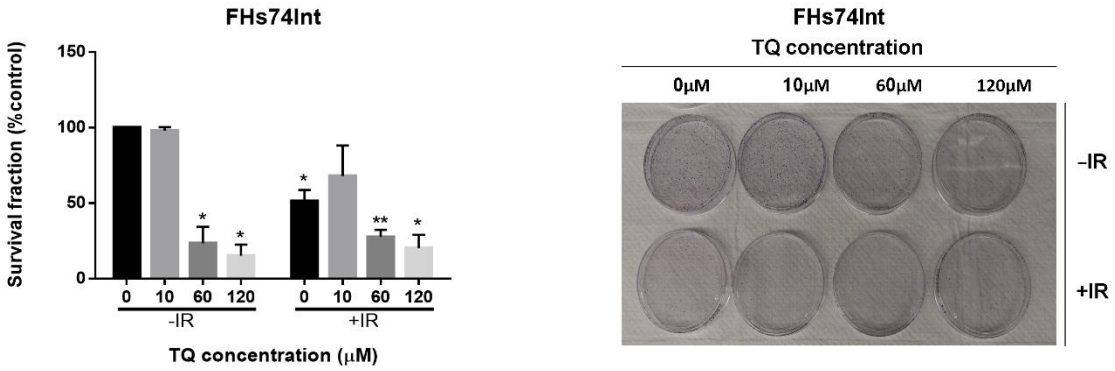

Figure 16. Effect of TQ and IR on colony forming ability of non-tumorigenic intestinal cells. Colony formation assay was used to determine effect of TQ and IR on the long-term survival of non-tumorigenic FHs74Int cells. Cells were treated with TQ, IR, or combinations, after which they were collected and seeded in treatment-free media at low density (2000-3500 cells). After 7-10 days, the resulting colonies were fixed, stained with 0.5% crystal violet, and counted. Representative images of colonies are shown. Results are expressed as percentage of the studied group as compared to its control. Data represent an average of three independent experiments. The data are reported as mean ± SEM (* P<0.05; ** P<0.01).

2. 3D clonogenic survival assay

For the 3D clonogenic survival assay, cells were treated with TQ, IR, or combinations for 48 hrs, as described above. At the specific timepoint, cells were collected and resuspended in serum-free media, after which cells were counted and mixed with Matrigel, and plated at low density around the rim of each well. Treatment-free media (+5% FBS) was added and cells were incubated for 8-12 days without treatment. Spheres were counted and images were obtained to determine effect of TQ and IR on SFU (Figure 17). The combination of 10 μM or 30 μM TQ and 2 Gy IR led to more than

3-fold decrease HCT116 sphere formation, and this decrease was significant when compared to either treatment alone (Figure 17A). In HCT116 p53 null cells, 30 µM TQ and 2 Gy IR combination resulted in significant decrease by 5.28-fold and was more significant than that of TQ alone (Figure 17B). Interestingly, HT29 SFU decreased by ~3-fold in response to 10 µM TQ and IR, and this reduction was greater than that of TQ alone (Figure 17C). Combining 60 µM TQ and IR inhibited the sphere formation ability of HT29 cells by a remarkable ~9-fold, and this inhibition was greater than that of TQ or IR alone. In DLD1 cells, treatment with 10 µM TQ and IR reduced SFU by 4.1-fold (Figure 17D). Interestingly, this decrease was significant when compared to either treatment alone. Moreover, combination of 30 µM TQ and IR combination led to a similar inhibition to 10 µM TQ and IR combination in these cells.

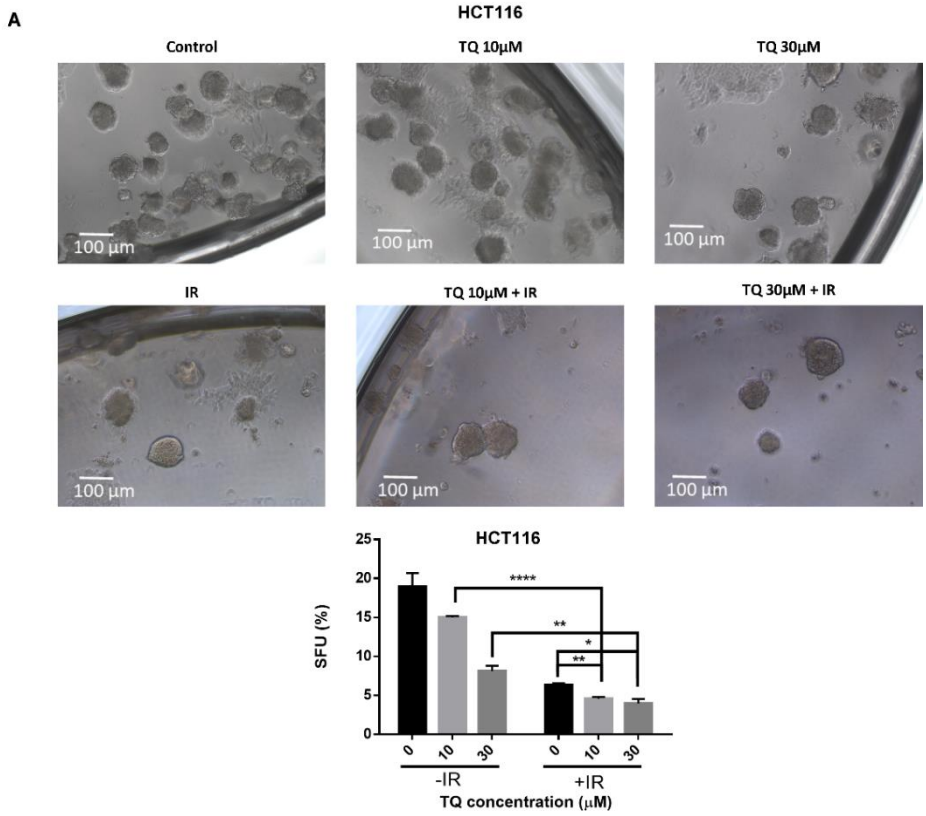
A
HCT116
Control
TQ 10μM
TQ 30μM
IR
TQ 10μM + IR
TQ 30μM + IR
100 μm
HCT116
SFU (%)
25
20
15
10
5
0
****
**
*
**
0
10
30
0
10
30
-IR
+IR
TQ concentration (μM)

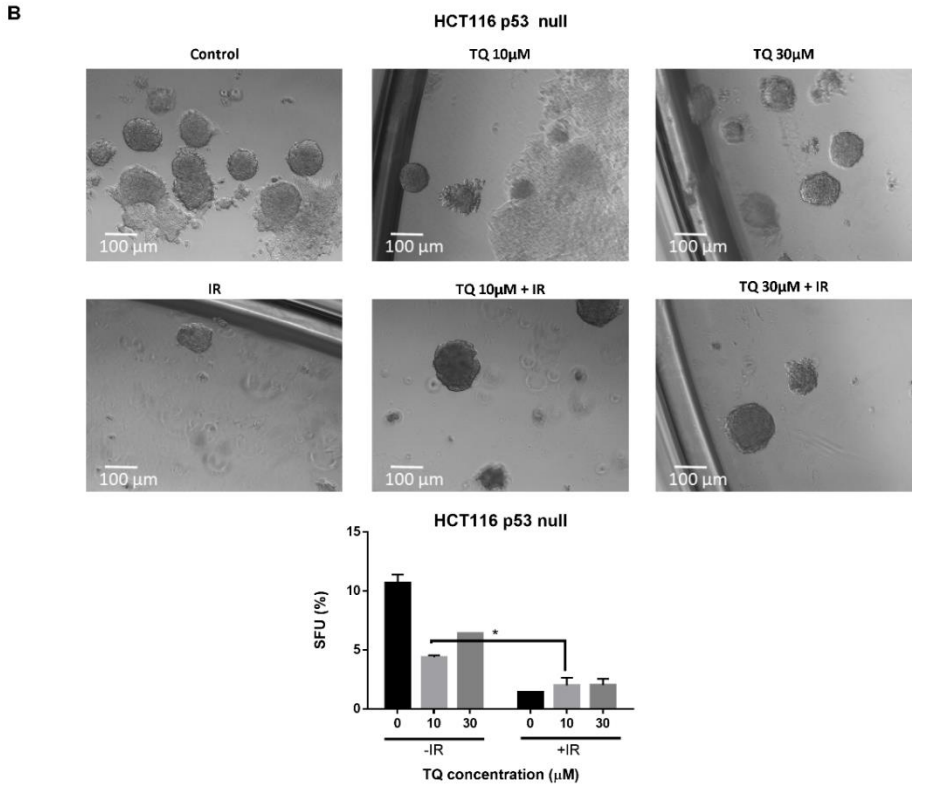
B
HCT116 p53 null
Control
TQ 10μM
TQ 30μM
IR
TQ 10μM + IR
TQ 30μM + IR
100 μm
HCT116 p53 null
SFU (%)
15
10
5
0
*
0
10
30
0
10
30
-IR
+IR
TQ concentration (μM)

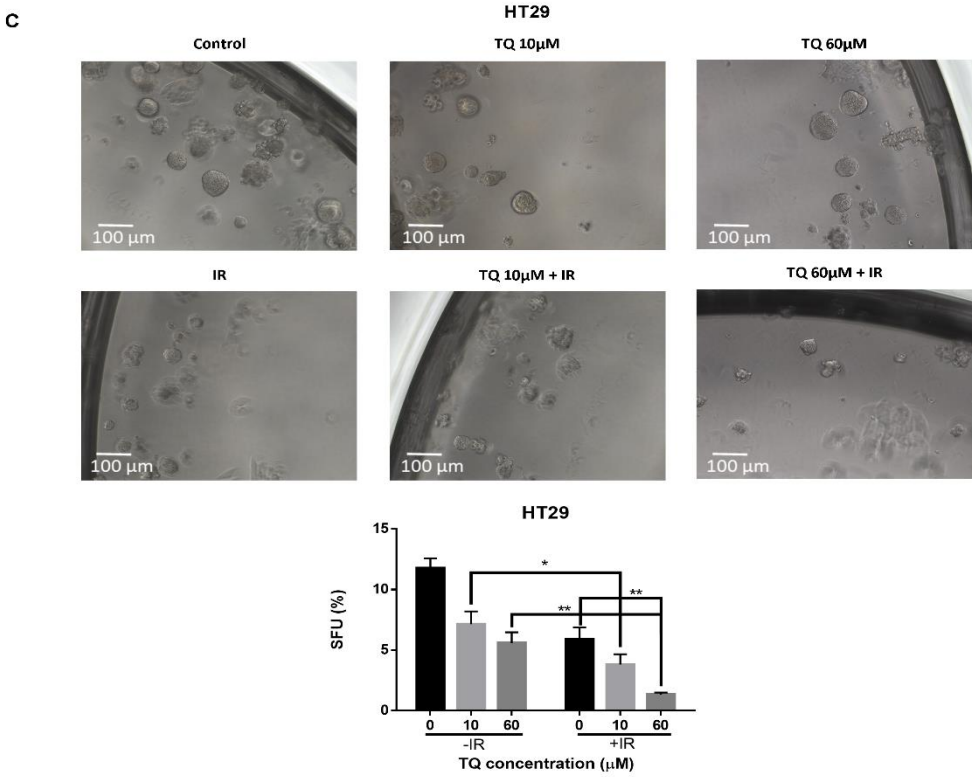
C
HT29
Control
TQ 10μM
TQ 60μM
IR
TQ 10μM + IR
TQ 60μM + IR
100 μm
HT29
SFU (%)
TQ concentration (μM)
-IR
+IR

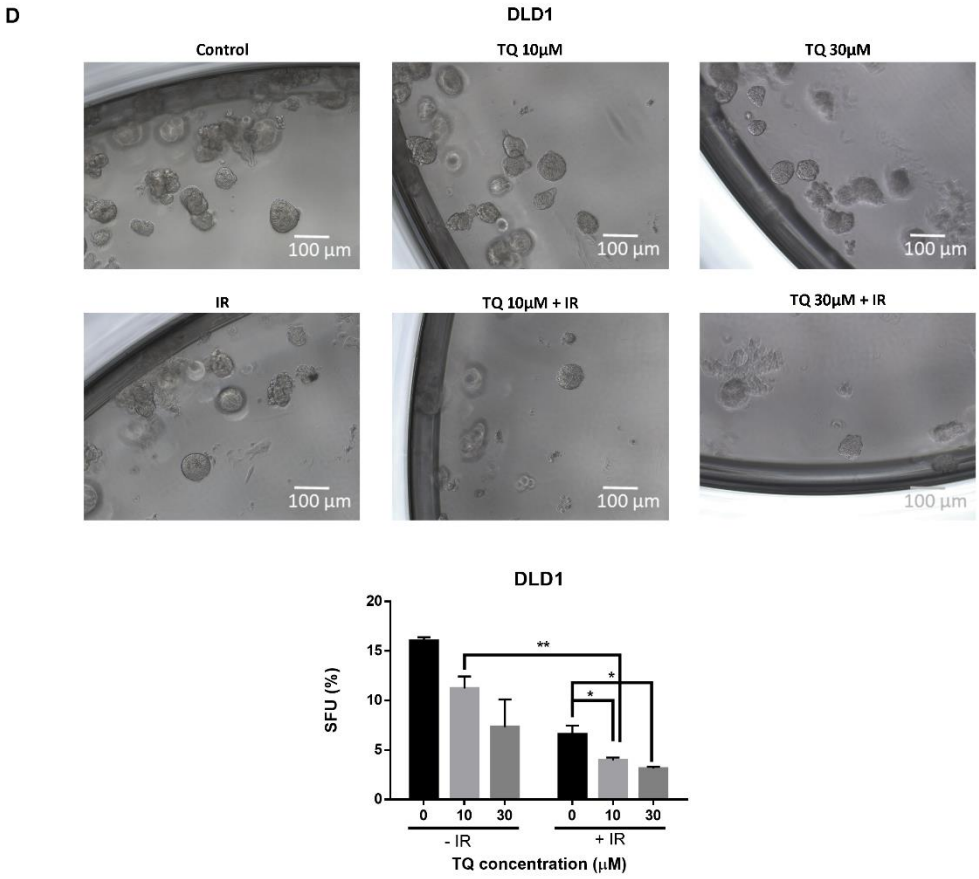
D
DLD1
Control
TQ 10μM
TQ 30μM
IR
TQ 10μM + IR
TQ 30μM + IR
100 μm
DLD1
SFU (%)
TQ concentration (μM)
- IR
+ IR

Figure 17. Inhibition of sphere-forming ability of spheres derived from colorectal cancer cells previously treated with TQ and IR. Sphere formation assay was used to determine the inhibitory effect on spheres derived from HCT116 (A), HCT116 p53 null (B), HT29 (C), and DLD1 (D) cells previously treated with TQ alone, IR (2 Gy) alone, or combinations for 48 hrs. At the specific time point, cells were collected and re-suspended in serum free media. Cells were then counted, mixed with growth factor-reduced Matrigel™ (1:1), and allowed to grow in media with 5% FBS without treatment. Sphere counts were performed at day 10-12 of culture. The sphere-forming unit (SFU) was calculated as the ratio of the number of spheres formed/ number of cells originally seeded x100. Data represent an average of three independent experiments and are reported as mean ± SEM (* P< 0.05; **P < 0.01; ***P< 0.001, **** P<0.0001). Representative bright-field images of spheres are shown next to the respective graph. Images were visualized by Axiovert inverted microscope at 10X magnification and analyzed by Carl Zeiss Zen 2012 image software. Scale bar 100 µm.

In FHs74Int cells, radiation alone reduced the sphere counts and combining TQ with IR had comparable effect to IR and TQ (60 µM) alone (Figure 18).

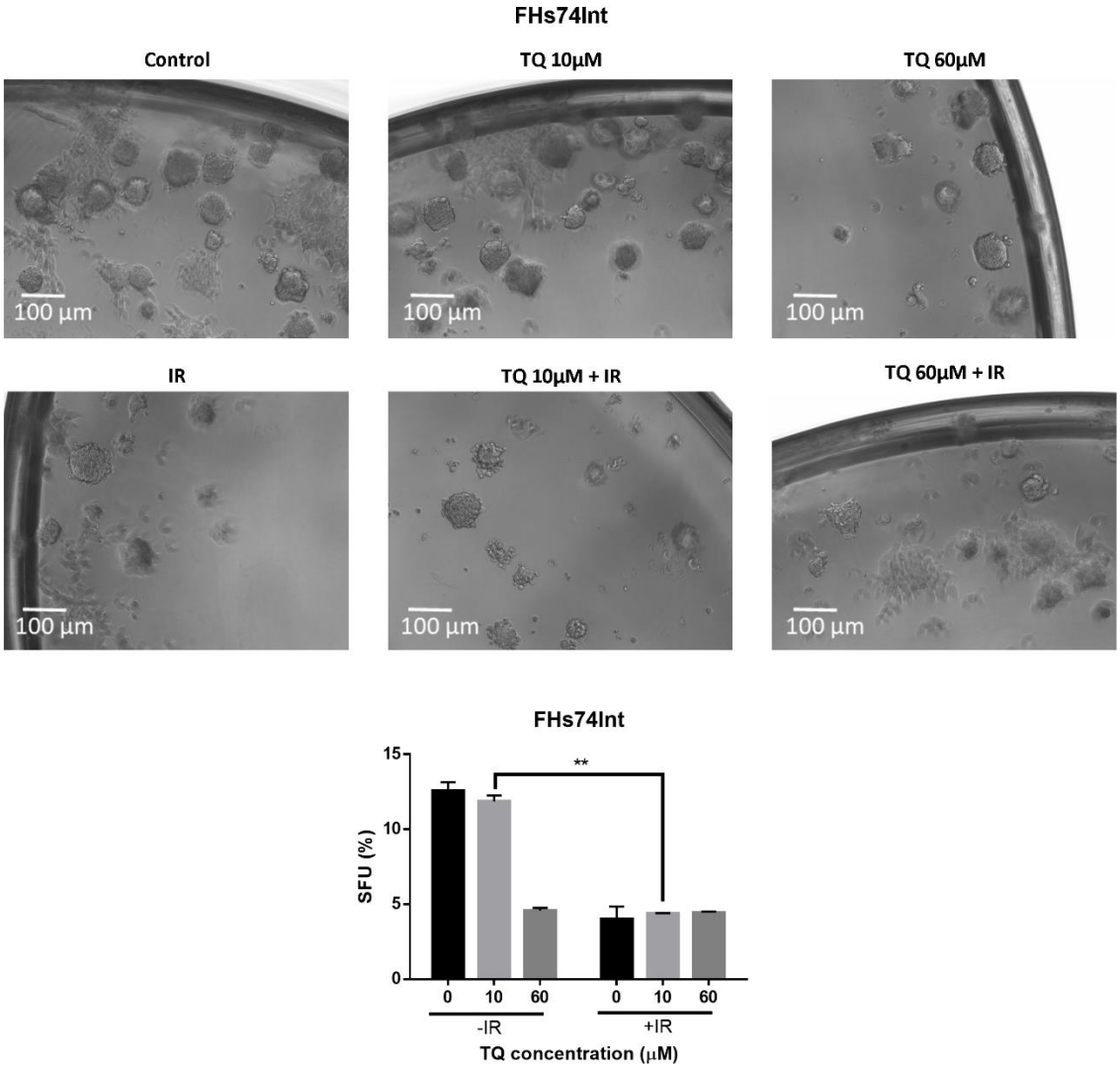

Figure 18. Sphere-forming ability of spheres derived from non-tumorigenic intestinal cells previously treated with TQ and IR. Sphere formation assay was used to determine the inhibitory effect on spheres derived from FHs74Int cells previously treated with TQ alone, IR (2 Gy) alone, or combinations for 48 hrs. At the specific time point, cells were collected and re-suspended in serum free media. Cells were then counted, mixed with growth factor-reduced Matrigel™ (1:1), and allowed to grow in media with 5%FBS without treatment. Sphere counts were performed at day 10-12 of culture. SFU was calculated as the ratio of the number of spheres formed/ number of cells originally seeded x100. Data represent an average of three independent experiments and are reported as mean ± SEM (**P < 0.01). Representative bright-field images of FHs74Int spheres are shown next to the respective graph. Images were visualized by Axiovert inverted microscope at 10X magnification and analyzed by Carl Zeiss Zen 2012 image software. Scale bar 100 µm.

D. Effect of TQ on IR-induced cell migration

We next evaluated the migration ability of HCT116 and HT29 cells in response to TQ and IR using wound healing assay (Figure 19). In HCT116, wound closure was slower in cells treated with a combination of 30 µM TQ and 2 Gy radiation, in comparison to cells treated with IR alone (wound width normalized to control: 82.20 vs. 63.44) (Figure 19A). Wound width in combination-treated cells was comparable to TQ-treated cells. Wound width in IR-treated HT29 cells decreased by 40% (Figure 19B). In contrast, wound width decreased by less than 4% in HT29 cells treated with TQ 60 µM and IR at 48 and 72 hrs, and this decrease was significant when compared to IR alone (Figure 19B).

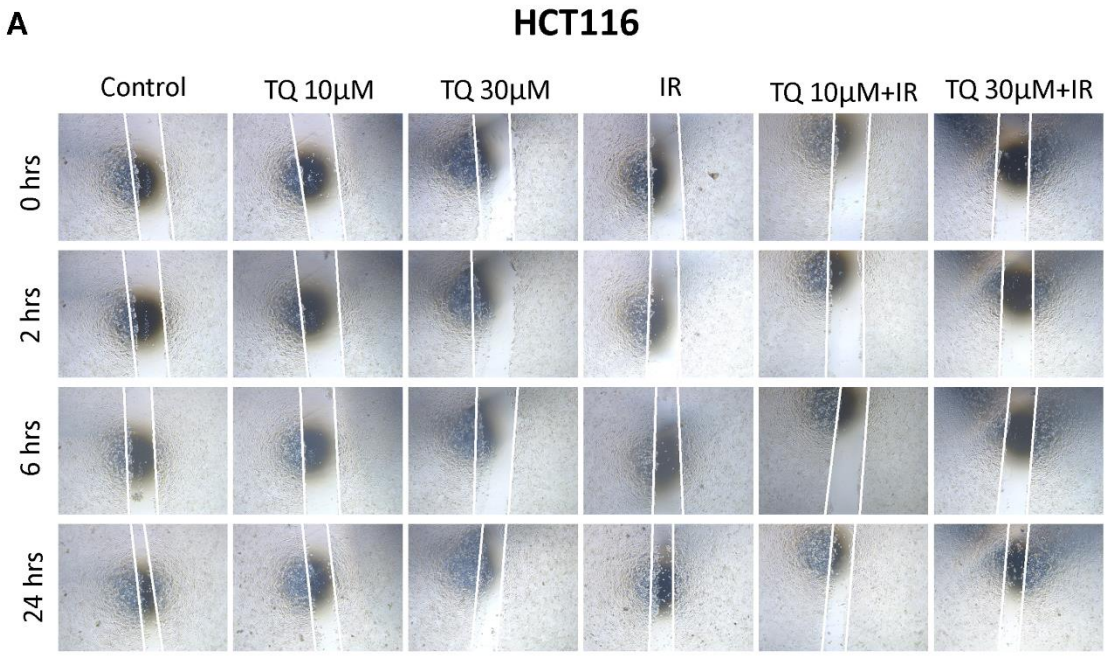

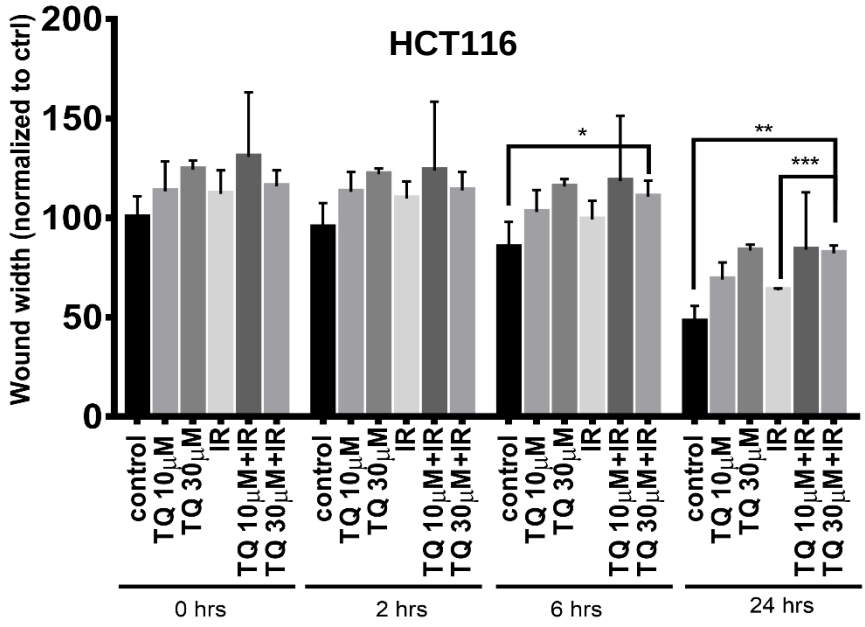
HCT116
Wound width (normalized to ctrl)
200
150
100
50
0
control
TQ 10μM
TQ 30μM
IR
TQ 10μM+IR
TQ 30μM+IR
0 hrs
2 hrs
6 hrs
24 hrs
*
**
***

B

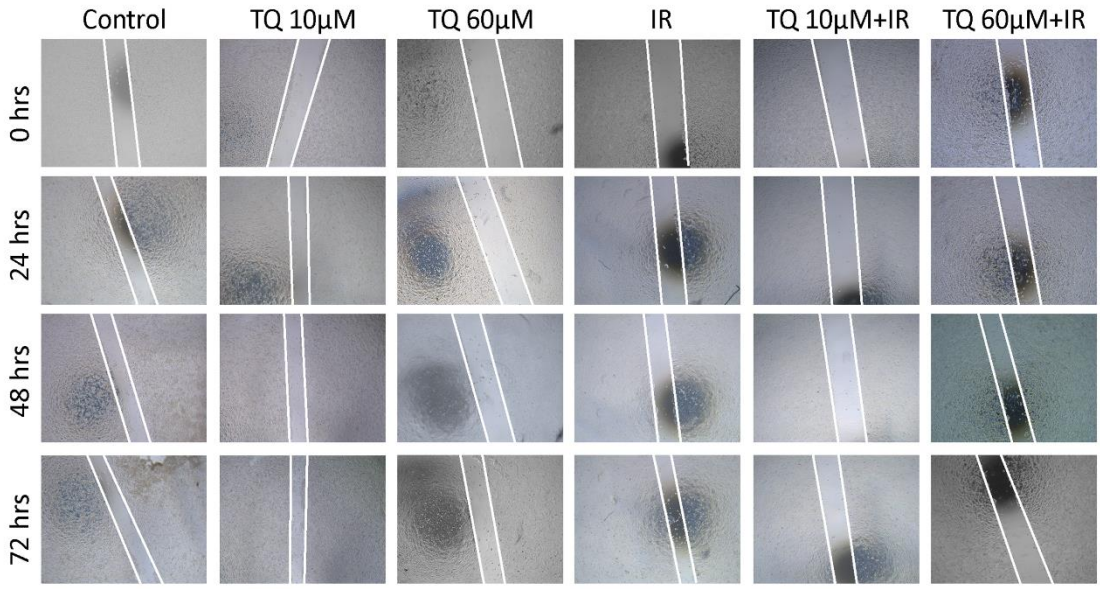
HT29
Control
TQ 10μM
TQ 60μM
IR
TQ 10μM+IR
TQ 60μM+IR
0 hrs
24 hrs
48 hrs
72 hrs

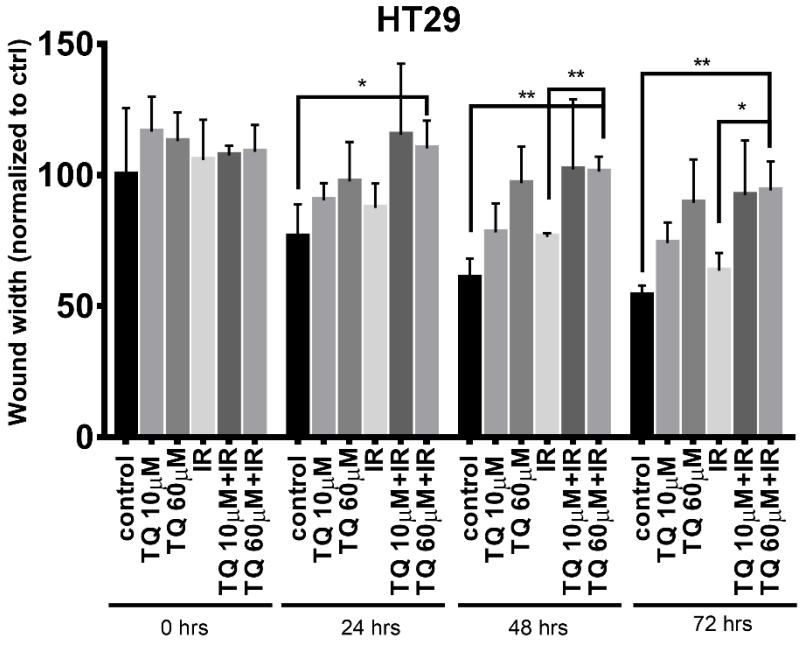

Figure 19. TQ inhibits IR-induced migration of colorectal cancer cells. Cell migration ability was tested using wound healing assay. HCT116 (A) and HT29 (B) cells were either treated or not with TQ, IR, or TQ+IR. For HCT116, wound width was measured at 0, 2, 6, and 24 hrs following treatment. For HT29 cells, wound width was measured at 0, 24, 48, and 72 hrs following treatment. The percentage of the wound width was calculated as follows: (wound width at specific time point)/(control wound width at 0 h) × 100. Data represent an average of three independent experiments. The data are reported as mean ± SEM (* $P < 0.05$; ** $P < 0.01$; *** $P < 0.001$).

E. Effect of TQ and radiation on cell cycle distribution in colorectal cancer cells

We then determined the effects of individual and combination treatments on HCT116 and HT29 cell cycle distribution using flow cytometry with PI staining of DNA (Figure 20). While IR (2 Gy) alone induced a slight increase in the percentage of HCT116 cells in G2/M phase, combining IR with TQ (10 μM and 30 μM) induced a significant increase in G2/M cell population by more than 1.5-fold (Figure 20A). Moreover, the 13% decrease in percentage of cells at G0/G1 was significant in HCT116 cells treated with 30 μM TQ and IR. In HT29, G2/M cell cycle arrest was observed in irradiated cells and in cells treated with high concentrations of TQ and was more pronounced in cells treated with combinations compared to either treatment alone (Figure 20B). Interestingly,

combining TQ and IR induced a significant increase in the G2/M population from 21% in the control to 26% and 31% at TQ concentrations of 10 µM and 60 µM, respectively.

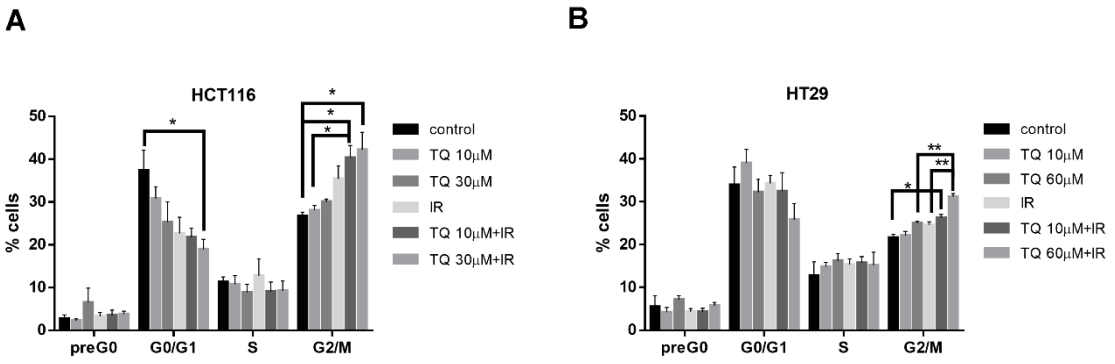

Figure 20. TQ enhances IR-induced cell cycle arrest at G2/M phase in colorectal cancer cells. Cell cycle was evaluated by flow cytometry using DNA staining of HCT116 (A) and HT29 (B) cells after each treatment (control, TQ, IR, and combinations) at 48 hrs. Data represent an average of three independent experiments and are reported as mean ± SEM (* $P < 0.05$; ** $P < 0.01$; *** $P<0.001$).

F. Effect of TQ and radiation on DNA repair in colorectal cancer cells

To elucidate the mechanism underlying the observed G2/M arrest in response to TQ and IR, we analyzed the dynamics of the DNA damage and repair maker, γH2AX and the kinases responsible for its phosphorylation during DDR, mainly ATM and ATR (Figure 21). ATM and ATR are also involved in the regulation of G2/M checkpoint. To check whether G2/M arrest is ATM- or ATR-dependent, we analyzed the dynamics of these kinases over a 48 hrs period in HCT116 and HT29 cells (Figure 21). Cells were treated with TQ for 24 hrs followed by irradiation at 2 Gy. Cells were then fixed at 0 mins, 10 mins, and 24 hrs post irradiation, followed by permeabilization and staining for p-ATM, p-ATR, and γ-H2AX. We observed similar activation of the kinases in both cell lines. Interestingly, combining 30 µM TQ and IR in HCT116 cells led to a significant 1.25-fold increase in p-ATM, 10 mins after irradiation (Figure 21A). At 24 hrs, the levels

of p-ATM were high in combination-treated HCT116 cells but were not significant when compared to the control. p-ATR was upregulated by more than 1.37-fold 10 mins post irradiation in HCT116 cells treated with IR alone or combination, and this increase was persistent and more pronounced at 24 hrs, especially in cells treated with combination of 30 µM TQ and IR (Table 3). In HT29 cells, the increase in p-ATM and p-ATR 10 mins post irradiation was insignificant compared to the control (Figure 21B). On the other hand, when cells were treated with either 10 µM or 60 µM TQ prior to irradiation, the levels of both kinases significantly increased by more than 1.7-fold 10 mins after irradiation (Figure 21B, Table 4). Importantly, at 24 hrs the levels of p-ATM in combination-treated cells were comparable to control cells. On the other hand, the level of p-ATR remained significantly high (1.57-fold greater than control cells) in cells treated with 60 µM TQ and IR.

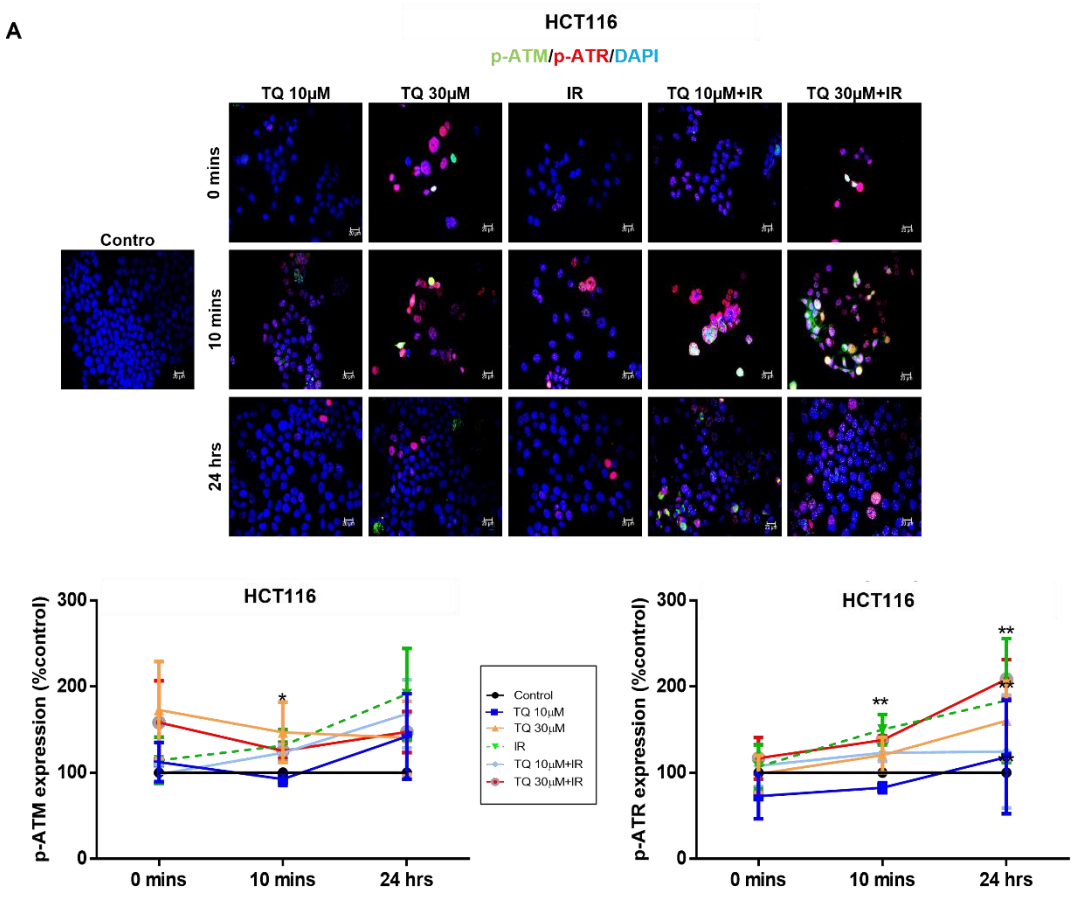
A
HCT116
p-ATM/p-ATR/DAPI
TQ 10μM
TQ 30μM
IR
TQ 10μM+IR
TQ 30μM+IR
0 mins
10 mins
24 hrs
Contro
HCT116
p-ATM expression (%control)
300
200
100
0
0 mins
10 mins
24 hrs
*
Control
TQ 10μM
TQ 30μM
IR
TQ 10μM+IR
TQ 30μM+IR
HCT116
p-ATR expression (%control)
300
200
100
0
0 mins
10 mins
24 hrs
**
**
**

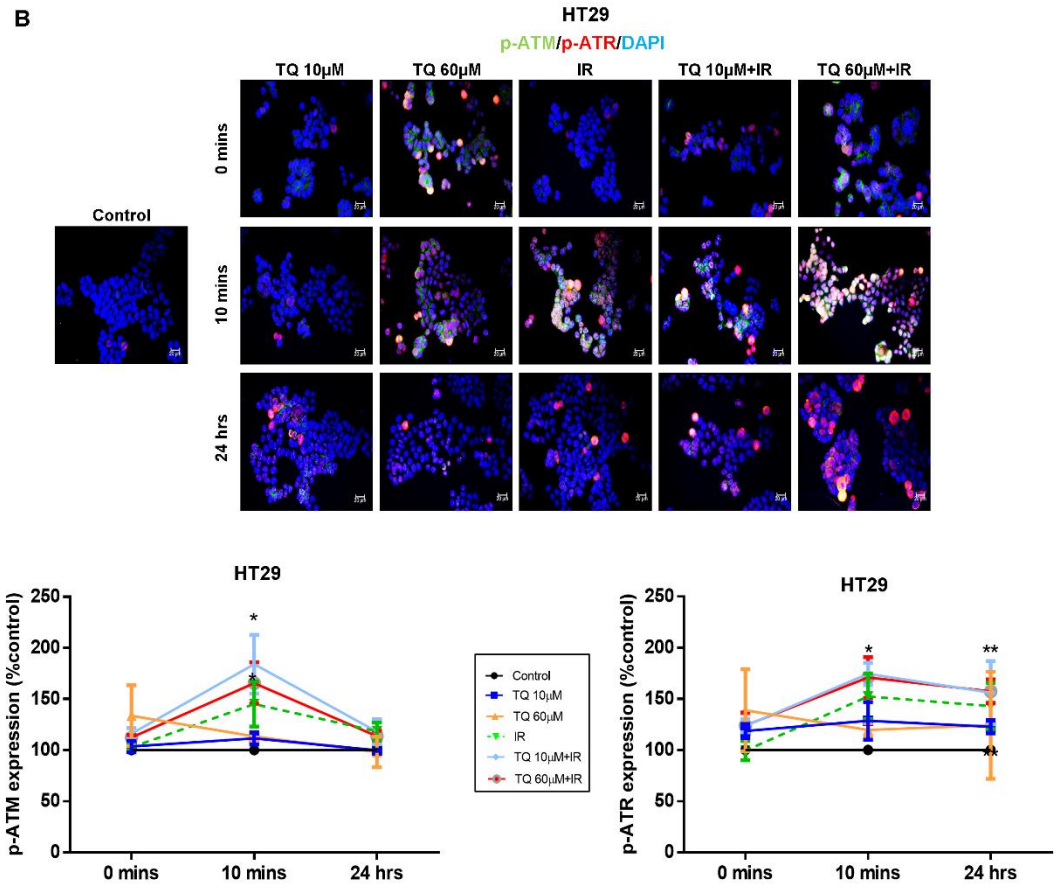

Figure 21. TQ radiosensitization of colorectal cancer cells is associated with upregulation of p-ATM and p-ATR expression in colorectal cancer cells. HCT116 (A) and HT29 (B) cells were either left untreated or incubated with TQ for 24 hrs followed by irradiation at 2 Gy. Cells were then fixed at 0 mins, 10 mins and 24 hrs post irradiation, followed by permeabilization and staining for p-ATR and p-ATM. Quantification and representative images are shown. Quantification of immunofluorescence intensity was performed using Carl Zeiss Zen 2012 image software. Data represent an average of three independent experiments and are reported as mean ± SEM (* P<0.05; ** P<0.01 significantly different from control). Scale bar for immunofluorescent images is 20 μm.

Table 3: Significance between different groups stained for p-ATM, p-ATR, and γ H2AX in HCT116 cells irradiated for 0 mins, 10 mins, or 24 hrs

HCT116		
Group	**Significance**	**Group**
	p-ATM	
10 mins	Control vs. TQ 30μM+IR	*p<0.05
	p-ATR	
10 mins	Control vs. TQ 10μM	*p<0.05
	Control vs. IR	* p<0.05
	Control vs. TQ30μM+IR	**p<0.01
24 hrs	Control vs. TQ30μM+IR	**p<0.01
	γH2AX	
0 mins	Control vs. TQ 10μM	*p<0.05
	Control vs. TQ 30μM	**p<0.01
	Control vs. TQ 10μM+IR	**p<0.01
	Control vs. TQ 30μM+IR	*p<0.05
	IR vs. TQ 10μM+IR	**p<0.01
	IR vs. TQ 30μM+IR	*p<0.05
10 mins	Control vs. TQ 10μM	*p<0.05
	Control vs. TQ 30μM	*p<0.05
	Control vs. IR	*p<0.05
	Control vs. TQ 10μM+IR	*p<0.05
	Control vs. TQ 30μM+IR	**p<0.01
	TQ 30μM vs. TQ 30μM+IR	*p<0.05
24 hrs	Control vs. IR	*p<0.05
	Control vs. TQ 10μM+IR	*p<0.05
	Control vs. TQ 30μM+IR	**p<0.01
	IR vs. TQ 30μM+IR	**p<0.01
	TQ 30μM vs. TQ 30μM+IR	*p<0.05

In HCT116 cells, γH2AX expression was upregulated in response to TQ alone (Figure 22A). γH2AX foci count in irradiated cells was comparable to cells treated with 10 or 30 μM TQ at 10 min after irradiation. The highest peak of γH2AX was observed at 10 mins in cells treated with 30 μM TQ and IR combination. Importantly, γH2AX expression remained significantly high (>2-fold increase) 24 hrs after radiation in cells treated with IR and TQ (10 μM or 30 μM) (Figure 22A). Importantly, the increase in the

levels of γH2AX in cells treated with 30 µM TQ and IR was significant when compared to TQ alone, 10 mins and 24 hrs post irradiation. In HT29 cells, a similar increase of γH2AX expression was observed (Figure 22B). TQ concentration as low as 10 µM TQ was sufficient to sensitize these cells to radiation and induce a ~12-fold and 6-fold increase in γ-H2AX counts at 10 mins and 24 hrs post IR, respectively. Combining 60 µM TQ and IR caused a more pronounced upregulation (~7-fold) of γH2AX expression than TQ or IR alone at 24 hrs (Figure 22B).

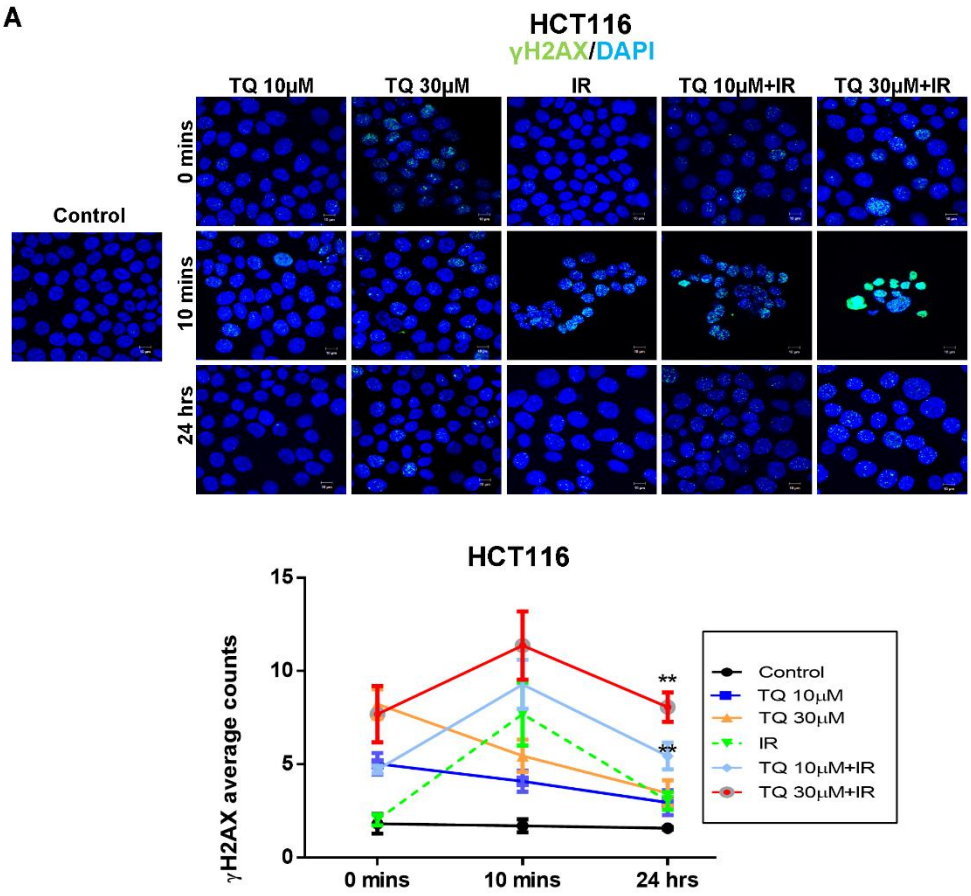

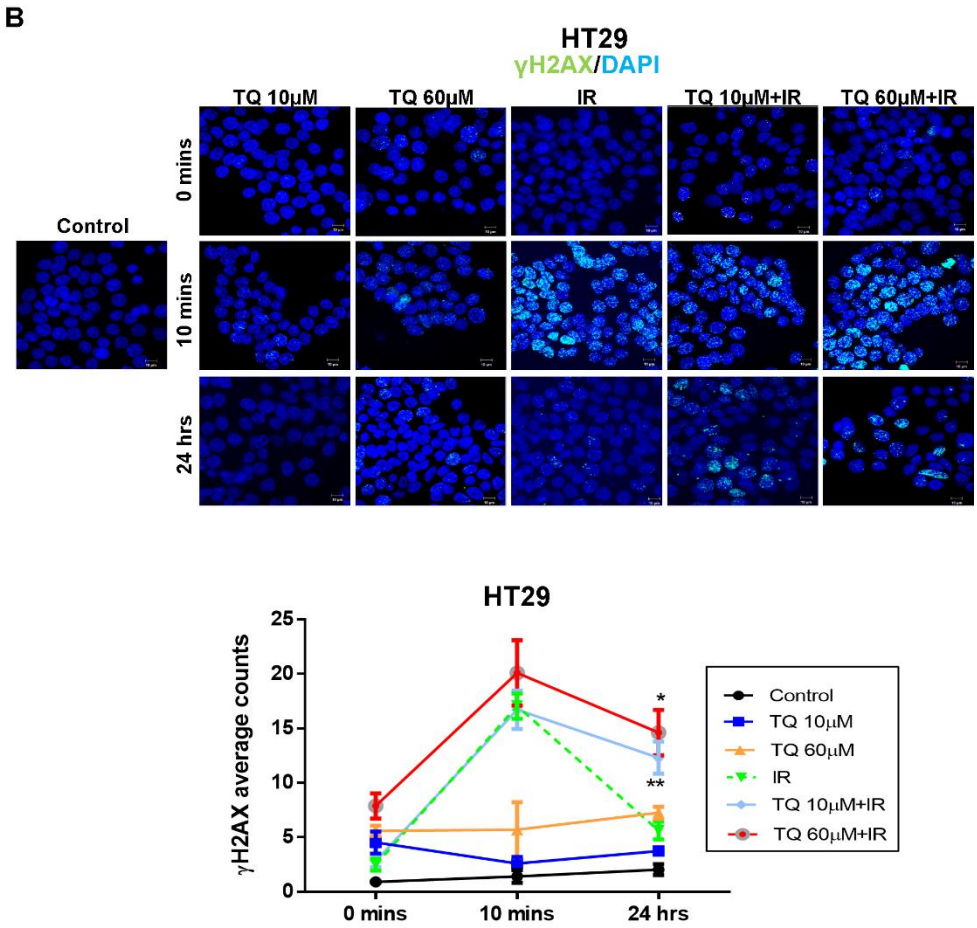

Figure 22. TQ radiosensitization of colorectal cancer cells is associated with an increase in γH2AX expression in colorectal cancer cells. HCT116 (A) and HT29 (B) cells were either left untreated or incubated with TQ for 24 hrs followed by irradiation at 2 Gy. Cells were then fixed at 0 mins, 10 mins and 24 hrs post irradiation, followed by permeabilization and staining for γH2AX. γH2AX foci were counted. Data represent an average of three independent experiments and are reported as mean ± SEM (* $P<0.05$; ** $P<0.01$ significantly different from IR). Scale bar for immunofluorescent images is 20 μm.

Table 4: Significance between different groups stained for p-ATM, p-ATR, and γ H2AX in HT29 cells irradiated for 0 mins, 10 mins, or 24 hrs.

HT29		
Group	**Significance**	**Group**
	p-ATM	
0 mins	Control vs. TQ 10μM+IR	* p<0.05
	Control vs. TQ 60μM+IR	**p<0.01
10 mins	Control vs. TQ 60 μM	*p<0.05
	Control vs. TQ 10μM+IR	*p<0.05
	Control vs. TQ 60μM+IR	*p<0.05
	p-ATR	
0 mins	Control vs. TQ 10μM	*p<0.05
	Control vs. TQ 10μM+IR	*p<0.05
10 mins	Control vs. TQ 60 μM	*p<0.05
	Control vs. TQ 10μM+IR	**p<0.01
	Control vs. TQ 60μM+IR	*p<0.05
24 hrs	Control vs. TQ 10 μM	*p<0.05
	Control vs. TQ 60μM+IR	**p<0.01
	γH2AX	
0 mins	Control vs. TQ 10μM	*p<0.05
	Control vs. TQ 60μM	***p<0.001
	Control vs. TQ 10μM+IR	*p<0.05
	Control vs. TQ 60μM+IR	**p<0.01
	IR vs. TQ 30μM+IR	*p<0.05
10 mins	Control vs. IR	***p<0.001
	Control vs. TQ 10μM+IR	**p<0.01
	Control vs. TQ 60μM+IR	**p<0.01
	TQ 10μM vs. TQ 10μM+IR	**p<0.01
	TQ 60μM vs. TQ 60μM+IR	*p<0.05
24 hrs	Control vs. TQ 60μM	**p<0.01
	Control vs. IR	*p<0.05
	Control vs. TQ 10μM+IR	**p<0.01
	Control vs. TQ 60μM+IR	**p<0.01
	IR vs. TQ 10μM+IR	*p<0.05
	IR vs. TQ 60μM+IR	*p<0.05
	TQ 10μM vs. TQ 10μM+IR	**p<0.01
	TQ 60μM vs. TQ 60μM+IR	*p<0.05

G. Effect of TQ and IR on oxidative stress

Reactive oxygen species (ROS) have been implicated in cellular proliferation and apoptosis [162]. As shown from cell cycle data, TQ in combination with IR was able to induce G2/M arrest, in parallel with DNA damage induction, in both HCT116 and

HT29 cells. Therefore, the ability of TQ to induce oxidative stress in the presence of radiation was tested using DHE as a fluorescent probe for ROS (Figure 23). In HCT116 cells, TQ or IR alone enhanced ROS production after 48 hrs treatment (Figure 23A). Importantly, when combined with IR, low (10µM) and relatively high (30µM) TQ concentrations were able to induce ROS accumulation by ~1.3 and 2-fold, respectively. A similar induction was also evident in cells treated TQ alone at 30µM. In HT29 cells, no significant ROS induction was shown in IR-treated cells, whereas ROS levels increased by ~46% in combination-treated cells, suggesting induction of oxidative stress by combination treatment (Figure 23B).

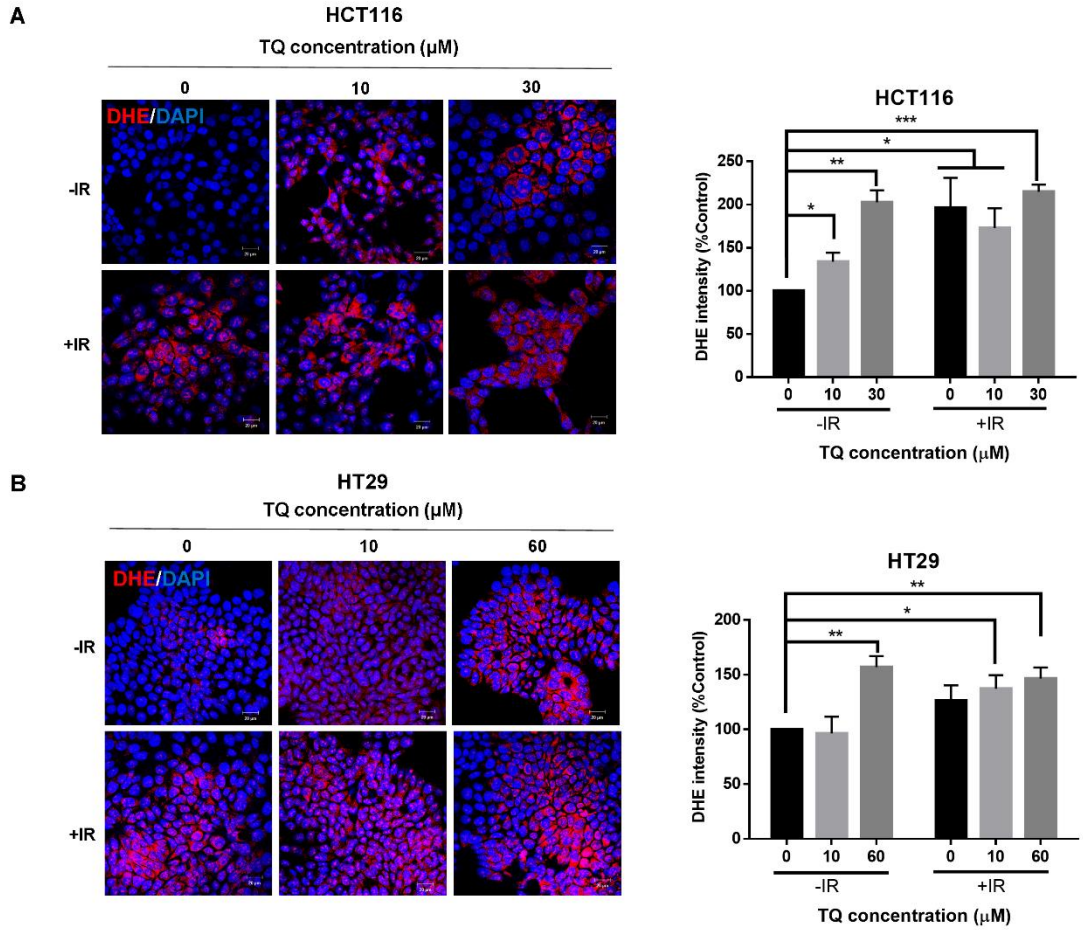

Figure 23. Effect of TQ and IR on oxidative stress in colorectal cancer cells. HCT116 (A) and HT29 (B) cells untreated and treated with TQ, IR, and combination of TQ and IR (TQ+IR) were immunofluorescently stained for ROS using DHE staining assay. Quantification and representative images are shown. Data represent an average of three independent experiments. The data are reported as mean ± SEM (* $P<0.05$; ** $P<0.01$; *** $P<0.001$). Scale bar is 20 µm.

H. Effect of TQ and radiation on pathways implicated in radioresistance

To determine the mechanism of TQ radiosensitization, we analyzed the expression of several molecules involved in survival and radioresistance (Figures 24-26). In HCT116, combination of 30 µM TQ and IR significantly reduced the expression of p-mTOR by 50%; however, this decrease in expression was comparable to TQ alone (Figure 24A). MEK was significantly reduced in combination-treated cells and the observed effect was comparable to individual treatments (Figure 25A). In HT29 cells, combining 10 µM TQ and IR resulted in a significant decrease in the expressions of p-mTOR (Figure 24B) and MEK (Figure 25B). Interestingly, a dose of 60 µM TQ was able to reverse p-mTOR induction by IR.

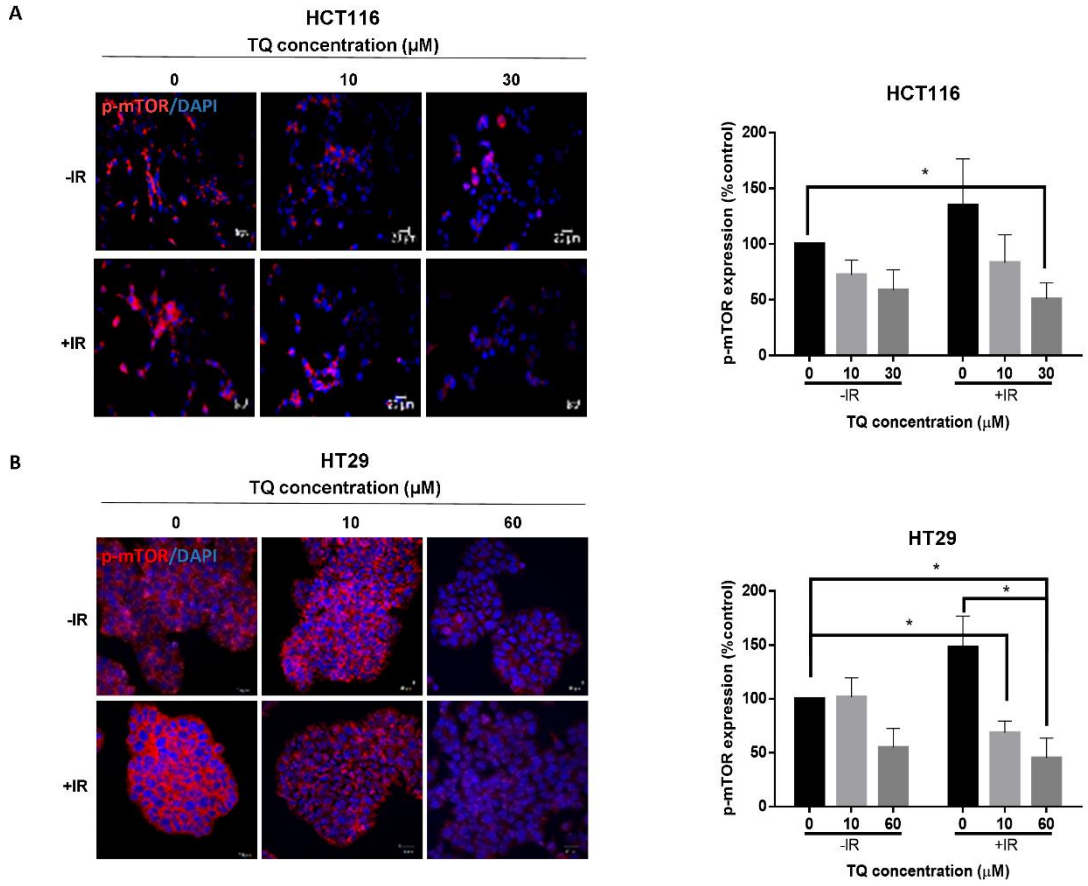

Figure 24. TQ and IR combination regulates p-mTOR expression in colorectal cancer cells. HCT116 (A) and HT29 (B) cells were treated or not with TQ alone, IR alone, or combinations (TQ+IR) and immunofluorescently stained for p-mTOR. Quantification and representative images are shown. Data represent an average of three independent experiments and are reported as mean ± SEM (* $P<0.05$). Scale bar for immunofluorescent images is 20 μm.

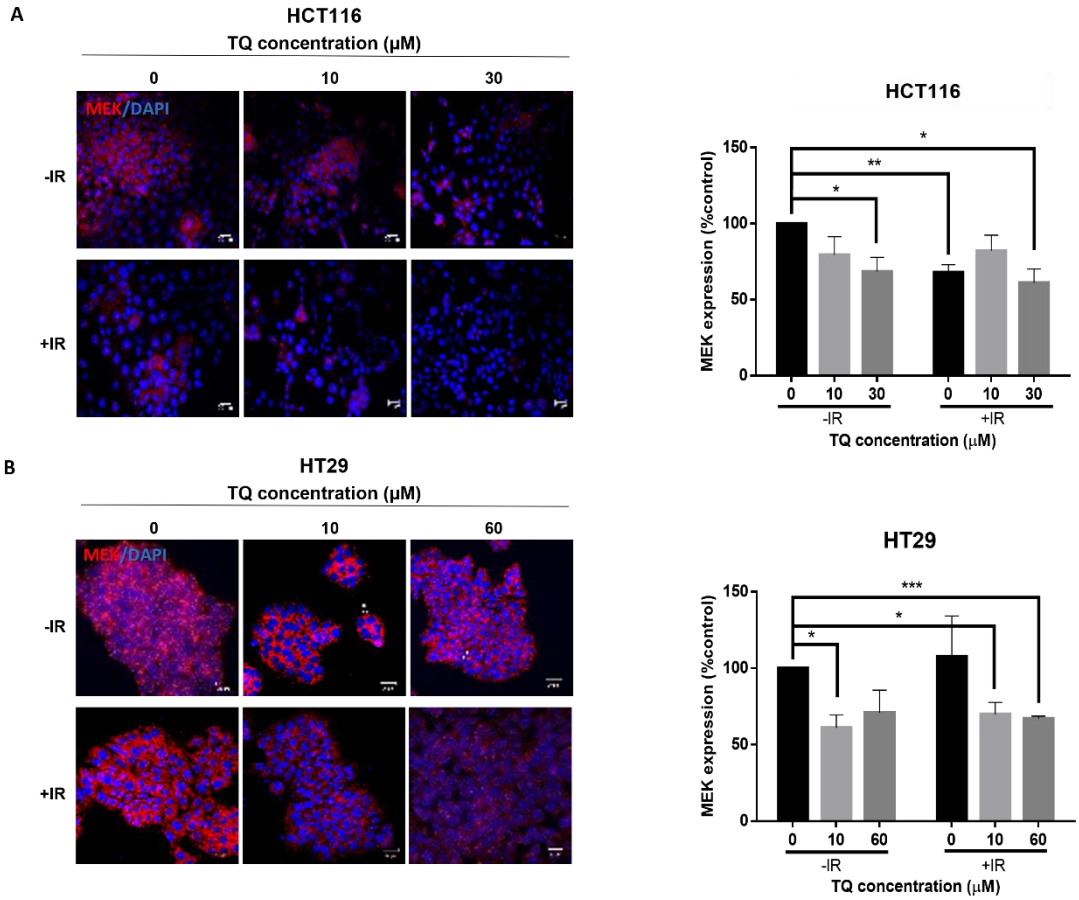

Figure 25. TQ and IR combination regulates MEK expression in colorectal cancer cells. HCT116 (A) and HT29 (B) cells were treated or not with TQ alone, IR alone, or combinations (TQ+IR) and immunofluorescently stained for MEK. Quantification and representative images are shown. Data represent an average of three independent experiments and are reported as mean ± SEM (* P<0.05; ** P<0.01; *** P<0.001). Scale bar for immunofluorescent images is 20 μm.

In HCT116 cells, Western blot analysis showed that 30 μM TQ and IR increased the expression of p53, and this increase was comparable to individual treatments, with slight enhancement in p53 expression in cells treated with combinations (Figure 26). A combination of TQ (10 μM or 30 μM) and IR induced an upregulation in p21 expression by ~1.7-fold, and this upregulation was comparable to IR alone. Combining TQ (10 μM or 30 μM) with IR led to a significant ~1.5-fold reduction in NF-κB expression and combining 30 μM TQ with IR reduced β-catenin expression by more than 2-fold. CD133

levels did not change upon treatment of HCT116 cells. In HT29 cells treated with TQ (10 µM or 60 µM) and IR, more than 1.6-fold increase in p53 expression was observed, whereas the increase in p21 was insignificant under these conditions (Figure 26). Importantly, 60 µM TQ and IR significantly reduced the expression of NF-κB by 1.82-fold and this reduction was significant when compared to IR alone. Notably, combining 60 µM TQ and IR led to a significant reduction in β- catenin and CD133 expression.

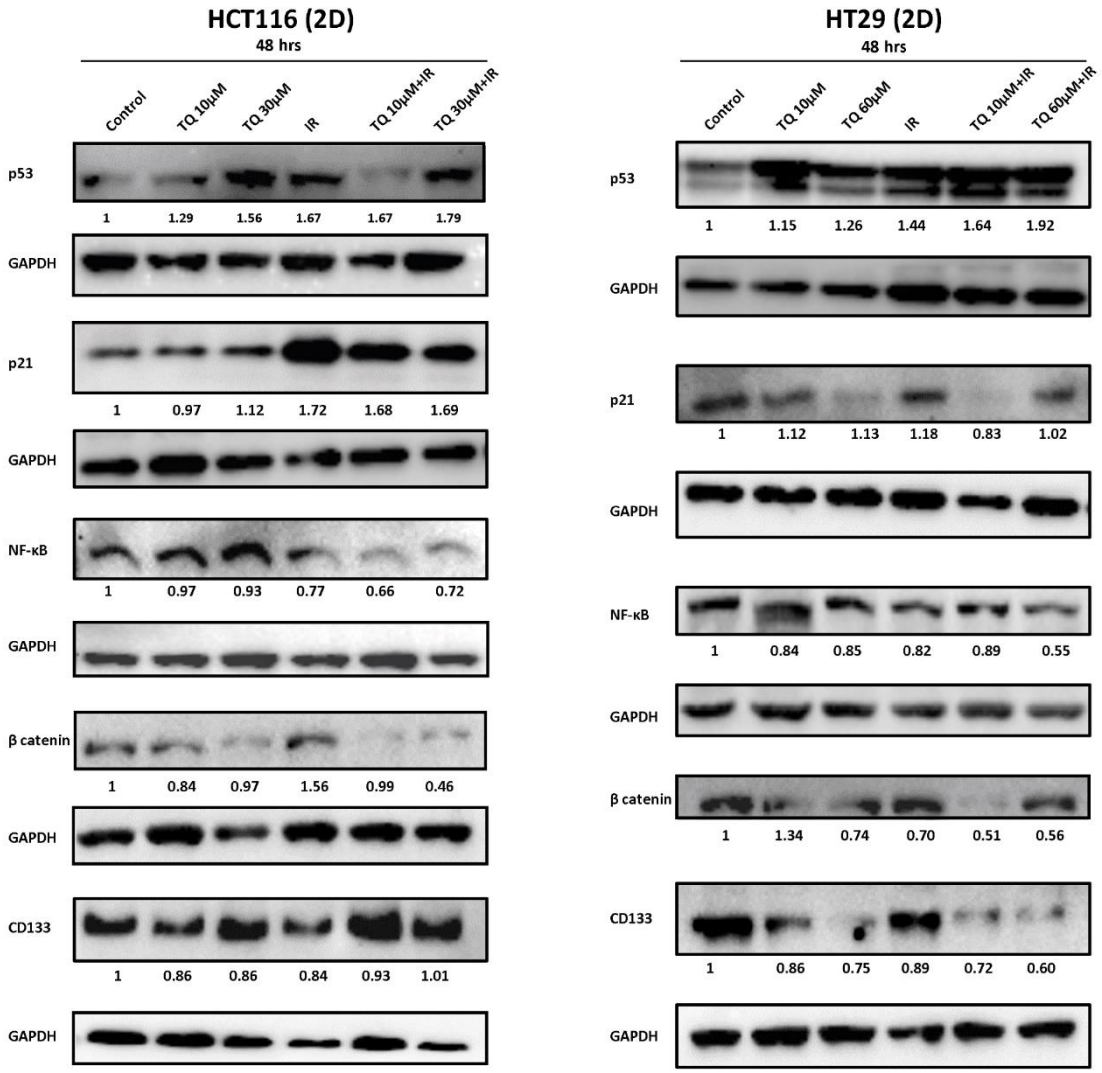

Figure 26. TQ sensitizes colorectal cancer cells to radiation through targeting major pathways implicated in survival and resistance to radiation. Western blot

analysis of p53, p21, NF-κB (p65), β-catenin, CD133 48 hrs post-treatment with TQ, IR, or combinations in HCT116 and HT29 cells. Fold expression changes normalized to GAPDH. Data represent an average of at least three independent experiments.

I. Effect of TQ and radiation on colorectal cancer stem/progenitor cells and their sphere-forming and self-renewal ability

Self-renewal is one of the major hallmarks of cancer stem/progenitor cells. To assess the effect of combination treatment on sphere-forming and self-renewal abilities, 3D culture sphere formation assay was employed and spheres were propagated till generation 5 (G5) (Figure 27). At each generation, cells were treated with TQ, IR, or combinations, after which spheres were imaged and counted. At G1, combining TQ (1 μM or 3 μM) with IR significantly reduced the sphere forming ability of HCT116, in comparison to IR alone (Figure 27A). Combining 1 μM TQ and IR decreased HCT116 SFU by more than 3-fold, whereas treatment with 3 μM TQ and IR decreased sphere count by a remarkable 12-fold. At G3, 3 μM TQ and IR resulted in inhibition that was greater than either treatment alone. Notably, at G5, 3 μM TQ and IR led to 97% reduction in sphere count. While treatment of HT29 cells with TQ or IR alone induced no significant decrease in sphere forming ability, combining 5 μM TQ and IR led to ~68% decrease at G1 (Figure 27B). Interestingly, successive propagation and treatment of HT29 cells with 3 μM TQ and IR significantly decreased sphere count by ~84% at G3 and by ~100% at G5. This decrease was greater than that either treatment alone.

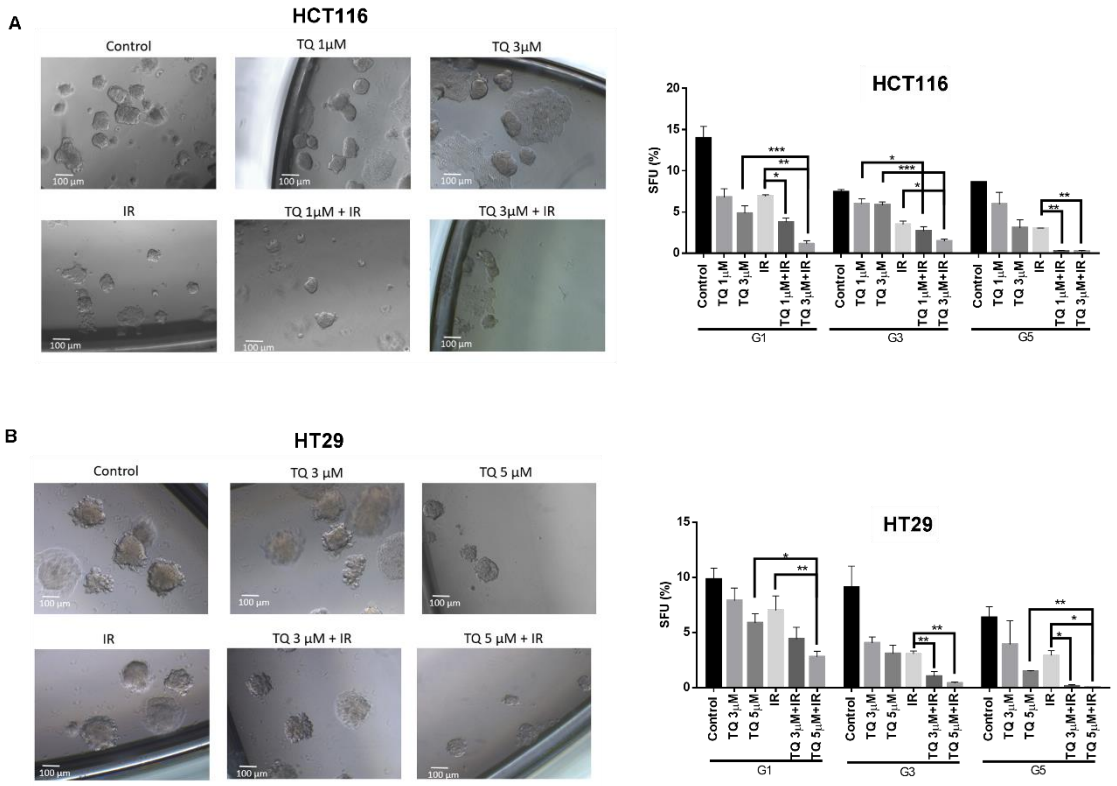

Figure 27. TQ sensitizes colorectal cancer stem/progenitor cells to IR and reduces their sphere-forming and self-renewal ability. SFU obtained from serially passaged colonopheres over five generations is shown for spheres derived from HCT116 (A) and HT29 (B) and treated with TQ (1, 3 and 5 μM), radiation (2 Gy), or combinations. SFU is calculated according to the following formula: SFU = (number of spheres counted/ number of input cells) ×100. Cells were suspended in Growth Factor reduced Matrigel/serum-free media (ratio 1:1) and allowed to grow in media with 5%FBS (with or without treatment) to enrich for CRC stem cells. Generated spheres are referred to as G1 (Generation 1) spheres. After each propagation, cells that were initially treated with TQ, IR, combinations, or media (control) were seeded into separate wells. Spheres were propagated for five generations in duplicates for each condition. Data represent an average of three independent experiments and are reported as mean ± SEM (* $P< 0.05$; ** $P < 0.01$; *** $P< 0.001$). Representative bright-field images showing the effect of TQ, IR, and combinations on SFU are shown next to the respective graphs. Images were visualized by Axiovert inverted microscope at 10X magnification and analyzed by Carl Zeiss Zen 2012 image software. Scale bar 100 μm.

Interestingly, upon withdrawal of combination treatment in the subsequent generations, HCT116 and HT29 spheres did regain some of their sphere-forming ability, yet they had lower sphere counts, when compared to the control at the same generation (Figure 28), suggesting that the treatment is partially irreversible.

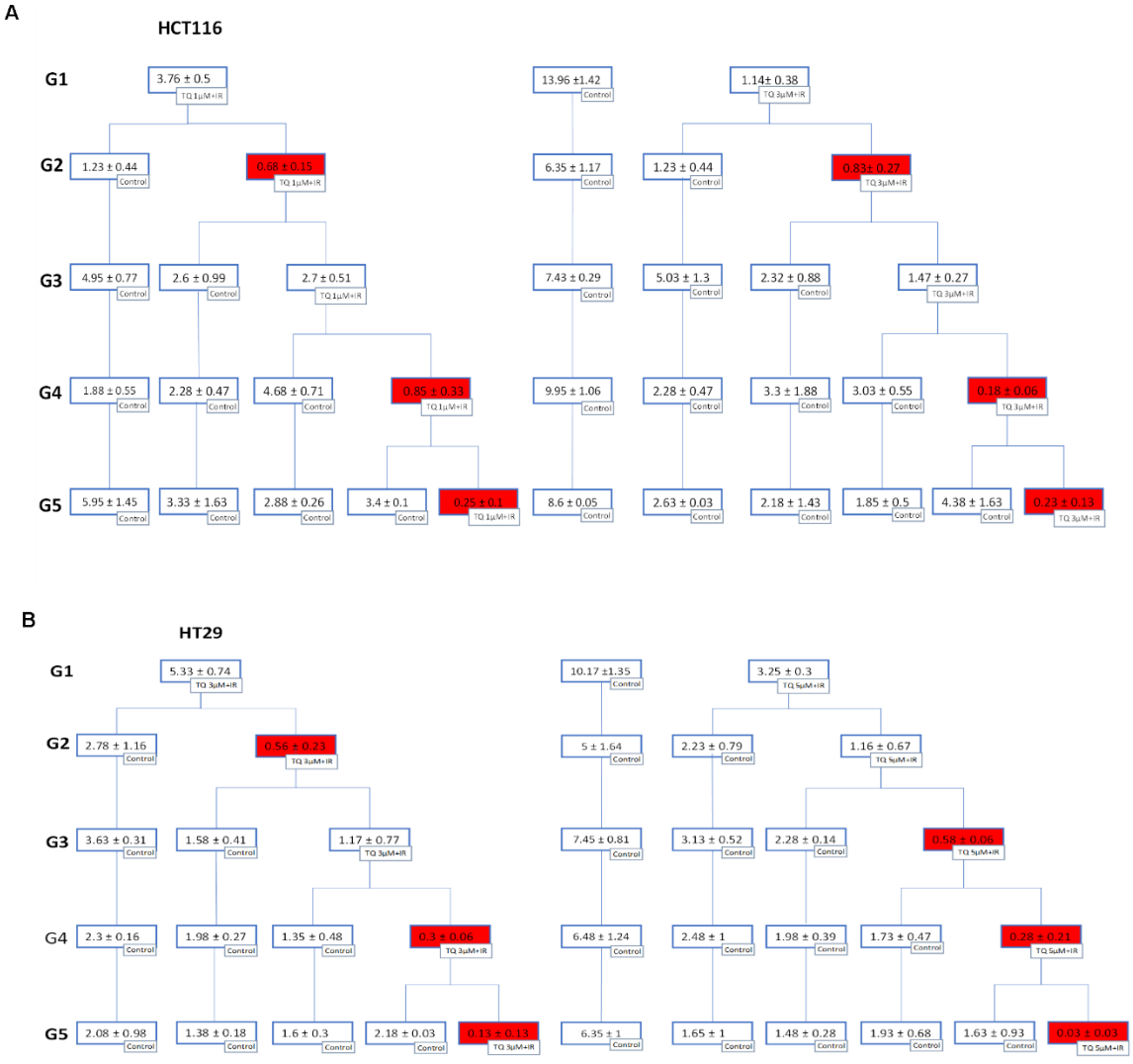

Figure 28. TQ enhances the effect of radiation on self-renewal capacity of colorectal cancer stem/progenitor cells. CRC stem cells were enriched from HCT116 (A) and HT29 (B) cell lines and treated with either TQ, IR, combinations, or media (control). After each propagation, cells that were initially treated with combinations or media (control) were seeded into separate wells and cultured with or without treatment. Spheres were propagated for five generations in duplicates of each condition. SFU is calculated according to the following formula: SFU = (number of spheres counted/ number of input cells) ×100 and an average of three experiments is represented. The data are reported as mean ± SEM.

We also aimed to study the effect of TQ and IR on G1 spheres enriched from HCT116 p53 null and DLD1 cells (Figure 29). Our preliminary data showed that

combination of 1 µM TQ and IR reduced sphere forming ability of HCT116 p53 null cells, and this reduction was significant when compared to TQ alone (Figure 29A). Combining higher TQ concentration (3 µM) with IR resulted in a decrease that is significant when compared to IR alone. Interestingly, IR alone had no effect on HCT116 p53 null SFU. In DLD1 cells, combining 3 µM TQ with IR led to a significant 5.16-fold reduction in sphere count, and this reduction was greater than that of either treatment alone (Figure 29B).

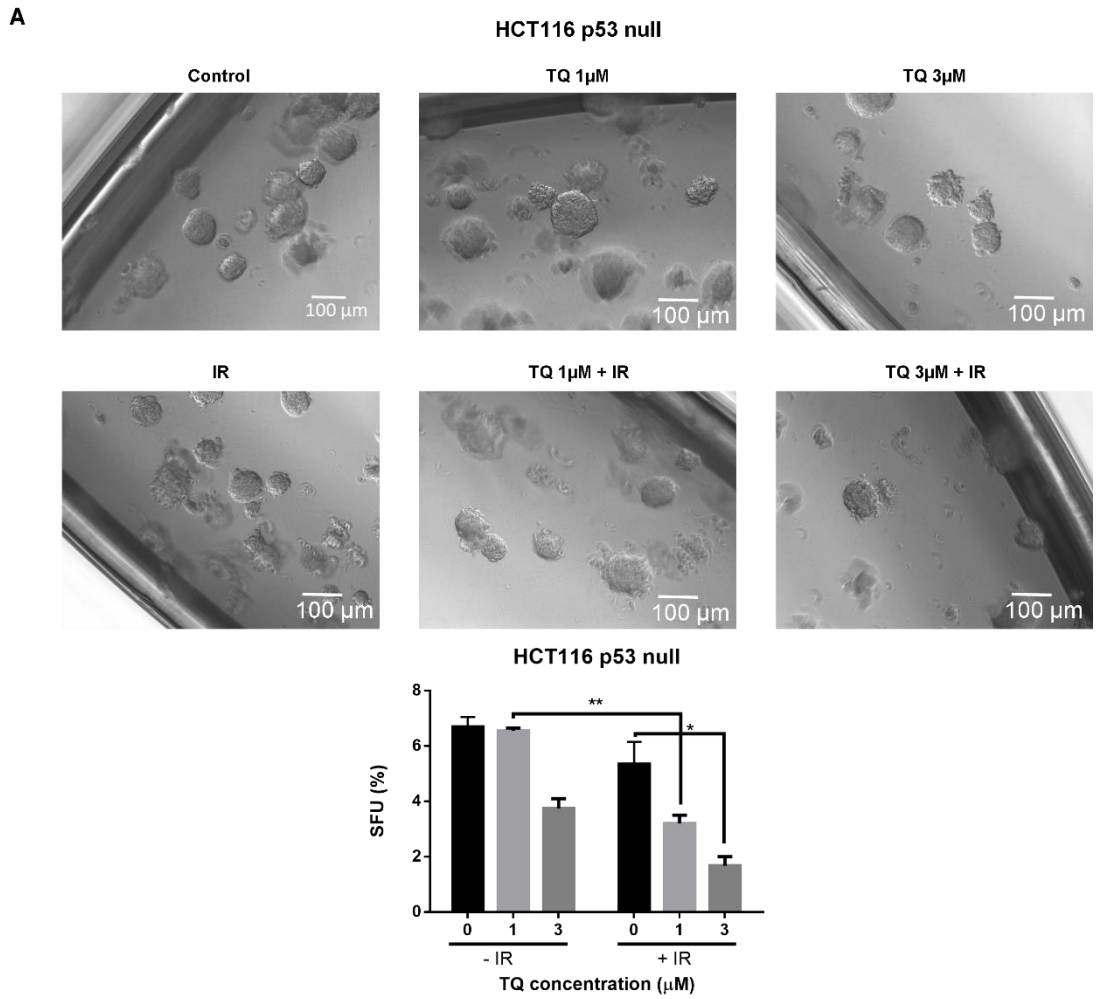

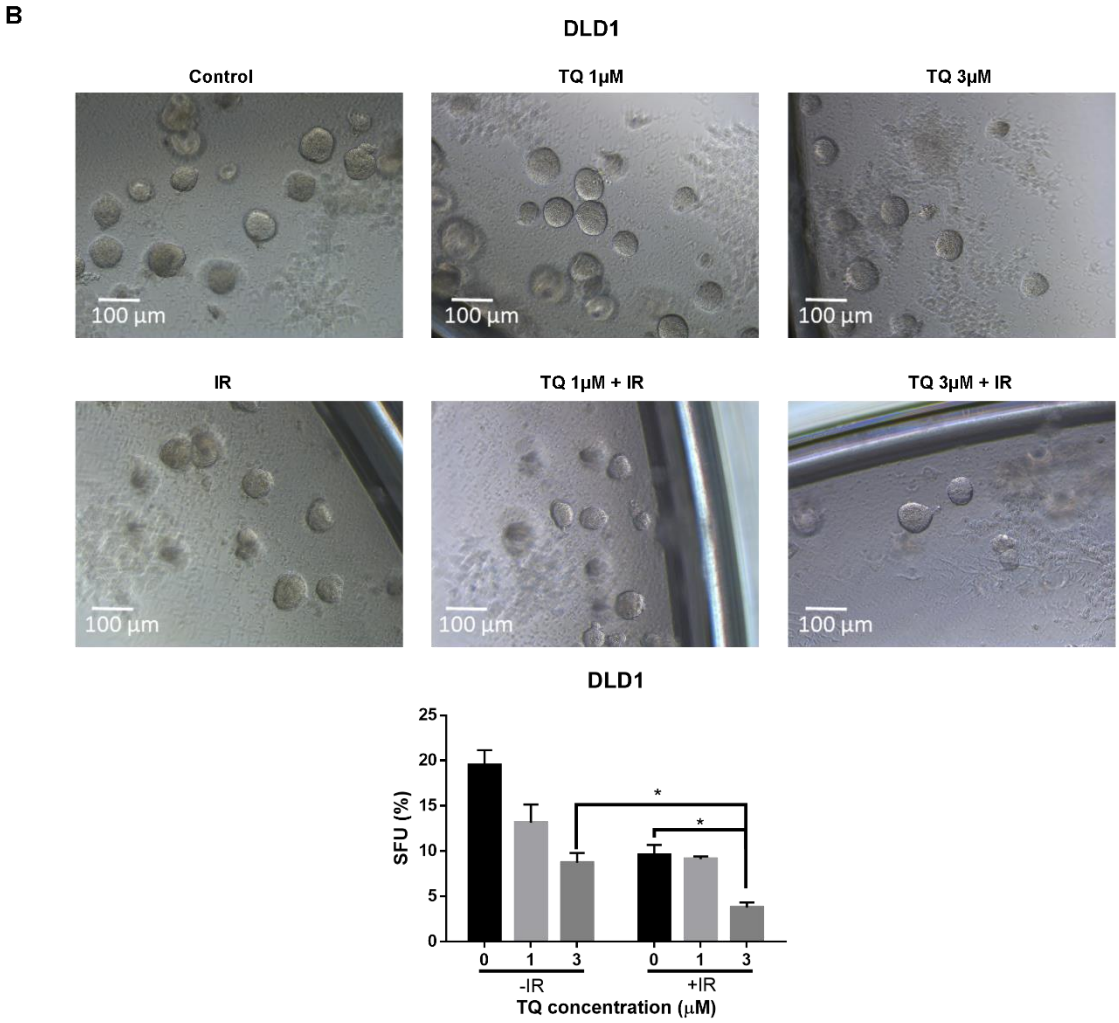

Figure 29. TQ sensitizes colorectal cancer stem/progenitor cells to IR and reduces their sphere-forming ability. Preliminary data showing effect of TQ and IR on CRC stem spheres enriched from HCT116 p53 null (A) and DLD1 (B) cell lines following treatment with either TQ, IR, combinations, or media (control) at G1. SFU is calculated according to the following formula: SFU = (number of spheres counted/ number of input cells) ×100. Data represent an average of two independent experiments and are reported as mean ± SEM (* P< 0.05; ** P < 0.01). Representative bright-field images showing the effect of TQ, IR, and combinations on SFU are shown next to the respective graphs. Images were visualized by Axiovert inverted microscope at 10X magnification and analyzed by Carl Zeiss Zen 2012 image software. Scale bar 100 μm.

Notably, IR alone and in combination with 3 μM TQ induced a slight reduction in SFU of FHs74Int cells, whereas TQ alone did not induce a significant reduction in

FHs74Int sphere count (Figure 30). Importantly, combination treatment induced comparable reduction to individual treatments.

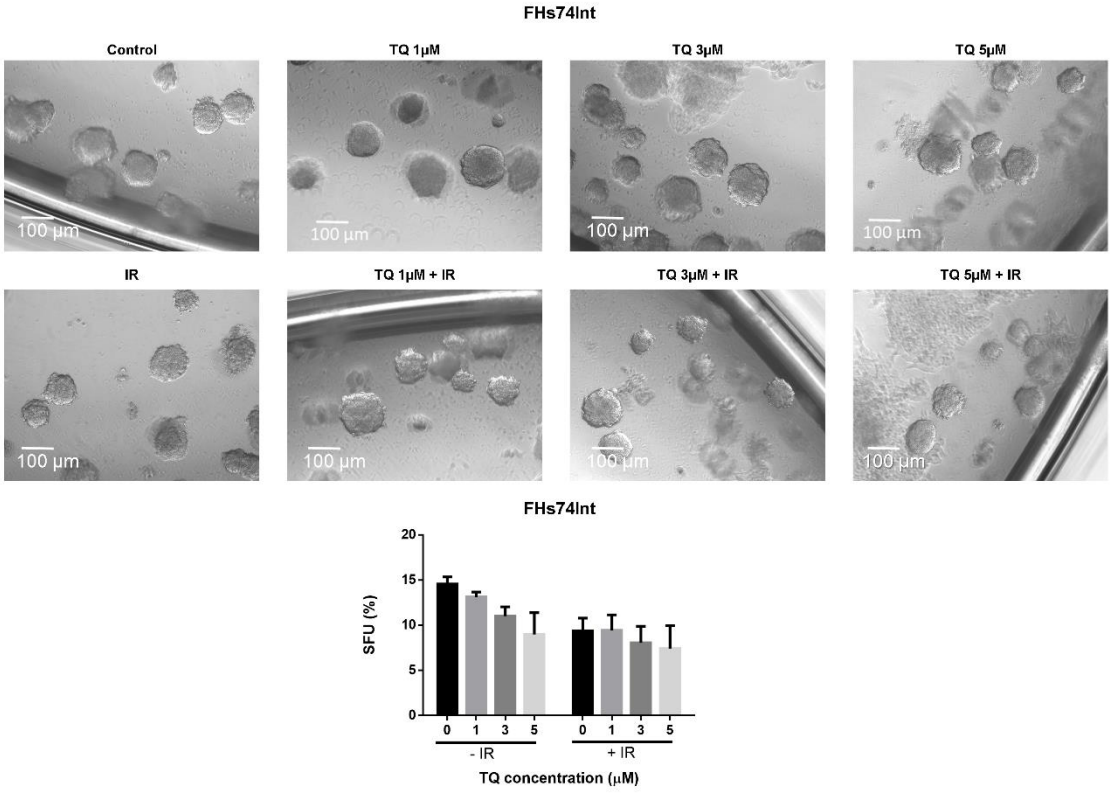

Figure 30. TQ and IR are non-toxic to colorectal cancer stem/progenitor cells enriched from non-tumorigenic intestinal cells. CRC stem cells enriched from FHs74Int cells following treatment with either TQ, IR, combinations, or media (control) at G1. SFU is calculated according to the following formula: SFU = (number of spheres counted/ number of input cells) ×100. Data represent an average of three independent experiments and are reported as mean ± SEM (* P< 0.05; ** P < 0.01). Representative bright-field images showing the effect of TQ, IR, and combinations on SFU are shown next to the respective graphs. Images were visualized by Axiovert inverted microscope at 10X magnification and analyzed by Carl Zeiss Zen 2012 image software. Scale bar 100 µm.

J. Effect of TQ and radiation on DNA repair and stemness in cancer stem/progenitor cells

We next checked for DNA damage in spheres treated with individual or combined treatment. Our results indicated that IR alone induced a significant increase in the γH2AX foci by ~2-fold in HCT116 spheres (Figure 31A). Interestingly, combining 3

μM TQ and IR led to a 4-fold increase in the expression of γH2AX, and this increase was more pronounced than either treatment alone. While TQ or IR alone did not induce a significant upregulation in γH2AX expression in HT29 spheres, combining TQ (3 μM or 5 μM) and IR treatment induced a ~4-fold upregulation in γH2AX expression, suggesting a delay in DNA damage repair after exposure to combination of TQ and IR (Figure 31B).

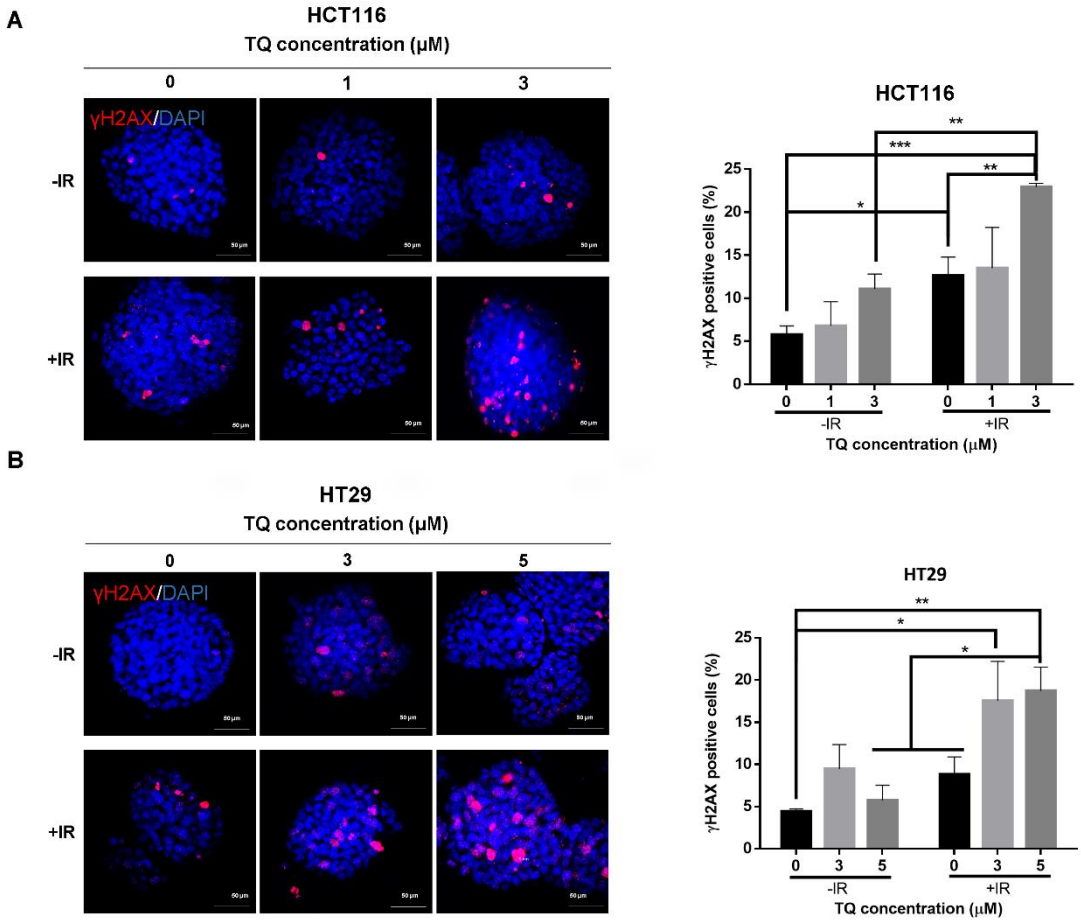

Figure 31. TQ radiosensitization of colorectal cancer stem/progenitor cells lead to inhibition of DNA repair. HCT116 (A) and HT29 (B) spheres were treated with TQ at day 0 of sphere culture and irradiated at day 4. Spheres were collected, fixed, and stained for γH2AX. Representative images were obtained using confocal microscopy and quantification of the intensity of γH2AX stain in HCT116 and HT29 G1 spheres untreated and treated with TQ, IR, and combinations (TQ+IR) was performed using Carl Zeiss Zen 2012 image software. γH2AX positive cells were counted and are normalized to size. Data represent an average of three independent experiments and are reported as mean ± SEM (* $P < 0.05$; ** $P < 0.01$; *** $P < 0.001$). Scale bar 50 μm.

Immunostaining analysis showed that 3 µM TQ alone and in combination with IR decreased expression of colorectal stem cell marker CD44 in HCT116 spheres by more than 1.2-fold (Figure 32A). In HT29 spheres, 5 µM TQ decreased CD44 expression level by ~1.5-fold, whereas combining the same dose of TQ with IR led to a ~1.8-fold reduction, and this reduction was significant when compared to IR alone (Figure 32B).

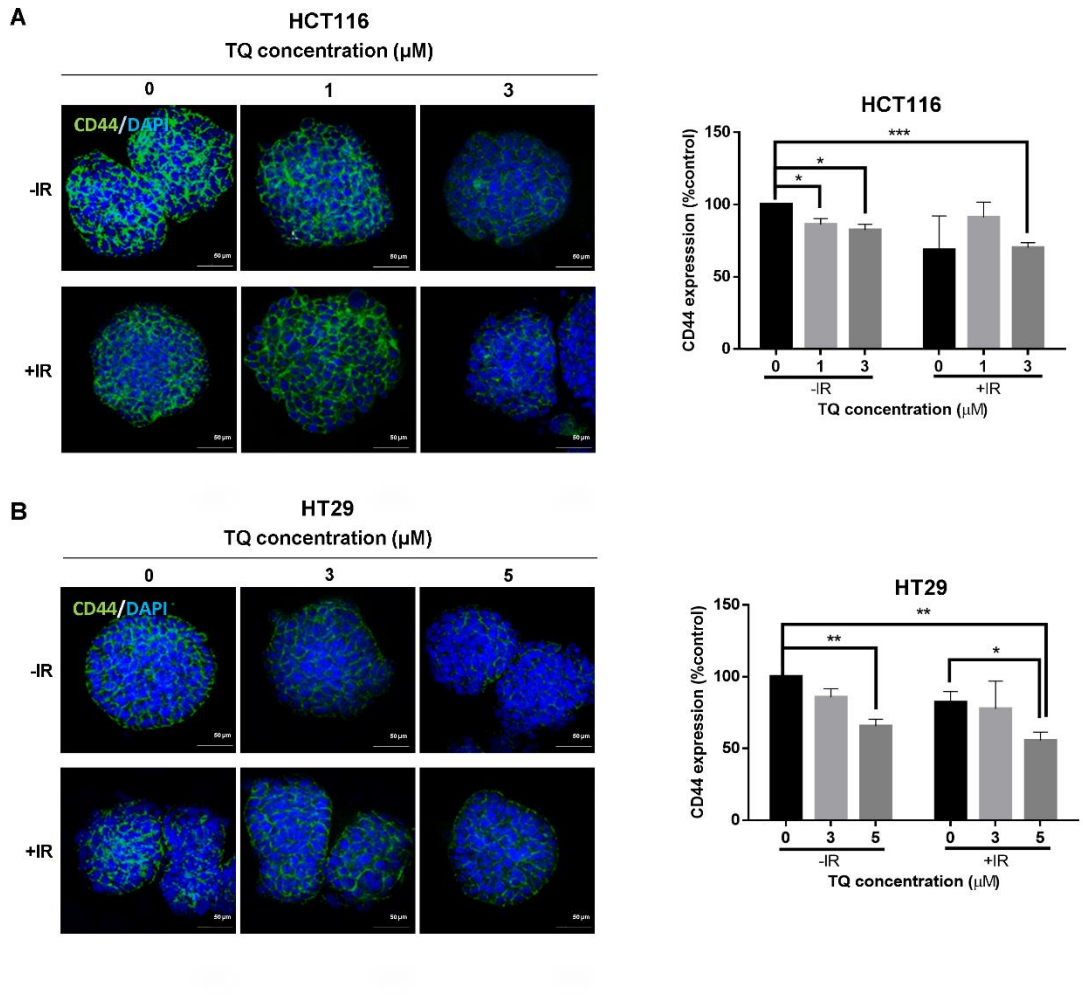

Figure 32. TQ radiosensitization of colorectal cancer stem/progenitor cells lead to reduction in the expression of CD44 cancer stem cell marker. TQ, IR, and TQ+IR treated HCT116 (A) and HT29 (B) G1 spheres were collected, fixed, and stained for CD44. Representative images were obtained using confocal and quantification of the intensity of CD44 stain was performed using Carl Zeiss Zen 2012 image software. Stain intensity was normalized to size. Data represent an average of three independent experiments and are reported as mean ± SEM (* $P < 0.05$; ** $P < 0.01$; *** $P < 0.001$). Scale bar 20 µm.

In HCT116 spheres, TQ or IR alone had no effect on the expression level of the epithelial marker CK8, while combining 3 µM TQ with IR resulted in a ~1.5-fold decrease (Figure 33A). Interestingly, combining TQ (1 µM or 3 µM) with IR significantly reduced the level of the stem cell marker CK19. In HT29 spheres, none of the treatments induced significant changes in the expression of CK8 or CK19 (Figure 33B), suggesting that the inhibitory mechanism is different in HCT116 and HT29 spheres.

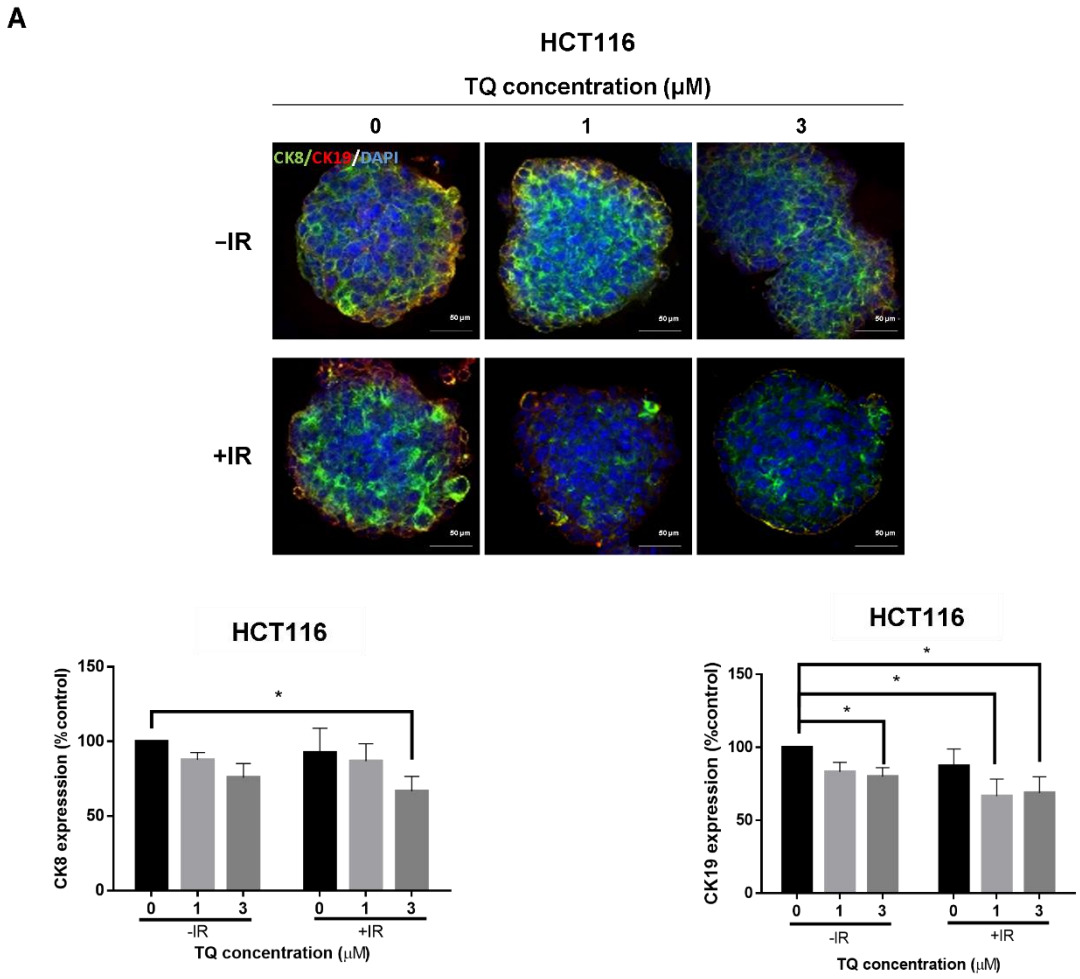

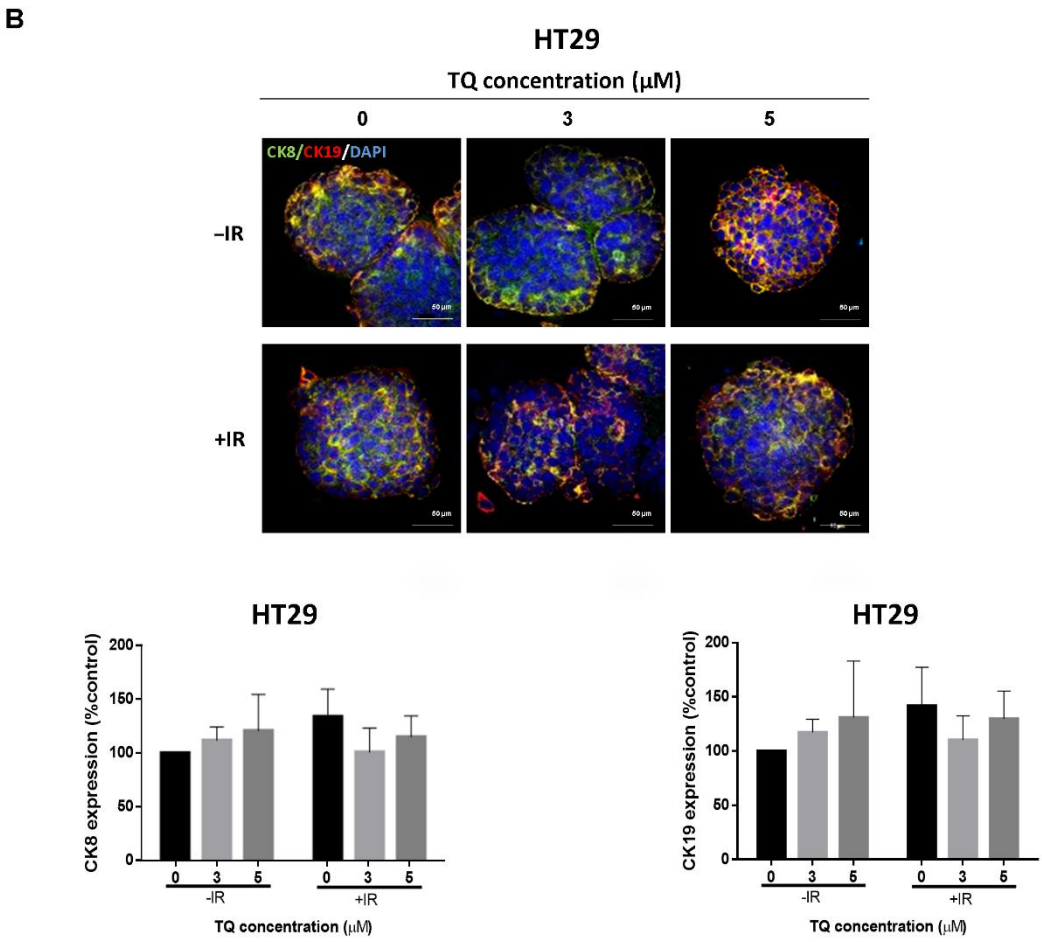

Figure 33. TQ radiosensitization of colorectal cancer stem/progenitor cells lead to reduction in the expression of CK8 and CK19. TQ, IR, and TQ+IR treated HCT116 (A) and HT29 (B) G1 spheres were collected, fixed, and stained for CK8 and CK19 epithelial cytokeratin markers. Representative images were obtained using confocal and quantification of the intensity of CK8 and CK19 stains was performed using Carl Zeiss Zen 2012 image software. Stain intensity was normalized to size. Data represent an average of three independent experiments and are reported as mean ± SEM (* $P < 0.05$; ** $P < 0.01$; *** $P < 0.001$). Scale bar 20 μm.

Analysis of p53 expression by Western blot showed a significant upregulation in HCT116 colonospheres in response to 3 μM TQ and IR combination and was significant when compared to TQ alone (Figure 34). p21 expression was upregulated by more than 1.2-fold in HCT116 spheres treated with 3 μM TQ alone and in combination with IR. Combining 3 μM TQ and IR resulted in a significant reduction in NF-κB

expression, and the reduction was more pronounced in comparison to TQ or IR alone. Combining 3 μM TQ and IR reduced the expression levels of β-catenin and CD133. In HT29 spheres, a combination of 5 μM TQ and IR led to a significant increase (1.54-fold) in p53, but not p21 expression (Figure 34). Combining 5 μM TQ and IR decreased the expression levels of NF-κB and β-catenin by ~2-fold. TQ (3 μM or 5 μM) and IR combination treatment reduced the levels of CD133 by more than 1.5-fold.

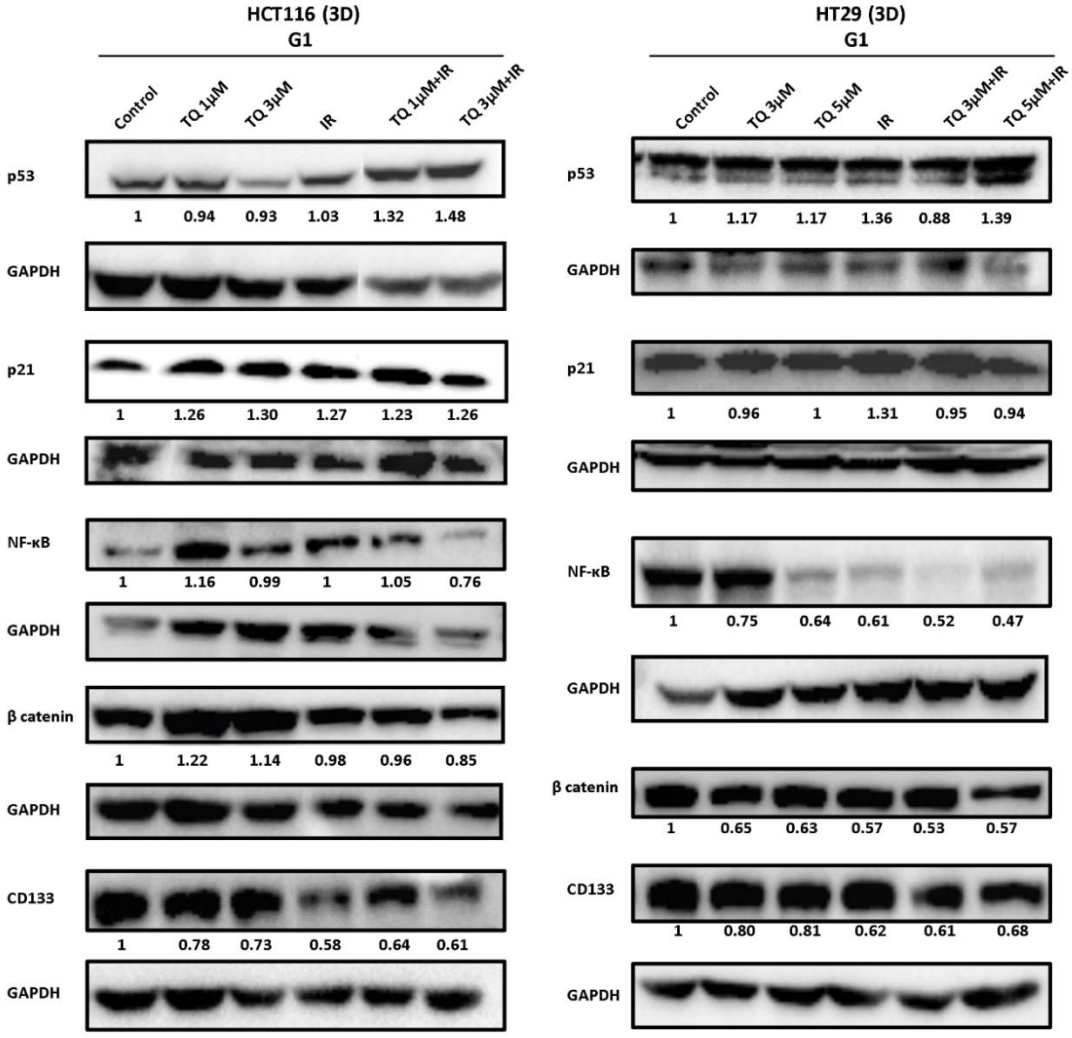

Figure 34. TQ radiosensitization of colorectal cancer stem/progenitor cells lead to inhibition of survival and stemness. Analysis of p53, p21, NF-κB (p65), β-catenin, and CD133 protein expression in HCT116 and HT29 G1 spheres following treatment with TQ, IR, and combinations (TQ+IR). Fold expression changes normalized to GAPDH.

K. Effect of TQ and IR on patient-derived tumor organoids

We succeeded in establishing PDOs from three different treatment-naïve patients and propagating them to model CRC disease in 3D culture. The three patients had different clinical manifestations whereby patient 1 had rectal mucinous adenocarcinoma (pT2 stage), and patients 2 and 3 had moderately differentiated (grade 2) pT2 and pT3 sigmoid colon adenocarcinoma, respectively (Table 5). Fresh unaffected and tumor tissues were processed as mentioned before (Figures 35-37). Interestingly only tumor samples successfully formed organoids in culture, which further confirms their tumorigenicity (Figures 35D-37D). Single cells from tumor tissues were allowed to form organoids, after which they were propagated and either treated with TQ (3 µM or 5 µM), IR (2 Gy), or combinations. After 10–12 days, the number and size of organoids were calculated. While IR or TQ alone had no significant effect on the count or size of PDOs derived from patient 1, combining TQ (3 µM or 5 µM) and IR significantly reduced both organoid count and size (Figure 35F). Combination treatment resulted in a ~1.7- fold and ~2-fold reduction in patient 1 OFC at TQ concentrations of 3 µM and 5 µM, respectively. The average organoid size was significantly reduced by ~1.4-fold in organoids treated with TQ (3 µM or 5 µM) and IR and was significant compared to either treatment alone. IR alone in patient 2 significantly reduced organoid count by ~1.5-fold, whereas combination of 5 µM TQ and IR reduced OFC by ~1.7-fold (Figure 36F). Combining 5 µM TQ with IR reduced the size of organoids by ~1.2-fold. In patient 3 (Figure 37F), IR alone significantly reduced the total count of organoids by ~5.2-fold and its effect was comparable to that of combination treatment. Combining 5 µM TQ and IR reduced the size of organoids by more than 1-fold and this reduction was significant when compared to TQ alone.

Immunofluorescent characterization of the established PDOs for CD44 and CK19 CRC stem cell markers showed that all organoids stained positive for these markers, demonstrating the presence of stem-like cells within the bulk of these organoids (Figures 35E–37E). Furthermore, treatment of patient 1 organoids with 3 μM TQ and IR significantly reduced the expression of CD44 (by 1.24-fold) and CK19 (by 1.45-fold), and this reduction was more pronounced than that of either treatment alone (Figure 35G).

Immunofluorescent staining of the parental tumor tissues with CK19 showed a positive expression, in consistency with the established PDOs. Tumor tissues were further characterized for other markers and showed positive immunofluorescent staining for CK8 and β-catenin (Figures 35B-37B) and positive immunohistochemical staining for Ki67 (Figures 35C-37C).

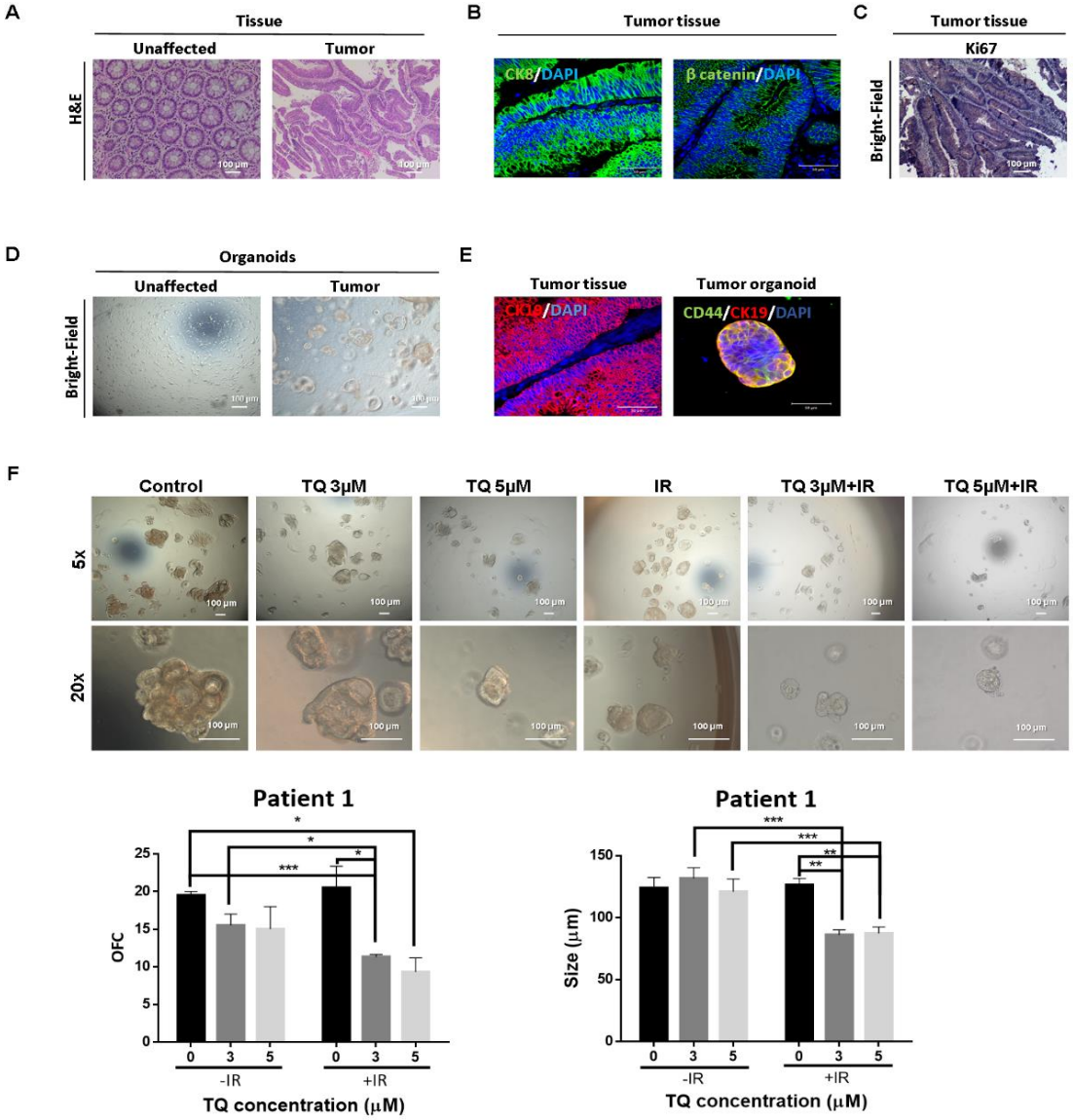
A
Tissue
Unaffected
Tumor
H&E
B
Tumor tissue
CK8/DAPI
β catenin/DAPI
C
Tumor tissue
Ki67
Bright-Field
D
Organoids
Unaffected
Tumor
Bright-Field
E
Tumor tissue
Tumor organoid
CK19/DAPI
CD44/CK19/DAPI
F
Control
TQ 3μM
TQ 5μM
IR
TQ 3μM+IR
TQ 5μM+IR
5x
20x
Patient 1
OFC
-IR
+IR
TQ concentration (μM)
Patient 1
Size (μm)
-IR
+IR
TQ concentration (μM)

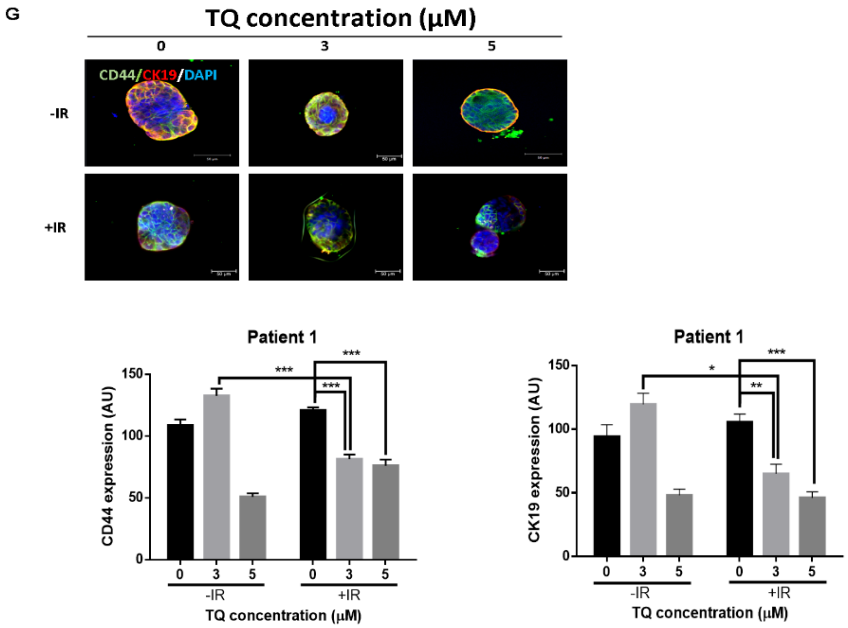

Figure 35. TQ radiosensitizes patient 1-derived rectal cancer organoids and reduces their organoid-forming ability and size. (A) Representative images of H&E stain of unaffected rectum and rectal cancer tissue from patient 1 with rectal mucinous adenocarcinoma (pT2 stage). Representative images of rectal cancer tissues stained for CK8, β-catenin (B) and Ki67 (C). (D) Representative bright-field images of organoids derived from unaffected rectum and rectal cancer samples. (E) Immunofluorescent images of rectal tumor issues and control organoids stained for CD44 and CK19. (F) Representative bright-field images of organoids derived from rectal cancer patient 1 sample and treated with TQ (3 and 5 µM), radiation (2 Gy), or combinations. (G) Immunofluorescent images of rectal tumor organoids treated with TQ, IR, and TQ+IR and stained for colorectal cancer stem cell markers CD44 and CK19. Images were obtained using confocal microscopy. Fresh unaffected and tumor tissues were digested, and single cells were resuspended in Matrigel and serum-free media (9:1) and allowed to grow without treatment. Generated organoids are referred to as G1 organoids. Organoids were propagated to G2 and treated with TQ, IR, or combinations (TQ+IR). Organoids-forming count (OFC) was calculated according to the following formula: (number of organoids counted/ number of input cells) ×100. Size of organoids was calculated. Average values were reported as mean ± SEM (* $P < 0.05$, ** $P < 0.01$, *** $P < 0.001$). Bright-filed and immunohistochemistry images were visualized by Axiovert inverted microscope at 10X magnification. Scale bar for bright-field images is 100 µm and for immunofluorescent images is 50 µm.

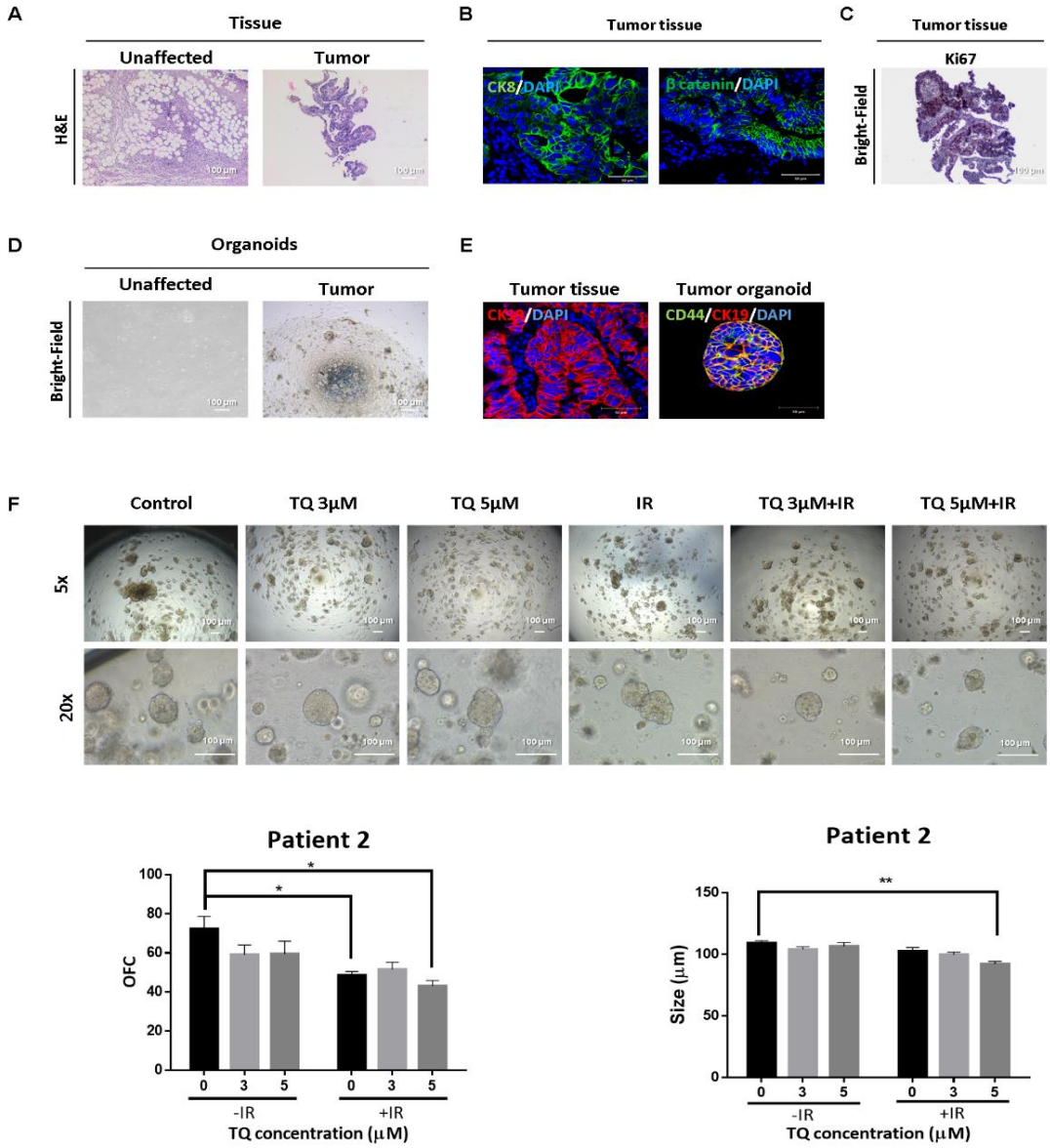

Figure 36. TQ and radiation inhibit patient 2-derived colon cancer organoids and reduce their organoid-forming ability and size. (A) Representative images of H&E stain of unaffected and tumor colon tissue from patient 2 with moderately differentiated (grade 2) pT2 sigmoid colon adenocarcinoma. Representative images of colon cancer tissues stained for CK8, β-catenin (B) and Ki67 (C). (D) Representative bright-field images of organoids derived from unaffected and tumor colon patient 2 samples. (E) Immunofluorescent images of tumor colon tissues and organoids stained for colorectal cancer stem cell markers CD44 and CK19. Images were obtained using confocal microscopy. (F) Representative bright-field images of organoids derived from tumor colon patient 2 sample and treated with TQ, IR, or combinations (TQ+IR). Fresh unaffected and tumor tissues were digested, and single cells were resuspended in Matrigel and serum-free colon media (9:1) and allowed to grow without treatment. Generated organoids are referred to as G1 organoids. Organoids were propagated to G4 and treated with TQ, IR, or combination (TQ+IR). OFC was calculated according to the following

formula: (number of organoids counted/ number of input cells) ×100. Size of organoids was calculated, and average values were reported as mean ± SEM (* $P < 0.05$, ** $P < 0.01$). Bright-filed and immunohistochemistry images were visualized by Axiovert inverted microscope at 10X magnification. Scale bar for bright-field images is 100 µm and for immunofluorescent images is 50 µm.

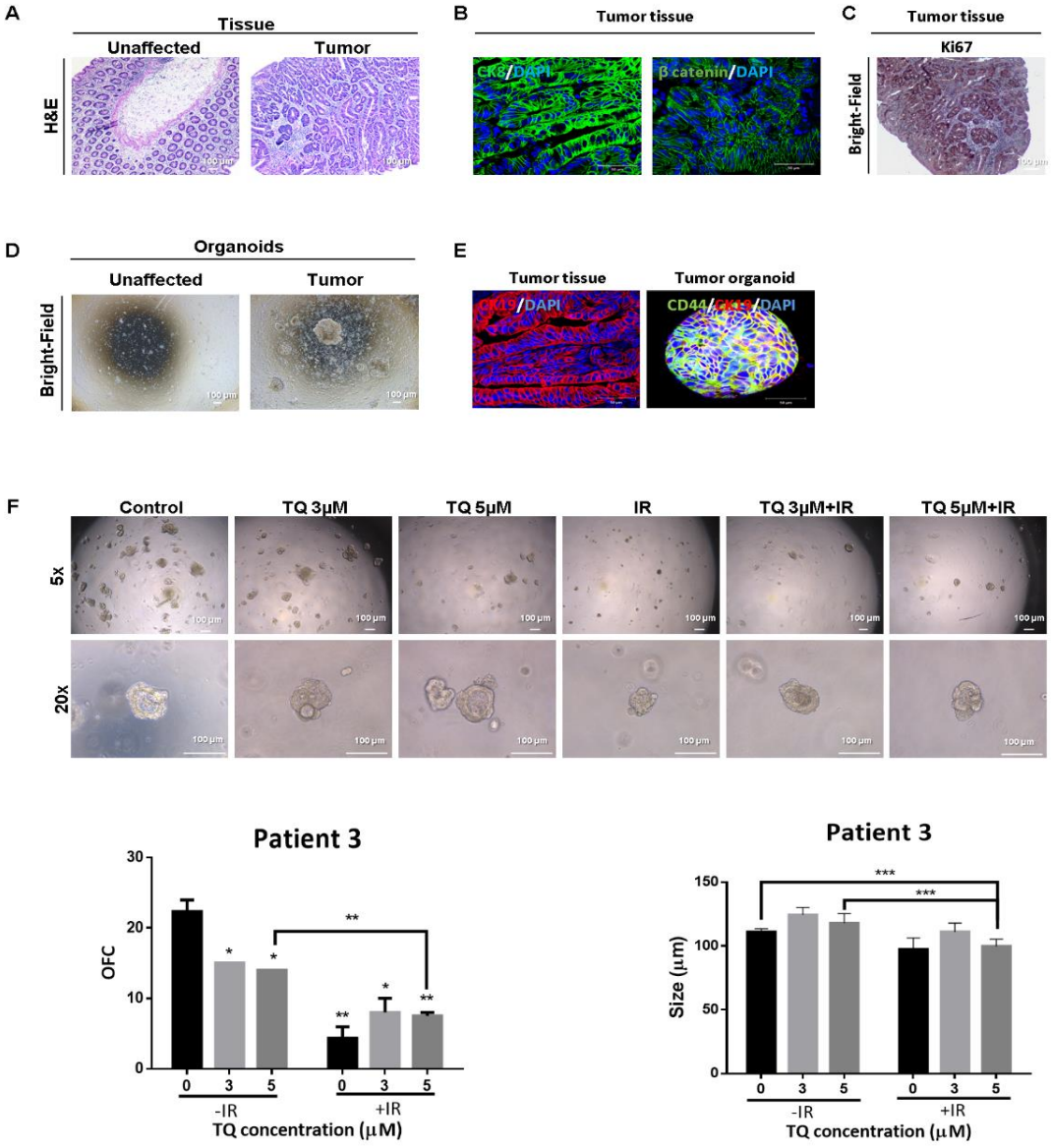

Figure 37. TQ and radiation inhibit patient 3-derived colon cancer organoids and reduce their organoid-forming ability and size. (A) Representative images of H&E stain of unaffected and tumor colon tissue from patient 3 with moderately differentiated (grade 2) pT3 sigmoid colon adenocarcinoma. Representative images of colon cancer tissues stained for CK8, β catenin (B), and Ki67 (C). (D) Representative bright-field images of organoids derived from unaffected and tumor colon patient 3 samples. (E) Immunofluorescent images of tumor colon tissues and organoids stained for colorectal

cancer stem cell markers CD44 and CK19. Images were obtained using confocal microscopy. (F) Representative bright-field images of organoids derived from tumor colon patient 3 sample and treated with TQ (3 and 5 µM), radiation (2 Gy), or combinations. Fresh unaffected and tumor tissues were digested, and single cells were resuspended in Matrigel and serum-free colon media (9:1) and allowed to grow without treatment. Generated organoids are referred to as G1 organoids. Organoids were propagated to G2 and treated with TQ, IR, or combination (TQ+IR). OFC was calculated according to the following formula: (number of organoids counted/ number of input cells) ×100. Size of organoids was calculated, and average values were reported as mean ± SEM (* $P < 0.05$, ** $P < 0.01$, *** $P < 0.001$). Bright-field and immunohistochemistry images were visualized by Axiovert inverted microscope at 10× magnification. Scale bar for bright-field images is 100 µm and for immunofluorescent images is 50 µm.

Table 5: Colorectal cancer patients' clinical and histopathologic characteristics

	Patient 1	Patient 2	Patient 3
Gender	Male	Female	Female
Age	62	55	61
BMI	29.7	25	21
Smoking	Yes	No	Yes
Chemotherapy preop	No	No	No
Radiation therapy preop	No	No	No
Location of tumor	Rectum	Sigmoid colon	Descending colon/ sigmoid colon
Type	Mucinous adenocarcinoma	Adenocarcinoma	Adenocarcinoma
T stage	pT2	pT2	pT3
N stage	pN0	pN0	pN0
M stage	N/A	N/A	N/A
Size of Tumor	6 cm	4.5 cm	2 cm
Grade	Not applicable: mucinous tumor	2: Moderately differentiated	2: Moderately differentiated

L. Effect of TQ and radiation on cell line-derived organoids

Given that HCT116 and HT29 are derived from colorectal adenocarcinoma patients, we next aimed to establish organoids from HCT116 and HT29 and assess the effect of TQ and IR combination on these organoids (Figures 38-39). Our results showed significant reduction in HCT116 OFC upon treatment with TQ (1 or 3 μM) with IR, and this reduction was comparable to TQ or IR alone (Figure 38A).

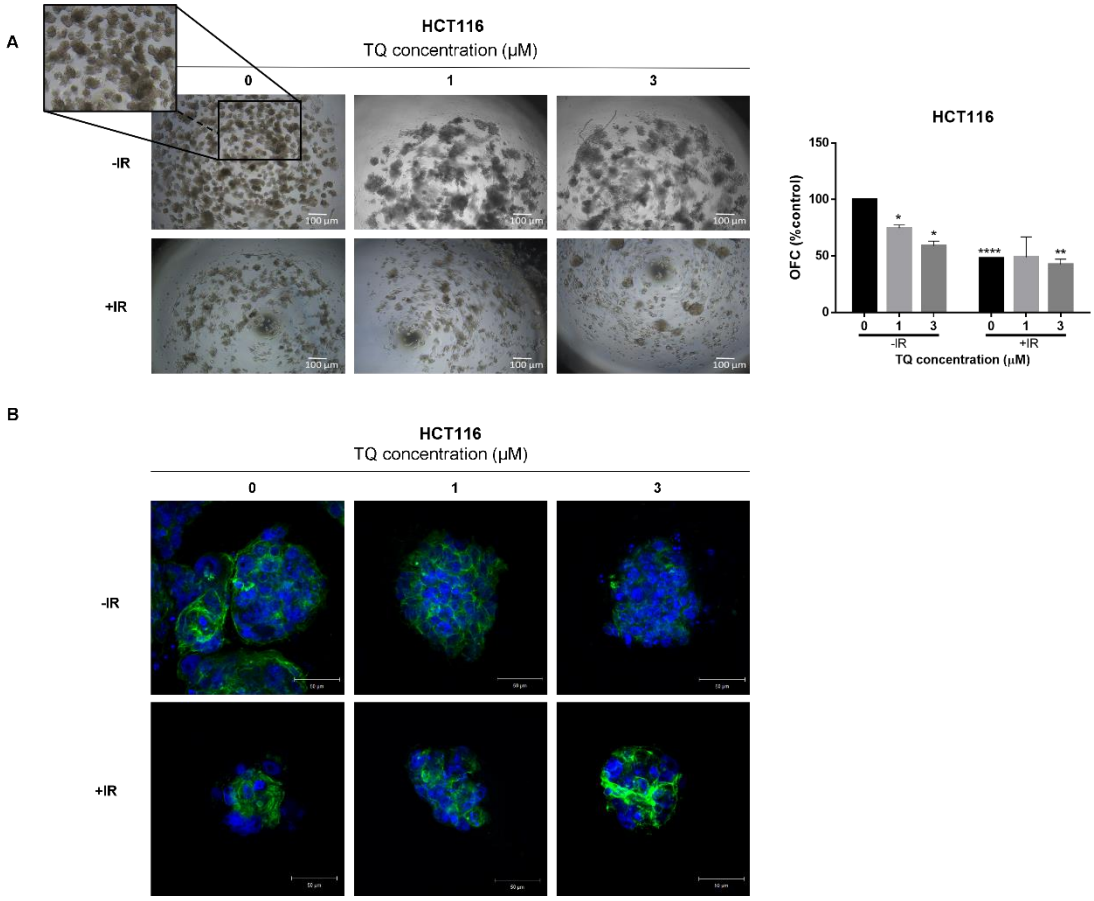

Figure 38. TQ and radiation inhibit HCT116 colorectal cancer cell line-derived organoids and reduce their organoid-forming ability. (A) Representative bright-field images of organoids derived from HCT116 cells and treated with TQ, IR (2 Gy), or combinations (TQ+IR). Images were visualized by Axiovert inverted microscope at 10X magnification and analyzed by Carl Zeiss Zen 2012 image software. Scale bar 100 µm. OFC was calculated and expressed as percentage of the treatment group as compared to its control according to the following formula: OFC (%control) = (number of organoids counted/number of organoids in control group) ×100. HCT116 cells were suspended in Matrigel and serum-free colon media (9:1) and allowed to grow in serum-free colon media (with or without treatment). Generated organoids are referred to as G1 organoids. Data represent an average of three independent experiments and are reported as mean ± SEM (**P* < 0.05). Representative immunofluorescence images of phalloidin-stained HCT116 organoids were obtained using confocal microscopy. Scale bar 50µm.

Interestingly, there was no significant effect of IR alone on HT29 organoid count, whereas treatment with 5 µM TQ alone led to a ~13% reduction (Figure 39A). Importantly, combining 5 µM TQ with IR resulted in a 2.26-fold decrease in OFC, and this decrease was significant when compared to individual treatments. Notably, organoids

established from the HT29 cells and treated with individual and combination treatments showed similar response to organoids from patient 1.

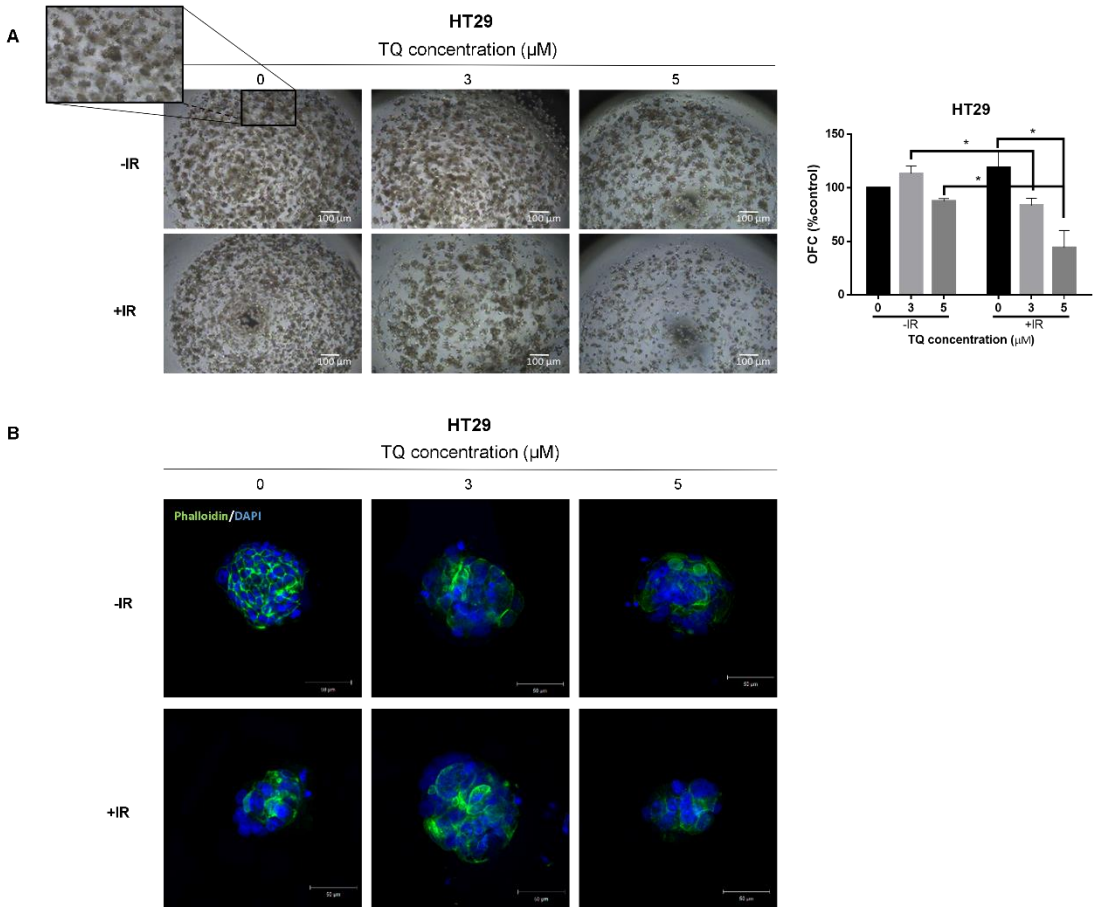

Figure 39. TQ radiosensitizes HT29 colorectal cancer cell line-derived organoids and reduces their organoid-forming ability. (A) Representative bright-field images of organoids derived from HT29 cells and treated with TQ, IR (2 Gy), or combinations (TQ+IR). Images were visualized by Axiovert inverted microscope at 10X magnification and analyzed by Carl Zeiss Zen 2012 image software. Scale bar 100 μm. OFC was calculated and expressed as percentage of the treatment group as compared to its control according to the following formula: OFC (%control) = (number of organoids counted/number of organoids in control group) ×100. HT29 cells were suspended in Matrigel and serum-free colon media (9:1) and allowed to grow in serum-free colon media (with or without treatment). Generated organoids are referred to as G1 organoids. Data represent an average of three independent experiments and are reported as mean ± SEM (*P < 0.05). Representative immunofluorescence images of phalloidin-stained HT29 organoids were obtained using confocal microscopy. Scale bar is 50 μm.

CHAPTER IV
DISCUSSION

Colorectal cancer is the third most common cancer affecting both men and women worldwide. It remains among the most lethal and prevalent malignancies worldwide with 14% survival for patients with metastatic CRC [163]. Despite the great advances made in detecting and treating CRC cancer, it remains a major burden in many countries. Treatments for CRC include surgical resection, radiotherapy, ablative therapies for metastases, and palliative chemotherapy [164]. However, in many cases, cancer recurrence may occur due to the resistance of CSCs to conventional therapies, including radiotherapy. Chemo- and radiotherapy are often combined and given as neoadjuvant therapy in cases of advanced rectal cancer disease (>T3), lymph node involvement, and after surgery to prevent local recurrence [165]. Several trimodality approaches have been devised for better management of the disease. Previously, the standard sequence was preoperative chemotherapy or radiotherapy, followed by surgery, and sometimes application of adjuvant multi-agent chemotherapy. Recent advances have been made to optimize the sequence of these approaches for better outcomes [166]. Total neoadjuvant therapy (TNT) is now being implemented in patients with higher risk of recurrence. This new approach consists of preoperative delivery of radio- and chemotherapy in sequence with multi-agent chemotherapy [166]. Delivering radiation before surgery led to lower recurrence, when compared to surgery alone [167-170]. Long-course chemoradiation (with concurrent 5-FU or capecitabine) and short course-radiotherapy have been studied in clinical trials; however, both involve the delivery of high radiation dose (>25 Gy) [171, 172].

The interest in the development of potential radiosensitizers in radiotherapy has expanded [173]. Mechanisms of radiosensitization may include inhibition of radiation-induced DNA damage repair, cell cycle progression, growth signaling pathways, energy metabolism pathways, angiogenesis, inflammation, hypoxia, and invasion and metastasis [174, 175].

Thymoquinone, the major bioactive compound found in Nigella sativa, exhibits several cytotoxic activities against many cancer types, including CRC, through the modulation of multiple hallmarks of cancer. However, no studies have investigated the radiosensitzing effect of TQ on CRC cells and stem/progenitor cells. This study was designed to investigate the radiosensitizing potential of TQ and the molecular mechanisms of TQ and IR combination in different 2D and 3D models of CRC cells, and in PDOs. Our study is the first to show a radiosensitizing potential of TQ in CRC stem/progenitor cells and in PDOs. In 3D colonosphere cultures, radiosensitization by TQ correlated with significant inhibition of DNA repair, stemness, and radioresistance through targeting CD44, CK19, and CD133 CRC stem cell markers, in addition to β-catenin and NF-κB molecules involved in survival and radioresistance. These findings confirm the efficacy of combination treatment in eradicating CSCs. On the other hand, combination treatment induced the expression of cell cycle regulators p53 and p21, suggesting cell cycle arrest in response to DNA damage. In our 2D model, combination of TQ and IR inhibited cell proliferation, viability, migration, and colony forming ability. It also induced DNA damage and G2/M cell cycle arrest, which was associated with persistent expression of γH2AX and p-ATR, in addition to induction of ROS and oxidative stress. Mechanistically, TQ and IR combination upregulated p53 and p21, and

targeted NF-κB, MEK/ERK, Wnt/β catenin, and p-mTOR pathways involved in radioresistance.

For the first part of the study, we used a panel of CRC cells with different mutations and sensitivity to TQ: HCT116 (Wild-type p53, mutant K-ras), HCT116 p53 null (absent p53, mutant K-ras), HT29 (mutant p53, wild-type K-ras), and DLD1 (mutant p53, mutant K-ras). We showed that TQ radiosensitized these cells, independent of their p53 or K-ras status. IR alone had reversible inhibitory effects on the proliferation of all cell lines and no cytotoxic effects on HT29 cells. Combining IR with TQ led to a dose-dependent reduction in proliferation of all CRC cells. Notably, MTT measures the level of cellular metabolic activity, which is associated with cell proliferation, and thus may not be the ideal assay to clearly see the effect of combination treatments. On the other hand, trypan blue assay showed that combining TQ with IR reduced the viability of CRC cells more than TQ or IR alone and was non-toxic to FHs74Int intestinal cells at low doses of TQ. Clonogenic survival of irradiated HCT116, HCT116 p53 null, HT29, and DLD1 cells was reduced by TQ, indicating radiosensitization through inhibition of long-term survival. This long-term inhibitory effect of TQ has been previously reported in breast cancer and HNSCC cell lines exposed to radiation [144, 176]. Importantly, using 3D clonogenic survival assay, we showed a reduction in sphere forming ability of CRC cells previously treated with combination treatment in 2D culture, indicating radiosensitization by TQ. Clonogenic survival assay showed inhibitory effect of IR alone on the FHs74Int non-tumorigenic intestinal cells, consistent with studies reporting radiation-induced toxicity in these cells [177, 178] and in normal tissues [179].

For subsequent experiments, HCT116 and HT29 cells were chosen to elucidate potential mechanisms of TQ radiosensitization. Interestingly, we showed that IR alone

induced migration of both HCT116 and HT29 cells, whereas combining TQ with IR reversed this induction. TQ is known to inhibit migration and invasion of cancer cells by targeting EMT markers, such as E cadherin and vimentin [159, 180]. When combined with IR, TQ was able to reverse the IR-induced upregulation of mesenchymal and metastasis markers (integrin αv, MMP2, MMP9) and downregulation of epithelial markers (E cadherin and CK19) in breast cancer cells [142].

Interestingly, our results showed that combining TQ with IR enhanced arrest at the G2/M phase, during which cells are most vulnerable for IR. The induction of G2/M arrest by TQ in irradiated cells is consistent with the mechanism of action of potent radiosensitizing agents studied in CRC models [181-184]. ATM and ATR play important roles in the cellular response to DNA damage and regulation of G2/M checkpoint [185]. Analysis of the active forms of ATM and ATR showed an upregulation at early times following irradiation in HCT116 and HT29 cells treated with TQ and IR. However, significant high levels of p-ATR but not p-ATM were maintained 24 hrs post irradiation in combination-treated cells. Following exposure to IR, double strand breaks (DSBs) activate ATM and ATR, which in turn phosphorylate and activate chk2 and chk1, respectively [66]. ATM is the major kinase that phosphorylates H2AX, but ATR and DNA-PKc kinases can substitute for ATM [186, 187]. Phosphorylation of H2AX is required for the assembly of the DNA repair machinery and for the activation of cell cycle checkpoints [188]. Importantly, an ATM-to-ATR switch is observed during DSB resection, which results in phosphorylation and activation of chk1 leading to G2/M phase arrest [66, 189]. These observations could explain the persistent high levels of p-ATR 24 hrs post irradiation, suggesting that DNA damage induced by combination treatment

results in the activation of both kinases at early times following irradiation, and are thereafter dependent on ATR activation and cell cycle arrest to repair DNA damage.

We next examined the changes in the expression of the DNA damage and repair marker, γH2AX in response to TQ and IR. Radiation-induced cytotoxicity is mediated through induction of DSBs, which are lethal to cells if not repaired [190]. We [159] and others [133, 191-193] have used γ-H2AX foci as a marker for TQ- and radiation-induced DNA damage. Our results showed that the repair of damage began early in CRC cells, as evident from the high number of γH2AX foci only 10 mins post IR. Interestingly, we found a persistent upregulation of this DNA damage marker upon treatment with TQ prior to irradiation. In contrast, cells treated with either TQ or IR had lower γH2AX levels 24 hrs post IR. This suggests that TQ is a potent inducer of DNA damage when combined with IR, whereby it sensitizes HCT116 and HT29 cells to radiation through maintaining constitutive activation of H2AX, resulting in a delayed repair of radiation-induced DSB, cell cycle arrest, and possibly apoptosis.

IR induces direct damage to cells through generation of ROS [194]. Similarly, TQ is also known to for its ROS generating effect in tumor cells [195, 196] Researchers have previously found that it increases ROS levels and decreases glutathione (GSH), an intracellular antioxidant, in prostate cancer cells [197]. This results in induction of growth arrest and DNA damage inducible gene (GADD45alpha) and apoptosis-inducing factor-1 and downregulation of several anti-apoptotic proteins [197]. Thus, we checked for ROS induction upon combining TQ with IR. IR alone induced oxidative stress in HCT116 cells but not in HT29 cells. On the other hand, TQ alone was able to induce ROS generation in both cell lines. Importantly combining TQ and IR led to a more pronounced increase in ROS generation, and this increase was comparable between the two cell lines at low

TQ concentration (10μM), suggesting that TQ radiosensitizes CRC cells to a similar extent, through modulating oxidative stress.

To understand what molecular pathways could be involved in radiosensitization, we focused on pathways implicated in radioresistance. mTOR has a central role in cell proliferation, growth, survival, metabolism. Its frequent activation has been documented in CRC liver metastasis [198]. Importantly, radiation induces mTOR phosphorylation and activation, which contributes to cancer metastasis and radioresistance. On the other hand, inhibiting mTOR sensitizes cancer cells to radiation via mechanisms that involve inhibition of survival and induction of DNA damage and apoptosis [199, 200]. In fact, PI3K/AKT/mTOR could be a potential target in the treatment of CRC [201]. Our results showed that p-mTOR was highly expressed in control and irradiated cancer cells and that combination treatment was successful in reversing this high expression. Importantly, the effect was greater in HT29 cells whereby treatment with low TQ concentrations prior to radiation inhibited mTOR activation and sensitized these cells to radiation. Wnt and MEK/ERK pathways are known to be involved in CRC tumorigenesis and thus, targeting them may be of clinical significance for patients with metastatic CRC [202]. Moreover, MEK/ERK pathway is known to play a role in cell survival and resistance in response to radiation [203]. Therefore, we were interested in studying the potential effects of TQ and IR on these pathways. According to our findings, combination treatment reduced the expression of β-catenin and MEK, suggesting that radiosensitization by TQ may be associated with inhibition of survival and metastasis of CRC cells through targeting these molecules. Interestingly, TQ and IR reduced the expression of NF-κB, which is involved in cellular survival in response to radiation exposure and oxidative stress, in addition to radioresistance [204]. It was shown that TQ sensitizes CRC cells to cisplatin by reducing

phosphorylation levels of NF- κB and thus inhibiting its activation [124]. The inhibition of NF-κB by TQ reduced metastasis of irinotecan-resistant LOVO colon cancer cells [135]. IR alone and in combination with TQ induced the upregulation of p53 and p21 in HCT116 cells, and this upregulation was associated with G2/M arrest. Cell cycle arrest through p53 and p21 activation following DNA damage is well studied [25]. TQ and IR combination upregulated p53 but not p21 in HT29 cells. Treating HCT116 and HT29 with combination treatment reduced the expression of the stem cell marker CD133 in HT29 but not in HCT116 cells, suggesting that combination treatment may be targeting different CRC stem cell markers in these cells. TQ was shown to sensitize cancer cells to radiation through targeting other molecular pathways [141, 142]. TQ alone or in combination with paclitaxel enhanced radiosensitivity of MCF7 and MDA-MB-231 breast cancer cells by inhibiting colony formation, migration and invasion, and EMT via targeting TGF-β, upregulating the epithelial marker E-cadherin and decreasing the expression of several mesenchymal markers including integrin αV and MMPs [142]. Morphologically, TQ reversed the fibroblast-like shape of breast cancer cells that is acquired following irradiation, further confirming inhibition of EMT and metastasis as a mechanism of sensitization. Another study showed that TQ radiosensitized MCF7 and T47D and this sensitization was associated with inhibition of proliferation, colony forming ability, and induction of cell cycle arrest and apoptosis [141]. A synergistic effect of TQ and radiation was observed in HNSCC through inhibition of proliferation [144]. Another study reported that TQ enhanced the effect of gamma knife on proliferation, survival, DNA damage, and apoptosis in melanoma cells by modulating the JAK2/STAT3 pathway [205].

Given that CSCs are the population responsible for radioresistance and tumor relapse, we aimed to study the radiosensitizing potential of TQ in stem/progenitor cells enriched from HCT116 and HT29 cell lines. TQ alone inhibited the sphere-forming and self-renewal capacity of spheres derived from both cell lines, which is consistent with recent findings from our lab [159]. The radiosensitizing effect of TQ was observed at low doses of TQ in colonospheres at G1 and led to depletion of spheres at G5, which suggests that combination of TQ and IR effectively targets resistant CRC stem/progenitor cells and exert a stronger inhibitory effect than either treatment alone. Studies investigating the effect of TQ on cancer stem/progenitor cells are very few. Recent studies have shown that combining TQ with chemotherapeutic agents or natural compounds increases treatment efficacy through enhancing inhibition of CSCs [206-208]. The co-delivery of TQ and Doxorubicin (DOX) in aragonite calcium carbonate nanoparticles (ACNP) attenuated the self-renewal abilities of breast CSCs, which was accompanied with downregulation of the breast CSC markers CD44, CD24, and ALDH1 [209]. Synergism from combining TQ with emodin was observed in breast CSCs against CD44+/CD24- CSCS population through downregulation of stemness markers, OCT-4 and SOX-2 [208]. The combined treatment of TQ and 5-FU depleted CD133+ CSCs and reduced self-renewal potential of CRC stem/progenitor cells, possibly through downregulation of Wnt and PI3K/AKT stemness pathways [140].

To evaluate the underlying mechanism of inhibition by TQ and IR in 3D colonospheres, we determined the effect of combination treatment on DNA damage and on the expression of several CRC stem cell markers and major stem cell regulatory pathways. Our results showed no change in γH2AX levels following treatment with TQ or IR alone, which translates into a highly efficient activation of DDR and repair in CSCs

[210]. Interestingly, combination of TQ and IR led to increased phosphorylation of H2AX, suggesting radiosensitization of resistant CSCs through diminishing their DNA damage repair ability. Moreover, we showed high expression of CD44 in control and irradiated HCT116 and HT29 spheres and that TQ sensitized spheres to radiation by reducing its expression. TQ alone downregulated CD44 expression, which is in agreement with our previous findings that showed a decrease in CD44 in spheres derived from HCT116 cells [159]. The inhibition of sphere forming ability seen here correlated with the decrease in this stem cell marker upon treatment with TQ alone or TQ and IR combination. Combination treatment led to reduction in the expression of CK8 and CK19 in CSCs enriched from HCT116 but not HT29 cells. This suggests a different mechanism of stemness inhibition by TQ and IR in different CSCs, whereby inhibition is mediated by downregulation of two CSC markers CD44 and CK19 in HCT116 spheres and of CD44 in HT29 spheres. Importantly, treating HCT116 and HT29 spheres with TQ and IR combination also reduced the expression of CD133, which is associated with migration and stemness in CRC, in addition to chemotherapy resistance [211]. CD44 and CD133 are recognized among others as putative stem cell markers in CRC [212, 213]. The high expression of CD44 and CD133 in CSCs that were derived from HCT116 and HT29 cells confirms enrichment of cells having stem-like properties in our 3D colonosphere cultures. Both markers have high prognostic impact, however the functional relevance of CD133 for the metastasis of CRC is still not very clear [213, 214]. CD44 is a surface glycoprotein that plays a role in several key processes including survival, growth, stemness, cell migration. CD44 is partly activated by Wnt/β catenin pathway [104], which explains the decrease in its expression, in line with the observed downregulation of β catenin in combination treated HCT116 and HT29 spheres. CK19, which was significantly

downregulated in HCT116 spheres treated with combination, is known to be a colon lineage epithelial and CSC marker and is therefore used to identify circulating CRC stem cells and to confirm their epithelial nature [215]. In fact, CK8 and CK19 have been reported to be the most abundant cytokeratin epithelial markers in sporadic CRC [216].

As for the PDOs established in this study, different responses to individual and combination treatments were observed, which could be explained by the differences in clinical and histopathological characteristics, such as tumor location and stage. Organoids derived from patient 1 were the most resistant to IR. Notably, TQ radiosensitized these organoids by reducing their total count and size. In patient 2, IR alone was good as standalone treatment for the established organoids. These organoids were partially sensitive to irradiation, and combination treatment had a similar effect, as compared to IR alone, on the organoid forming ability. Only combination treatment had an inhibitory effect on organoid size, suggesting inhibition of proliferation in response to TQ and IR combinations. OFC of organoids from patient 3 were drastically reduced by IR alone, indicating high sensitivity to IR, and combination of TQ with IR resulted in similar inhibition by IR alone on OFC. Interestingly, TQ was good as a standalone treatment for organoids derived from this patient. Similar to patient 2, organoid size was reduced in combination-treated organoids.

Interestingly, organoids derived from HT29 cells and patient 1 tumor tissue showed similar response to individual and combination treatments. On the other hand, combining TQ and IR in HCT116 organoids showed comparable effect to TQ or IR alone, suggesting that higher TQ concentration should be used to sensitize these organoids to radiation.

CD44 has prognostic and clinical value in CRC and has been used to predict unfavorable prognosis and cancer aggressiveness [217]. High expression of CD44 has been associated with self-renewal, tumor initiation and metastasis, as well as resistance to apoptosis and to chemo- and radiotherapy [218, 219]. CK19 expression has been also shown to be associated with carcinogenesis of colon cancer [220]. Therefore, the high expression of these CRC stem cell markers in the established PDOs, as well as in the corresponding parental tumor tissues, confirms the presence of CSCs and the maintenance of tumor tissue molecular characteristics in these disease models. Interestingly, data from patient 1-derived organoids showed a decrease in the expression of CD44 and CK19 upon treatment with TQ and IR, suggesting that combination treatment is effective in targeting stemness pathways in radiation-resistant CSCs.

Further analysis of parental tumor tissues showed positive staining for the proliferation marker Ki67, in addition to the epithelial marker CK8 and stemness marker β-catenin. The epithelial cytokeratin CK8 is found in most cancers and has prognostic value in colon cancer [221].

Patient-derived organoids are superior models to identify and study potential anti-cancer drugs and compounds and have been shown to be a powerful preclinical platform for drug testing and personalized therapy. These models retain and thus recapitulate basic biological functions and characteristics of their source tumor, including histological complexity and genetic heterogeneity of cancer tissue, in contrast to 2D monolayer cultures [222, 223]. We have succeeded in establishing patient-derived CRC organoids and characterizing the expression of some CSC markers in primary tumor tissue and patient-matched organoids and we showed a positive expression in our PDOs and their corresponding tissue of origin.

The present study has several limitations. We acknowledge that the patient sample size is small and dependent on the availability of tissues at the time of the study. Additionally, among the few tissue samples we received, only three successfully formed PDOs in culture, possibly due to limitations in tissue quality and size, which hindered organoid derivation. Also, PDO staining was limited by the low number of organoids generated, mainly in treated groups. Future investigations are essential to validate the radiosensitizing effects of TQ on additional colon/rectal patient samples and to link the differential responses to clinical variables. It remains essential to determine the radiosensitizing effects of TQ on more CRC cell lines and the mechanisms of radiosensitization in 2D and 3D cultures. It would be interesting to study effect on several pathways and molecules implicated in radioresistance and survival (PI3K/Akt/mTOR and Notch) and DNA damage repair (DNA-PKc, RAD51, and BRCA). Mechanistic studies in vitro could be followed by validation in PDOs, which have more physiological and clinical relevance relative to 2D and 3D spheroid cultures and offer a suitable tool for predicting patients' drug response and implementing personalized medicine. Based on future experiments, our data hold promise for the potential use of TQ as a potent radiosensitizing agent in clinical practice, with minimal toxicity on normal tissue.

In summary, we reported for the first time a radiosensitizing potential of TQ in 2D and 3D cultures of CRC cells and in PDOs. Importantly, radiosensitization was associated with inhibition of cell viability, colony forming ability, migration, cell cycle progression, and DNA repair ability. TQ in combination with IR also targeted pathways implicated in survival, stemness, and radioresistance in cancer cells and cancer stem/progenitor cells. Based on these results, combination of TQ with radiation might

represent a useful tool for targeting radiation-resistant cancer cells and stem/progenitor cells.

BIBLIOGRAPHY

[1] P. Kahai, P. Mandiga, C.J. Wehrle, S. Lobo, Anatomy, Abdomen and Pelvis, Large Intestine, StatPearls, Treasure Island (FL), 2022.
[2] P. Minoo, I. Zlobec, M. Peterson, L. Terracciano, A. Lugli, Characterization of rectal, proximal and distal colon cancers based on clinicopathological, molecular and protein profiles, Int J Oncol, 37 (2010) 707-718.
[3] N. Barker, J.H. van Es, V. Jaks, M. Kasper, H. Snippert, R. Toftgard, H. Clevers, Very long-term self-renewal of small intestine, colon, and hair follicles from cycling Lgr5+ve stem cells, Cold Spring Harb Symp Quant Biol, 73 (2008) 351-356.
[4] E. Sancho, E. Batlle, H. Clevers, Live and let die in the intestinal epithelium, Curr Opin Cell Biol, 15 (2003) 763-770.
[5] N. Barker, M. van de Wetering, H. Clevers, The intestinal stem cell, Genes Dev, 22 (2008) 1856-1864.
[6] D.J. Huels, O.J. Sansom, Stem vs non-stem cell origin of colorectal cancer, Br J Cancer, 113 (2015) 1-5.
[7] N. Barker, J.H. van Es, J. Kuipers, P. Kujala, M. van den Born, M. Cozijnsen, A. Haegebarth, J. Korving, H. Begthel, P.J. Peters, H. Clevers, Identification of stem cells in small intestine and colon by marker gene Lgr5, Nature, 449 (2007) 1003-1007.
[8] D. Hu, H. Yan, X.C. He, L. Li, Recent advances in understanding intestinal stem cell regulation, F1000Res, 8 (2019).
[9] M. Yousefi, L. Li, C.J. Lengner, Hierarchy and Plasticity in the Intestinal Stem Cell Compartment, Trends Cell Biol, 27 (2017) 753-764.
[10] A.J.M. Santos, Y.H. Lo, A.T. Mah, C.J. Kuo, The Intestinal Stem Cell Niche: Homeostasis and Adaptations, Trends Cell Biol, 28 (2018) 1062-1078.
[11] Colorectal Cancer Facts & Figures 2020-2022., American Cancer Society, (2022).
[12] P.H. Viale, The American Cancer Society's Facts & Figures: 2020 Edition, J Adv Pract Oncol, 11 (2020) 135-136.
[13] R.L. Siegel, K.D. Miller, H.E. Fuchs, A. Jemal, Cancer statistics, 2022, CA Cancer J Clin, 72 (2022) 7-33.
[14] R.L. Siegel, K.D. Miller, H.E. Fuchs, A. Jemal, Cancer Statistics, 2021, CA Cancer J Clin, 71 (2021) 7-33.
[15] F.A. Haggar, R.P. Boushey, Colorectal cancer epidemiology: incidence, mortality, survival, and risk factors, Clin Colon Rectal Surg, 22 (2009) 191-197.
[16] V. Janout, H. Kollarova, Epidemiology of colorectal cancer, Biomed Pap Med Fac Univ Palacky Olomouc Czech Repub, 145 (2001) 5-10.
[17] M.B. Yurgelun, M.H. Kulke, C.S. Fuchs, B.A. Allen, H. Uno, J.L. Hornick, C.I. Ukaegbu, L.K. Brais, P.G. McNamara, R.J. Mayer, D. Schrag, J.A. Meyerhardt, K. Ng, J. Kidd, N. Singh, A.R. Hartman, R.J. Wenstrup, S. Syngal, Cancer Susceptibility Gene Mutations in Individuals With Colorectal Cancer, J Clin Oncol, 35 (2017) 1086-1095.
[18] J. Bogaert, H. Prenen, Molecular genetics of colorectal cancer, Ann Gastroenterol, 27 (2014) 9-14.
[19] H. Yamagishi, H. Kuroda, Y. Imai, H. Hiraishi, Molecular pathogenesis of sporadic colorectal cancers, Chin J Cancer, 35 (2016) 4.
[20] E.R. Fearon, B. Vogelstein, A genetic model for colorectal tumorigenesis, Cell, 61 (1990) 759-767.

[21] K.W. Kinzler, B. Vogelstein, Lessons from hereditary colorectal cancer, Cell, 87 (1996) 159-170.
[22] B. Rubinfeld, I. Albert, E. Porfiri, S. Munemitsu, P. Polakis, Loss of beta-catenin regulation by the APC tumor suppressor protein correlates with loss of structure due to common somatic mutations of the gene, Cancer Res, 57 (1997) 4624-4630.
[23] E.J. Kuipers, W.M. Grady, D. Lieberman, T. Seufferlein, J.J. Sung, P.G. Boelens, C.J. van de Velde, T. Watanabe, Colorectal cancer, Nat Rev Dis Primers, 1 (2015) 15065.
[24] S.J. Baker, A.C. Preisinger, J.M. Jessup, C. Paraskeva, S. Markowitz, J.K. Willson, S. Hamilton, B. Vogelstein, p53 gene mutations occur in combination with 17p allelic deletions as late events in colorectal tumorigenesis, Cancer Res, 50 (1990) 7717-7722.
[25] S. Al Bitar, H. Gali-Muhtasib, The Role of the Cyclin Dependent Kinase Inhibitor p21(cip1/waf1) in Targeting Cancer: Molecular Mechanisms and Novel Therapeutics, Cancers (Basel), 11 (2019).
[26] A.J. Levine, p53, the cellular gatekeeper for growth and division, Cell, 88 (1997) 323-331.
[27] M. Bettington, N. Walker, A. Clouston, I. Brown, B. Leggett, V. Whitehall, The serrated pathway to colorectal carcinoma: current concepts and challenges, Histopathology, 62 (2013) 367-386.
[28] J.P. Issa, Colon cancer: it's CIN or CIMP, Clin Cancer Res, 14 (2008) 5939-5940.
[29] M.S. Pino, D.C. Chung, The chromosomal instability pathway in colon cancer, Gastroenterology, 138 (2010) 2059-2072.
[30] D.J. Weisenberger, K.D. Siegmund, M. Campan, J. Young, T.I. Long, M.A. Faasse, G.H. Kang, M. Widschwendter, D. Weener, D. Buchanan, H. Koh, L. Simms, M. Barker, B. Leggett, J. Levine, M. Kim, A.J. French, S.N. Thibodeau, J. Jass, R. Haile, P.W. Laird, CpG island methylator phenotype underlies sporadic microsatellite instability and is tightly associated with BRAF mutation in colorectal cancer, Nat Genet, 38 (2006) 787-793.
[31] L. Shen, M. Toyota, Y. Kondo, E. Lin, L. Zhang, Y. Guo, N.S. Hernandez, X. Chen, S. Ahmed, K. Konishi, S.R. Hamilton, J.P. Issa, Integrated genetic and epigenetic analysis identifies three different subclasses of colon cancer, Proc Natl Acad Sci U S A, 104 (2007) 18654-18659.
[32] B.A. Cisterna, N. Kamaly, W.I. Choi, A. Tavakkoli, O.C. Farokhzad, C. Vilos, Targeted nanoparticles for colorectal cancer, Nanomedicine (Lond), 11 (2016) 2443-2456.
[33] A. Varghese, Chemotherapy for Stage II Colon Cancer, Clin Colon Rectal Surg, 28 (2015) 256-261.
[34] L.H. Biller, D. Schrag, Diagnosis and Treatment of Metastatic Colorectal Cancer: A Review, JAMA, 325 (2021) 669-685.
[35] M.F. Hafner, J. Debus, Radiotherapy for Colorectal Cancer: Current Standards and Future Perspectives, Visc Med, 32 (2016) 172-177.
[36] T. Lapidot, C. Sirard, J. Vormoor, B. Murdoch, T. Hoang, J. Caceres-Cortes, M. Minden, B. Paterson, M.A. Caligiuri, J.E. Dick, A cell initiating human acute myeloid leukaemia after transplantation into SCID mice, Nature, 367 (1994) 645-648.
[37] D. Bonnet, J.E. Dick, Human acute myeloid leukemia is organized as a hierarchy that originates from a primitive hematopoietic cell, Nat Med, 3 (1997) 730-737.

[38] M. Shimokawa, Y. Ohta, S. Nishikori, M. Matano, A. Takano, M. Fujii, S. Date, S. Sugimoto, T. Kanai, T. Sato, Visualization and targeting of LGR5(+) human colon cancer stem cells, Nature, 545 (2017) 187-192.
[39] M. Shibata, M.O. Hoque, Targeting Cancer Stem Cells: A Strategy for Effective Eradication of Cancer, Cancers (Basel), 11 (2019).
[40] G. Bhardwaj, B. Murdoch, D. Wu, D.P. Baker, K.P. Williams, K. Chadwick, L.E. Ling, F.N. Karanu, M. Bhatia, Sonic hedgehog induces the proliferation of primitive human hematopoietic cells via BMP regulation, Nat Immunol, 2 (2001) 172-180.
[41] J. Wang, T.P. Wakeman, J.D. Lathia, A.B. Hjelmeland, X.F. Wang, R.R. White, J.N. Rich, B.A. Sullenger, Notch promotes radioresistance of glioma stem cells, Stem Cells, 28 (2010) 17-28.
[42] S.S. Kanwar, Y. Yu, J. Nautiyal, B.B. Patel, A.P. Majumdar, The Wnt/beta-catenin pathway regulates growth and maintenance of colonospheres, Mol Cancer, 9 (2010) 212.
[43] S.K. Singh, C. Hawkins, I.D. Clarke, J.A. Squire, J. Bayani, T. Hide, R.M. Henkelman, M.D. Cusimano, P.B. Dirks, Identification of human brain tumour initiating cells, Nature, 432 (2004) 396-401.
[44] P. Dalerba, S.J. Dylla, I.K. Park, R. Liu, X. Wang, R.W. Cho, T. Hoey, A. Gurney, E.H. Huang, D.M. Simeone, A.A. Shelton, G. Parmiani, C. Castelli, M.F. Clarke, Phenotypic characterization of human colorectal cancer stem cells, Proc Natl Acad Sci U S A, 104 (2007) 10158-10163.
[45] L. Ricci-Vitiani, D.G. Lombardi, E. Pilozzi, M. Biffoni, M. Todaro, C. Peschle, R. De Maria, Identification and expansion of human colon-cancer-initiating cells, Nature, 445 (2007) 111-115.
[46] A.V. Krivtsov, D. Twomey, Z. Feng, M.C. Stubbs, Y. Wang, J. Faber, J.E. Levine, J. Wang, W.C. Hahn, D.G. Gilliland, T.R. Golub, S.A. Armstrong, Transformation from committed progenitor to leukaemia stem cell initiated by MLL-AF9, Nature, 442 (2006) 818-822.
[47] B.J. Huntly, H. Shigematsu, K. Deguchi, B.H. Lee, S. Mizuno, N. Duclos, R. Rowan, S. Amaral, D. Curley, I.R. Williams, K. Akashi, D.G. Gilliland, MOZ-TIF2, but not BCR-ABL, confers properties of leukemic stem cells to committed murine hematopoietic progenitors, Cancer Cell, 6 (2004) 587-596.
[48] S.A. Mani, W. Guo, M.J. Liao, E.N. Eaton, A. Ayyanan, A.Y. Zhou, M. Brooks, F. Reinhard, C.C. Zhang, M. Shipitsin, L.L. Campbell, K. Polyak, C. Brisken, J. Yang, R.A. Weinberg, The epithelial-mesenchymal transition generates cells with properties of stem cells, Cell, 133 (2008) 704-715.
[49] S. Schwitalla, A.A. Fingerle, P. Cammareri, T. Nebelsiek, S.I. Goktuna, P.K. Ziegler, O. Canli, J. Heijmans, D.J. Huels, G. Moreaux, R.A. Rupec, M. Gerhard, R. Schmid, N. Barker, H. Clevers, R. Lang, J. Neumann, T. Kirchner, M.M. Taketo, G.R. van den Brink, O.J. Sansom, M.C. Arkan, F.R. Greten, Intestinal tumorigenesis initiated by dedifferentiation and acquisition of stem-cell-like properties, Cell, 152 (2013) 25-38.
[50] Z. Huang, T. Wu, A.Y. Liu, G. Ouyang, Differentiation and transdifferentiation potentials of cancer stem cells, Oncotarget, 6 (2015) 39550-39563.
[51] A.Q. Khan, E.I. Ahmed, N.R. Elareer, K. Junejo, M. Steinhoff, S. Uddin, Role of miRNA-Regulated Cancer Stem Cells in the Pathogenesis of Human Malignancies, Cells, 8 (2019).

[52] M.C. Cleophas, L.A. Joosten, L.K. Stamp, N. Dalbeth, O.M. Woodward, T.R. Merriman, ABCG2 polymorphisms in gout: insights into disease susceptibility and treatment approaches, Pharmgenomics Pers Med, 10 (2017) 129-142.
[53] W. Gao, L. Chen, Z. Ma, Z. Du, Z. Zhao, Z. Hu, Q. Li, Isolation and phenotypic characterization of colorectal cancer stem cells with organ-specific metastatic potential, Gastroenterology, 145 (2013) 636-646 e635.
[54] I.M. Shih, T.L. Wang, G. Traverso, K. Romans, S.R. Hamilton, S. Ben-Sasson, K.W. Kinzler, B. Vogelstein, Top-down morphogenesis of colorectal tumors, Proc Natl Acad Sci U S A, 98 (2001) 2640-2645.
[55] S.L. Preston, W.M. Wong, A.O. Chan, R. Poulsom, R. Jeffery, R.A. Goodlad, N. Mandir, G. Elia, M. Novelli, W.F. Bodmer, I.P. Tomlinson, N.A. Wright, Bottom-up histogenesis of colorectal adenomas: origin in the monocryptal adenoma and initial expansion by crypt fission, Cancer Res, 63 (2003) 3819-3825.
[56] S. Basu, G. Haase, A. Ben-Ze'ev, Wnt signaling in cancer stem cells and colon cancer metastasis, F1000Res, 5 (2016).
[57] N. Takebe, P.J. Harris, R.Q. Warren, S.P. Ivy, Targeting cancer stem cells by inhibiting Wnt, Notch, and Hedgehog pathways, Nat Rev Clin Oncol, 8 (2011) 97-106.
[58] R. Vadde, S. Vemula, R. Jinka, N. Merchant, P.V. Bramhachari, G.P. Nagaraju, Role of hypoxia-inducible factors (HIF) in the maintenance of stemness and malignancy of colorectal cancer, Crit Rev Oncol Hematol, 113 (2017) 22-27.
[59] J.Y. Wang, C.C. Chang, C.C. Chiang, W.M. Chen, S.C. Hung, Silibinin suppresses the maintenance of colorectal cancer stem-like cells by inhibiting PP2A/AKT/mTOR pathways, J Cell Biochem, 113 (2012) 1733-1743.
[60] Y. Zhou, L. Xia, H. Wang, L. Oyang, M. Su, Q. Liu, J. Lin, S. Tan, Y. Tian, Q. Liao, D. Cao, Cancer stem cells in progression of colorectal cancer, Oncotarget, 9 (2018) 33403-33415.
[61] S. Toden, H.M. Tran, O.A. Tovar-Camargo, Y. Okugawa, A. Goel, Epigallocatechin-3-gallate targets cancer stem-like cells and enhances 5-fluorouracil chemosensitivity in colorectal cancer, Oncotarget, 7 (2016) 16158-16171.
[62] F. Li, K. Zhou, L. Gao, B. Zhang, W. Li, W. Yan, X. Song, H. Yu, S. Wang, N. Yu, Q. Jiang, Radiation induces the generation of cancer stem cells: A novel mechanism for cancer radioresistance, Oncol Lett, 12 (2016) 3059-3065.
[63] Y.K. Su, P.H. Shih, W.H. Lee, O.A. Bamodu, A.T.H. Wu, C.C. Huang, Y.M. Tzeng, M. Hsiao, C.T. Yeh, C.M. Lin, Antrodia cinnamomea sensitizes radio-/chemo-therapy of cancer stem-like cells by modulating microRNA expression, J Ethnopharmacol, 207 (2017) 47-56.
[64] Y.C. He, F.L. Zhou, Y. Shen, D.F. Liao, D. Cao, Apoptotic death of cancer stem cells for cancer therapy, Int J Mol Sci, 15 (2014) 8335-8351.
[65] C.G. Broustas, H.B. Lieberman, DNA damage response genes and the development of cancer metastasis, Radiat Res, 181 (2014) 111-130.
[66] A. Marechal, L. Zou, DNA damage sensing by the ATM and ATR kinases, Cold Spring Harb Perspect Biol, 5 (2013).
[67] H.C. Reinhardt, M.B. Yaffe, Kinases that control the cell cycle in response to DNA damage: Chk1, Chk2, and MK2, Curr Opin Cell Biol, 21 (2009) 245-255.
[68] M. Donzelli, G.F. Draetta, Regulating mammalian checkpoints through Cdc25 inactivation, EMBO Rep, 4 (2003) 671-677.

[69] N. Kangwan, Y.J. Kim, Y.M. Han, M. Jeong, J.M. Park, E.J. Go, K.B. Hahm, Sonic hedgehog inhibitors prevent colitis-associated cancer via orchestrated mechanisms of IL-6/gp130 inhibition, 15-PGDH induction, Bcl-2 abrogation, and tumorsphere inhibition, Oncotarget, 7 (2016) 7667-7682.
[70] Y.L. Sun, A. Patel, P. Kumar, Z.S. Chen, Role of ABC transporters in cancer chemotherapy, Chin J Cancer, 31 (2012) 51-57.
[71] L.G. Bastos, P.G. de Marcondes, J.C. de-Freitas-Junior, F. Leve, A.L. Mencalha, W.F. de Souza, W.M. de Araujo, M.N. Tanaka, E.S. Abdelhay, J.A. Morgado-Diaz, Progeny from irradiated colorectal cancer cells acquire an EMT-like phenotype and activate Wnt/beta-catenin pathway, J Cell Biochem, 115 (2014) 2175-2187.
[72] P.A. Sotiropoulou, M.S. Christodoulou, A. Silvani, C. Herold-Mende, D. Passarella, Chemical approaches to targeting drug resistance in cancer stem cells, Drug Discov Today, 19 (2014) 1547-1562.
[73] L.B. Weiswald, D. Bellet, V. Dangles-Marie, Spherical cancer models in tumor biology, Neoplasia, 17 (2015) 1-15.
[74] B. Bao, A. Ahmad, A.S. Azmi, S. Ali, F.H. Sarkar, Overview of cancer stem cells (CSCs) and mechanisms of their regulation: implications for cancer therapy, Curr Protoc Pharmacol, Chapter 14 (2013) Unit 14 25.
[75] G. Mehta, A.Y. Hsiao, M. Ingram, G.D. Luker, S. Takayama, Opportunities and challenges for use of tumor spheroids as models to test drug delivery and efficacy, J Control Release, 164 (2012) 192-204.
[76] Y.S. Torisawa, A. Takagi, H. Shiku, T. Yasukawa, T. Matsue, A multicellular spheroid-based drug sensitivity test by scanning electrochemical microscopy, Oncol Rep, 13 (2005) 1107-1112.
[77] D.E. Discher, D.J. Mooney, P.W. Zandstra, Growth factors, matrices, and forces combine and control stem cells, Science, 324 (2009) 1673-1677.
[78] D. Dutta, I. Heo, H. Clevers, Disease Modeling in Stem Cell-Derived 3D Organoid Systems, Trends Mol Med, 23 (2017) 393-410.
[79] M.A. Lancaster, J.A. Knoblich, Organogenesis in a dish: modeling development and disease using organoid technologies, Science, 345 (2014) 1247125.
[80] M. Huch, B.K. Koo, Modeling mouse and human development using organoid cultures, Development, 142 (2015) 3113-3125.
[81] A. Ootani, X. Li, E. Sangiorgi, Q.T. Ho, H. Ueno, S. Toda, H. Sugihara, K. Fujimoto, I.L. Weissman, M.R. Capecchi, C.J. Kuo, Sustained in vitro intestinal epithelial culture within a Wnt-dependent stem cell niche, Nat Med, 15 (2009) 701-706.
[82] T. Sato, R.G. Vries, H.J. Snippert, M. van de Wetering, N. Barker, D.E. Stange, J.H. van Es, A. Abo, P. Kujala, P.J. Peters, H. Clevers, Single Lgr5 stem cells build crypt-villus structures in vitro without a mesenchymal niche, Nature, 459 (2009) 262-265.
[83] T. Sato, D.E. Stange, M. Ferrante, R.G. Vries, J.H. Van Es, S. Van den Brink, W.J. Van Houdt, A. Pronk, J. Van Gorp, P.D. Siersema, H. Clevers, Long-term expansion of epithelial organoids from human colon, adenoma, adenocarcinoma, and Barrett's epithelium, Gastroenterology, 141 (2011) 1762-1772.
[84] T. Seidlitz, S.R. Merker, A. Rothe, F. Zakrzewski, C. von Neubeck, K. Grutzmann, U. Sommer, C. Schweitzer, S. Scholch, H. Uhlemann, A.M. Gaebler, K. Werner, M. Krause, G.B. Baretton, T. Welsch, B.K. Koo, D.E. Aust, B. Klink, J. Weitz, D.E. Stange, Human gastric cancer modelling using organoids, Gut, 68 (2019) 207-217.

[85] H.H.N. Yan, H.C. Siu, S. Law, S.L. Ho, S.S.K. Yue, W.Y. Tsui, D. Chan, A.S. Chan, S. Ma, K.O. Lam, S. Bartfeld, A.H.Y. Man, B.C.H. Lee, A.S.Y. Chan, J.W.H. Wong, P.S.W. Cheng, A.K.W. Chan, J. Zhang, J. Shi, X. Fan, D.L.W. Kwong, T.W. Mak, S.T. Yuen, H. Clevers, S.Y. Leung, A Comprehensive Human Gastric Cancer Organoid Biobank Captures Tumor Subtype Heterogeneity and Enables Therapeutic Screening, Cell Stem Cell, 23 (2018) 882-897 e811.
[86] R.M. Engel, W.H. Chan, D. Nickless, S. Hlavca, E. Richards, G. Kerr, K. Oliva, P.J. McMurrick, T. Jarde, H.E. Abud, Patient-Derived Colorectal Cancer Organoids Upregulate Revival Stem Cell Marker Genes following Chemotherapeutic Treatment, J Clin Med, 9 (2020).
[87] S.N. Ooft, F. Weeber, K.K. Dijkstra, C.M. McLean, S. Kaing, E. van Werkhoven, L. Schipper, L. Hoes, D.J. Vis, J. van de Haar, W. Prevoo, P. Snaebjornsson, D. van der Velden, M. Klein, M. Chalabi, H. Boot, M. van Leerdam, H.J. Bloemendal, L.V. Beerepoot, L. Wessels, E. Cuppen, H. Clevers, E.E. Voest, Patient-derived organoids can predict response to chemotherapy in metastatic colorectal cancer patients, Sci Transl Med, 11 (2019).
[88] E. Driehuis, A. van Hoeck, K. Moore, S. Kolders, H.E. Francies, M.C. Gulersonmez, E.C.A. Stigter, B. Burgering, V. Geurts, A. Gracanin, G. Bounova, F.H. Morsink, R. Vries, S. Boj, J. van Es, G.J.A. Offerhaus, O. Kranenburg, M.J. Garnett, L. Wessels, E. Cuppen, L.A.A. Brosens, H. Clevers, Pancreatic cancer organoids recapitulate disease and allow personalized drug screening, Proc Natl Acad Sci U S A, (2019).
[89] L. Broutier, G. Mastrogiovanni, M.M. Verstegen, H.E. Francies, L.M. Gavarro, C.R. Bradshaw, G.E. Allen, R. Arnes-Benito, O. Sidorova, M.P. Gaspersz, N. Georgakopoulos, B.K. Koo, S. Dietmann, S.E. Davies, R.K. Praseedom, R. Lieshout, I.J. JNM, S.J. Wigmore, K. Saeb-Parsy, M.J. Garnett, L.J. van der Laan, M. Huch, Human primary liver cancer-derived organoid cultures for disease modeling and drug screening, Nat Med, 23 (2017) 1424-1435.
[90] S.H. Lee, W. Hu, J.T. Matulay, M.V. Silva, T.B. Owczarek, K. Kim, C.W. Chua, L.J. Barlow, C. Kandoth, A.B. Williams, S.K. Bergren, E.J. Pietzak, C.B. Anderson, M.C. Benson, J.A. Coleman, B.S. Taylor, C. Abate-Shen, J.M. McKiernan, H. Al-Ahmadie, D.B. Solit, M.M. Shen, Tumor Evolution and Drug Response in Patient-Derived Organoid Models of Bladder Cancer, Cell, 173 (2018) 515-528 e517.
[91] X. Li, H.E. Francies, M. Secrier, J. Perner, A. Miremadi, N. Galeano-Dalmau, W.J. Barendt, L. Letchford, G.M. Leyden, E.K. Goffin, A. Barthorpe, H. Lightfoot, E. Chen, J. Gilbert, A. Noorani, G. Devonshire, L. Bower, A. Grantham, S. MacRae, N. Grehan, D.C. Wedge, R.C. Fitzgerald, M.J. Garnett, Organoid cultures recapitulate esophageal adenocarcinoma heterogeneity providing a model for clonality studies and precision therapeutics, Nat Commun, 9 (2018) 2983.
[92] F. Jacob, R.D. Salinas, D.Y. Zhang, P.T.T. Nguyen, J.G. Schnoll, S.Z.H. Wong, R. Thokala, S. Sheikh, D. Saxena, S. Prokop, D.A. Liu, X. Qian, D. Petrov, T. Lucas, H.I. Chen, J.F. Dorsey, K.M. Christian, Z.A. Binder, M. Nasrallah, S. Brem, D.M. O'Rourke, G.L. Ming, H. Song, A Patient-Derived Glioblastoma Organoid Model and Biobank Recapitulates Inter- and Intra-tumoral Heterogeneity, Cell, 180 (2020) 188-204 e122.
[93] M. Kim, H. Mun, C.O. Sung, E.J. Cho, H.J. Jeon, S.M. Chun, D.J. Jung, T.H. Shin, G.S. Jeong, D.K. Kim, E.K. Choi, S.Y. Jeong, A.M. Taylor, S. Jain, M. Meyerson, S.J.

Jang, Patient-derived lung cancer organoids as in vitro cancer models for therapeutic screening, Nat Commun, 10 (2019) 3991.
[94] M. Boretto, N. Maenhoudt, X. Luo, A. Hennes, B. Boeckx, B. Bui, R. Heremans, L. Perneel, H. Kobayashi, I. Van Zundert, H. Brems, B. Cox, M. Ferrante, I.H. Uji, K.P. Koh, T. D'Hooghe, A. Vanhie, I. Vergote, C. Meuleman, C. Tomassetti, D. Lambrechts, J. Vriens, D. Timmerman, H. Vankelecom, Patient-derived organoids from endometrial disease capture clinical heterogeneity and are amenable to drug screening, Nat Cell Biol, 21 (2019) 1041-1051.
[95] J. Azar, H.F. Bahmad, D. Daher, M.M. Moubarak, O. Hadadeh, A. Monzer, S. Al Bitar, M. Jamal, M. Al-Sayegh, W. Abou-Kheir, The Use of Stem Cell-Derived Organoids in Disease Modeling: An Update, Int J Mol Sci, 22 (2021).
[96] D. Ohlund, A. Handly-Santana, G. Biffi, E. Elyada, A.S. Almeida, M. Ponz-Sarvise, V. Corbo, T.E. Oni, S.A. Hearn, E.J. Lee, Chio, II, C.I. Hwang, H. Tiriac, L.A. Baker, D.D. Engle, C. Feig, A. Kultti, M. Egeblad, D.T. Fearon, J.M. Crawford, H. Clevers, Y. Park, D.A. Tuveson, Distinct populations of inflammatory fibroblasts and myofibroblasts in pancreatic cancer, J Exp Med, 214 (2017) 579-596.
[97] K. Ganesh, C. Wu, K.P. O'Rourke, B.C. Szeglin, Y. Zheng, C.G. Sauve, M. Adileh, I. Wasserman, M.R. Marco, A.S. Kim, M. Shady, F. Sanchez-Vega, W.R. Karthaus, H.H. Won, S.H. Choi, R. Pelossof, A. Barlas, P. Ntiamoah, E. Pappou, A. Elghouayel, J.S. Strong, C.T. Chen, J.W. Harris, M.R. Weiser, G.M. Nash, J.G. Guillem, I.H. Wei, R.N. Kolesnick, H. Veeraraghavan, E.J. Ortiz, I. Petkovska, A. Cercek, K.O. Manova-Todorova, L.B. Saltz, J.A. Lavery, R.P. DeMatteo, J. Massague, P.B. Paty, R. Yaeger, X. Chen, S. Patil, H. Clevers, M.F. Berger, S.W. Lowe, J. Shia, P.B. Romesser, L.E. Dow, J. Garcia-Aguilar, C.L. Sawyers, J.J. Smith, A rectal cancer organoid platform to study individual responses to chemoradiation, Nat Med, 25 (2019) 1607-1614.
[98] Y. Yao, X. Xu, L. Yang, J. Zhu, J. Wan, L. Shen, F. Xia, G. Fu, Y. Deng, M. Pan, Q. Guo, X. Gao, Y. Li, X. Rao, Y. Zhou, L. Liang, Y. Wang, J. Zhang, H. Zhang, G. Li, L. Zhang, J. Peng, S. Cai, C. Hu, J. Gao, H. Clevers, Z. Zhang, G. Hua, Patient-Derived Organoids Predict Chemoradiation Responses of Locally Advanced Rectal Cancer, Cell Stem Cell, 26 (2020) 17-26 e16.
[99] A. Costales-Carrera, A. Fernandez-Barral, P. Bustamante-Madrid, L. Guerra, R. Cantero, A. Barbachano, A. Munoz, Plocabulin Displays Strong Cytotoxic Activity in a Personalized Colon Cancer Patient-Derived 3D Organoid Assay, Mar Drugs, 17 (2019).
[100] M.A. Koppens, G. Bounova, P. Cornelissen-Steijger, N. de Vries, O.J. Sansom, L.F. Wessels, M. van Lohuizen, Large variety in a panel of human colon cancer organoids in response to EZH2 inhibition, Oncotarget, 7 (2016) 69816-69828.
[101] P.G. Staff, Correction: Heterogeneous pathway activation and drug response modelled in colorectal-tumor-derived 3D cultures, PLoS Genet, 15 (2019) e1008183.
[102] S.F. Zerp, Z. Bibi, I. Verbrugge, E.E. Voest, M. Verheij, Enhancing radiation response by a second-generation TRAIL receptor agonist using a new in vitro organoid model system, Clin Transl Radiat Oncol, 24 (2020) 1-9.
[103] M. Riihimaki, A. Hemminki, J. Sundquist, K. Hemminki, Patterns of metastasis in colon and rectal cancer, Sci Rep, 6 (2016) 29765.
[104] M.J. Munro, S.K. Wickremesekera, L. Peng, S.T. Tan, T. Itinteang, Cancer stem cells in colorectal cancer: a review, J Clin Pathol, 71 (2018) 110-116.

[105] W.A. Hammond, A. Swaika, K. Mody, Pharmacologic resistance in colorectal cancer: a review, Ther Adv Med Oncol, 8 (2016) 57-84.
[106] R. Akhtar, S. Chandel, P. Sarotra, B. Medhi, Current status of pharmacological treatment of colorectal cancer, World J Gastrointest Oncol, 6 (2014) 177-183.
[107] N. Ikoma, K. Raghav, G. Chang, An Update on Randomized Clinical Trials in Metastatic Colorectal Carcinoma, Surg Oncol Clin N Am, 26 (2017) 667-687.
[108] Y.H. Xie, Y.X. Chen, J.Y. Fang, Comprehensive review of targeted therapy for colorectal cancer, Signal Transduct Target Ther, 5 (2020) 22.
[109] M.H. Frank, B.J. Wilson, J.S. Gold, N.Y. Frank, Clinical Implications of Colorectal Cancer Stem Cells in the Age of Single-Cell Omics and Targeted Therapies, Gastroenterology, 160 (2021) 1947-1960.
[110] A. Passardi, M. Canale, M. Valgiusti, P. Ulivi, Immune Checkpoints as a Target for Colorectal Cancer Treatment, Int J Mol Sci, 18 (2017).
[111] W.F. Taylor, E. Jabbarzadeh, The use of natural products to target cancer stem cells, Am J Cancer Res, 7 (2017) 1588-1605.
[112] A.F. Majdalawieh, M.W. Fayyad, G.K. Nasrallah, Anti-cancer properties and mechanisms of action of thymoquinone, the major active ingredient of Nigella sativa, Crit Rev Food Sci Nutr, 57 (2017) 3911-3928.
[113] A. Ahmad, A. Husain, M. Mujeeb, S.A. Khan, A.K. Najmi, N.A. Siddique, Z.A. Damanhouri, F. Anwar, A review on therapeutic potential of Nigella sativa: A miracle herb, Asian Pac J Trop Biomed, 3 (2013) 337-352.
[114] A. Ahmad, R.K. Mishra, A. Vyawahare, A. Kumar, M.U. Rehman, W. Qamar, A.Q. Khan, R. Khan, Thymoquinone (2-Isoprpyl-5-methyl-1, 4-benzoquinone) as a chemopreventive/anticancer agent: Chemistry and biological effects, Saudi Pharm J, 27 (2019) 1113-1126.
[115] M. Asaduzzaman Khan, M. Tania, S. Fu, J. Fu, Thymoquinone, as an anticancer molecule: from basic research to clinical investigation, Oncotarget, 8 (2017) 51907-51919.
[116] C. Sankaranarayanan, L. Pari, Thymoquinone ameliorates chemical induced oxidative stress and beta-cell damage in experimental hyperglycemic rats, Chem Biol Interact, 190 (2011) 148-154.
[117] K.M. Fararh, Y. Atoji, Y. Shimizu, T. Shiina, H. Nikami, T. Takewaki, Mechanisms of the hypoglycaemic and immunopotentiating effects of Nigella sativa L. oil in streptozotocin-induced diabetic hamsters, Res Vet Sci, 77 (2004) 123-129.
[118] E. Taka, E.A. Mazzio, C.B. Goodman, N. Redmon, H. Flores-Rozas, R. Reams, S. Darling-Reed, K.F. Soliman, Anti-inflammatory effects of thymoquinone in activated BV-2 microglial cells, J Neuroimmunol, 286 (2015) 5-12.
[119] M.K. Cobourne-Duval, E. Taka, P. Mendonca, K.F.A. Soliman, Thymoquinone increases the expression of neuroprotective proteins while decreasing the expression of pro-inflammatory cytokines and the gene expression NFkappaB pathway signaling targets in LPS/IFNgamma -activated BV-2 microglia cells, J Neuroimmunol, 320 (2018) 87-97.
[120] Y. Lu, Y. Feng, D. Liu, Z. Zhang, K. Gao, W. Zhang, H. Tang, Thymoquinone Attenuates Myocardial Ischemia/Reperfusion Injury Through Activation of SIRT1 Signaling, Cell Physiol Biochem, 47 (2018) 1193-1206.

[121] N.M. Elsherbiny, M. El-Sherbiny, Thymoquinone attenuates Doxorubicin-induced nephrotoxicity in rats: Role of Nrf2 and NOX4, Chem Biol Interact, 223 (2014) 102-108.
[122] Y. Yang, T. Bai, Y.L. Yao, D.Q. Zhang, Y.L. Wu, L.H. Lian, J.X. Nan, Upregulation of SIRT1-AMPK by thymoquinone in hepatic stellate cells ameliorates liver injury, Toxicol Lett, 262 (2016) 80-91.
[123] Y.K. Mahmoud, H.M.A. Abdelrazek, Cancer: Thymoquinone antioxidant/pro-oxidant effect as potential anticancer remedy, Biomed Pharmacother, 115 (2019) 108783.
[124] L. Zhang, Y. Bai, Y. Yang, Thymoquinone chemosensitizes colon cancer cells through inhibition of NF-kappaB, Oncol Lett, 12 (2016) 2840-2845.
[125] C. El-Baba, V. Mahadevan, F.B. Fahlbusch, S.S. Mohan, T.T. Rau, H. Gali-Muhtasib, R. Schneider-Stock, Thymoquinone-induced conformational changes of PAK1 interrupt prosurvival MEK-ERK signaling in colorectal cancer, Mol Cancer, 13 (2014) 201.
[126] N. El-Najjar, M. Chatila, H. Moukadem, H. Vuorela, M. Ocker, M. Gandesiri, R. Schneider-Stock, H. Gali-Muhtasib, Reactive oxygen species mediate thymoquinone-induced apoptosis and activate ERK and JNK signaling, Apoptosis, 15 (2010) 183-195.
[127] H. Gali-Muhtasib, M. Ocker, D. Kuester, S. Krueger, Z. El-Hajj, A. Diestel, M. Evert, N. El-Najjar, B. Peters, A. Jurjus, A. Roessner, R. Schneider-Stock, Thymoquinone reduces mouse colon tumor cell invasion and inhibits tumor growth in murine colon cancer models, J Cell Mol Med, 12 (2008) 330-342.
[128] L.M. Feng, X.F. Wang, Q.X. Huang, Thymoquinone induces cytotoxicity and reprogramming of EMT in gastric cancer cells by targeting PI3K/Akt/mTOR pathway, J Biosci, 42 (2017) 547-554.
[129] B. Kou, W. Liu, W. Zhao, P. Duan, Y. Yang, Q. Yi, F. Guo, J. Li, J. Zhou, Q. Kou, Thymoquinone inhibits epithelial-mesenchymal transition in prostate cancer cells by negatively regulating the TGF-beta/Smad2/3 signaling pathway, Oncol Rep, 38 (2017) 3592-3598.
[130] M. Zhang, H. Du, Z. Huang, P. Zhang, Y. Yue, W. Wang, W. Liu, J. Zeng, J. Ma, G. Chen, X. Wang, J. Fan, Thymoquinone induces apoptosis in bladder cancer cell via endoplasmic reticulum stress-dependent mitochondrial pathway, Chem Biol Interact, 292 (2018) 65-75.
[131] O.H. Alobaedi, W.H. Talib, I.A. Basheti, Antitumor effect of thymoquinone combined with resveratrol on mice transplanted with breast cancer, Asian Pac J Trop Med, 10 (2017) 400-408.
[132] J. Yang, X.R. Kuang, P.T. Lv, X.X. Yan, Thymoquinone inhibits proliferation and invasion of human nonsmall-cell lung cancer cells via ERK pathway, Tumour Biol, 36 (2015) 259-269.
[133] M. Roepke, A. Diestel, K. Bajbouj, D. Walluscheck, P. Schonfeld, A. Roessner, R. Schneider-Stock, H. Gali-Muhtasib, Lack of p53 augments thymoquinone-induced apoptosis and caspase activation in human osteosarcoma cells, Cancer Biol Ther, 6 (2007) 160-169.
[134] H.H. Hsu, M.C. Chen, C.H. Day, Y.M. Lin, S.Y. Li, C.C. Tu, V.V. Padma, H.N. Shih, W.W. Kuo, C.Y. Huang, Thymoquinone suppresses migration of LoVo human colon cancer cells by reducing prostaglandin E2 induced COX-2 activation, World J Gastroenterol, 23 (2017) 1171-1179.

[135] M.C. Chen, N.H. Lee, H.H. Hsu, T.J. Ho, C.C. Tu, R.J. Chen, Y.M. Lin, V.P. Viswanadha, W.W. Kuo, C.Y. Huang, Inhibition of NF-kappaB and metastasis in irinotecan (CPT-11)-resistant LoVo colon cancer cells by thymoquinone via JNK and p38, Environ Toxicol, 32 (2017) 669-678.
[136] J. Kundu, B.Y. Choi, C.H. Jeong, J.K. Kundu, K.S. Chun, Thymoquinone induces apoptosis in human colon cancer HCT116 cells through inactivation of STAT3 by blocking JAK2- and Srcmediated phosphorylation of EGF receptor tyrosine kinase, Oncol Rep, 32 (2014) 821-828.
[137] H. Gali-Muhtasib, D. Kuester, C. Mawrin, K. Bajbouj, A. Diestel, M. Ocker, C. Habold, C. Foltzer-Jourdainne, P. Schoenfeld, B. Peters, M. Diab-Assaf, U. Pommrich, W. Itani, H. Lippert, A. Roessner, R. Schneider-Stock, Thymoquinone triggers inactivation of the stress response pathway sensor CHEK1 and contributes to apoptosis in colorectal cancer cells, Cancer Res, 68 (2008) 5609-5618.
[138] H. Jrah-Harzallah, S. Ben-Hadj-Khalifa, W.Y. Almawi, A. Maaloul, Z. Houas, T. Mahjoub, Effect of thymoquinone on 1,2-dimethyl-hydrazine-induced oxidative stress during initiation and promotion of colon carcinogenesis, Eur J Cancer, 49 (2013) 1127-1135.
[139] A. Wirries, S. Breyer, K. Quint, R. Schobert, M. Ocker, Thymoquinone hydrazone derivatives cause cell cycle arrest in p53-competent colorectal cancer cells, Exp Ther Med, 1 (2010) 369-375.
[140] B. Ndreshkjana, A. Capci, V. Klein, P. Chanvorachote, J.K. Muenzner, K. Huebner, S. Steinmann, K. Erlenbach-Wuensch, C.I. Geppert, A. Agaimy, F. Ballout, C. El-Baba, H. Gali-Muhtasib, A.V. Roehe, A. Hartmann, S.B. Tsogoeva, R. Schneider-Stock, Combination of 5-fluorouracil and thymoquinone targets stem cell gene signature in colorectal cancer cells, Cell Death Dis, 10 (2019) 379.
[141] R. Velho-Pereira, A. Kumar, B.N. Pandey, A.G. Jagtap, K.P. Mishra, Radiosensitization in human breast carcinoma cells by thymoquinone: role of cell cycle and apoptosis, Cell Biol Int, 35 (2011) 1025-1029.
[142] S. Rajput, B.N. Kumar, P. Banik, S. Parida, M. Mandal, Thymoquinone restores radiation-induced TGF-beta expression and abrogates EMT in chemoradiotherapy of breast cancer cells, J Cell Physiol, 230 (2015) 620-629.
[143] J. Kundu, K.S. Chun, O.I. Aruoma, J.K. Kundu, Mechanistic perspectives on cancer chemoprevention/chemotherapeutic effects of thymoquinone, Mutat Res, 768 (2014) 22-34.
[144] U. Kotowski, G. Heiduschka, L. Kadletz, T. Fahim, R. Seemann, R. Schmid, S. Schneider, A. Mitterbauer, D. Thurnher, Effect of thymoquinone on head and neck squamous cell carcinoma cells in vitro: Synergism with radiation, Oncol Lett, 14 (2017) 1147-1151.
[145] E. Demir, S. Taysi, H. Ulusal, D.S. Kaplan, K. Cinar, M. Tarakcioglu, Nigella sativa oil and thymoquinone reduce oxidative stress in the brain tissue of rats exposed to total head irradiation, Int J Radiat Biol, 96 (2020) 228-235.
[146] A. Ahlatci, A. Kuzhan, S. Taysi, O.C. Demirtas, H.E. Alkis, M. Tarakcioglu, A. Demirci, D. Caglayan, E. Saricicek, K. Cinar, Radiation-modifying abilities of Nigella sativa and thymoquinone on radiation-induced nitrosative stress in the brain tissue, Phytomedicine, 21 (2014) 740-744.
[147] M.S. Guida, A. Abd El-Aal, Y. Kafafy, S.F. Salama, B.M. Badr, G. Badr, Thymoquinone Rescues T Lymphocytes from Gamma Irradiation-Induced Apoptosis

and Exhaustion by Modulating Pro-Inflammatory Cytokine Levels and PD-1, Bax, and Bcl-2 Signaling, Cell Physiol Biochem, 38 (2016) 786-800.
[148] C.C. Woo, A.P. Kumar, G. Sethi, K.H. Tan, Thymoquinone: potential cure for inflammatory disorders and cancer, Biochem Pharmacol, 83 (2012) 443-451.
[149] A. Ahmad, R.M. Khan, K.M. Alkharfy, M. Raish, F.I. Al-Jenoobi, A.M. Al-Mohizea, Effects of Thymoquinone on the Pharmacokinetics and Pharmacodynamics of Glibenclamide in a Rat Model, Nat Prod Commun, 10 (2015) 1395-1398.
[150] S.A. Pathan, G.K. Jain, S.M. Zaidi, S. Akhter, D. Vohora, P. Chander, P.L. Kole, F.J. Ahmad, R.K. Khar, Stability-indicating ultra-performance liquid chromatography method for the estimation of thymoquinone and its application in biopharmaceutical studies, Biomed Chromatogr, 25 (2011) 613-620.
[151] F. Ballout, Z. Habli, O.N. Rahal, M. Fatfat, H. Gali-Muhtasib, Thymoquinone-based nanotechnology for cancer therapy: promises and challenges, Drug Discov Today, 23 (2018) 1089-1098.
[152] Clinical and Immunohisochemical Evaluation of Chemopreventive Effect of Thymoquinone on Oral Potentially Malignant Lesions., clinicaltrials.gov, 2021.
[153] B.A.O. Al Amri A.M., Phase I Safety And Clinical Activity Study Of Thymoquinone In Patients With Advanced Refractory Malignant Disease, SHIRAZ E MEDICAL JOURNAL, 10 (2009) 107-111.
[154] E. Perez-Herrero, A. Fernandez-Medarde, Advanced targeted therapies in cancer: Drug nanocarriers, the future of chemotherapy, Eur J Pharm Biopharm, 93 (2015) 52-79.
[155] A.G.M. Mostofa, M.K. Hossain, D. Basak, M.S. Bin Sayeed, Thymoquinone as a Potential Adjuvant Therapy for Cancer Treatment: Evidence from Preclinical Studies, Front Pharmacol, 8 (2017) 295.
[156] S.B. Al Bitar, F.; Monzer, A.; Kanso, M.; Saheb, N.; Mukherji, D.; Faraj, W.; Tawil, A.; Doughan, S.; Hussein, M.; Abou-Kheir, W.; Gali-Muhtasib, H. , Thymoquinone Radiosensitizes Human Colorectal Cancer Cells in 2D and 3D Culture Models, Cancers, 14 (2022) 1363.
[157] H.F. Bahmad, K. Cheaito, R.M. Chalhoub, O. Hadadeh, A. Monzer, F. Ballout, A. El-Hajj, D. Mukherji, Y.N. Liu, G. Daoud, W. Abou-Kheir, Sphere-Formation Assay: Three-Dimensional in vitro Culturing of Prostate Cancer Stem/Progenitor Sphere-Forming Cells, Front Oncol, 8 (2018) 347.
[158] K. Boehnke, P.W. Iversen, D. Schumacher, M.J. Lallena, R. Haro, J. Amat, J. Haybaeck, S. Liebs, M. Lange, R. Schafer, C.R. Regenbrecht, C. Reinhard, J.A. Velasco, Assay Establishment and Validation of a High-Throughput Screening Platform for Three-Dimensional Patient-Derived Colon Cancer Organoid Cultures, J Biomol Screen, 21 (2016) 931-941.
[159] F. Ballout, A. Monzer, M. Fatfat, H.E. Ouweini, M.A. Jaffa, R. Abdel-Samad, N. Darwiche, W. Abou-Kheir, H. Gali-Muhtasib, Thymoquinone induces apoptosis and DNA damage in 5-Fluorouracil-resistant colorectal cancer stem/progenitor cells, Oncotarget, 11 (2020) 2959-2972.
[160] D. Ahmed, P.W. Eide, I.A. Eilertsen, S.A. Danielsen, M. Eknaes, M. Hektoen, G.E. Lind, R.A. Lothe, Epigenetic and genetic features of 24 colon cancer cell lines, Oncogenesis, 2 (2013) e71.
[161] H. Gali-Muhtasib, M. Diab-Assaf, C. Boltze, J. Al-Hmaira, R. Hartig, A. Roessner, R. Schneider-Stock, Thymoquinone extracted from black seed triggers

apoptotic cell death in human colorectal cancer cells via a p53-dependent mechanism, Int J Oncol, 25 (2004) 857-866.
[162] J.M. Mates, J.A. Segura, F.J. Alonso, J. Marquez, Intracellular redox status and oxidative stress: implications for cell proliferation, apoptosis, and carcinogenesis, Arch Toxicol, 82 (2008) 273-299.
[163] J. Wang, S. Li, Y. Liu, C. Zhang, H. Li, B. Lai, Metastatic patterns and survival outcomes in patients with stage IV colon cancer: A population-based analysis, Cancer Med, 9 (2020) 361-373.
[164] E. Dekker, P.J. Tanis, J.L.A. Vleugels, P.M. Kasi, M.B. Wallace, Colorectal cancer, Lancet, 394 (2019) 1467-1480.
[165] R. Glynne-Jones, L. Wyrwicz, E. Tiret, G. Brown, C. Rodel, A. Cervantes, D. Arnold, E.G. Committee, Rectal cancer: ESMO Clinical Practice Guidelines for diagnosis, treatment and follow-up, Ann Oncol, 28 (2017) iv22-iv40.
[166] W. Feng, B. Yu, Z. Zhang, J. Li, Y. Wang, Current status of total neoadjuvant therapy for locally advanced rectal cancer, Asia Pac J Clin Oncol, (2021).
[167] R. Sauer, T. Liersch, S. Merkel, R. Fietkau, W. Hohenberger, C. Hess, H. Becker, H.R. Raab, M.T. Villanueva, H. Witzigmann, C. Wittekind, T. Beissbarth, C. Rodel, Preoperative versus postoperative chemoradiotherapy for locally advanced rectal cancer: results of the German CAO/ARO/AIO-94 randomized phase III trial after a median follow-up of 11 years, J Clin Oncol, 30 (2012) 1926-1933.
[168] M.S. Roh, L.H. Colangelo, M.J. O'Connell, G. Yothers, M. Deutsch, C.J. Allegra, M.S. Kahlenberg, L. Baez-Diaz, C.S. Ursiny, N.J. Petrelli, N. Wolmark, Preoperative multimodality therapy improves disease-free survival in patients with carcinoma of the rectum: NSABP R-03, J Clin Oncol, 27 (2009) 5124-5130.
[169] D. Sebag-Montefiore, R.J. Stephens, R. Steele, J. Monson, R. Grieve, S. Khanna, P. Quirke, J. Couture, C. de Metz, A.S. Myint, E. Bessell, G. Griffiths, L.C. Thompson, M. Parmar, Preoperative radiotherapy versus selective postoperative chemoradiotherapy in patients with rectal cancer (MRC CR07 and NCIC-CTG C016): a multicentre, randomised trial, Lancet, 373 (2009) 811-820.
[170] J.H. Song, J.U. Jeong, J.H. Lee, S.H. Kim, H.M. Cho, J.W. Um, H.S. Jang, C. Korean Clinical Practice Guideline for, C. Rectal Cancer, Preoperative chemoradiotherapy versus postoperative chemoradiotherapy for stage II-III resectable rectal cancer: a meta-analysis of randomized controlled trials, Radiat Oncol J, 35 (2017) 198-207.
[171] S.Y. Ngan, B. Burmeister, R.J. Fisher, M. Solomon, D. Goldstein, D. Joseph, S.P. Ackland, D. Schache, B. McClure, S.A. McLachlan, J. McKendrick, T. Leong, C. Hartopeanu, J. Zalcberg, J. Mackay, Randomized trial of short-course radiotherapy versus long-course chemoradiation comparing rates of local recurrence in patients with T3 rectal cancer: Trans-Tasman Radiation Oncology Group trial 01.04, J Clin Oncol, 30 (2012) 3827-3833.
[172] S.A. McLachlan, R.J. Fisher, J. Zalcberg, M. Solomon, B. Burmeister, D. Goldstein, T. Leong, S.P. Ackland, J. McKendrick, B. McClure, J. Mackay, S.Y. Ngan, The impact on health-related quality of life in the first 12 months: A randomised comparison of preoperative short-course radiation versus long-course chemoradiation for T3 rectal cancer (Trans-Tasman Radiation Oncology Group Trial 01.04), Eur J Cancer, 55 (2016) 15-26.

[173] L. Gong, Y. Zhang, C. Liu, M. Zhang, S. Han, Application of Radiosensitizers in Cancer Radiotherapy, Int J Nanomedicine, 16 (2021) 1083-1102.
[174] A.M. Buckley, N. Lynam-Lennon, H. O'Neill, J. O'Sullivan, Targeting hallmarks of cancer to enhance radiosensitivity in gastrointestinal cancers, Nat Rev Gastroenterol Hepatol, 17 (2020) 298-313.
[175] K. Hintelmann, M. Kriegs, K. Rothkamm, T. Rieckmann, Improving the Efficacy of Tumor Radiosensitization Through Combined Molecular Targeting, Front Oncol, 10 (2020) 1260.
[176] O.R. Kaaden, E. Bartel, L. Haas, D. Kierek-Jaczszuk, M. Lochelt, F. Muller, R. Neth, S. Roth, B. Stolze, S. Van Dawen, et al., Mechanisms contributing to the virus persistence in Aleutian disease, Dtsch Tierarztl Wochenschr, 97 (1990) 96-99.
[177] A. Estrada-Bernal, M. Chatterjee, S.J. Haque, L. Yang, M.A. Morgan, S. Kotian, D. Morrell, A. Chakravarti, T.M. Williams, MEK inhibitor GSK1120212-mediated radiosensitization of pancreatic cancer cells involves inhibition of DNA double-strand break repair pathways, Cell Cycle, 14 (2015) 3713-3724.
[178] G. Li, A. Wu, D. Qi, F. Cui, Y. Zeng, F. Xie, H. Wu, Y. Gu, Q. Chen, X. Zhang, Differential effects of peptidoglycan on colorectal tumors and intestinal tissue post-pelvic radiotherapy, Oncotarget, 7 (2016) 75685-75697.
[179] R. Baskar, J. Dai, N. Wenlong, R. Yeo, K.W. Yeoh, Biological response of cancer cells to radiation treatment, Front Mol Biosci, 1 (2014) 24.
[180] M.A. Khan, M. Tania, C. Wei, Z. Mei, S. Fu, J. Cheng, J. Xu, J. Fu, Thymoquinone inhibits cancer metastasis by downregulating TWIST1 expression to reduce epithelial to mesenchymal transition, Oncotarget, 6 (2015) 19580-19591.
[181] X.T. Xu, W.T. Hu, J.Y. Zhou, Y. Tu, Celecoxib enhances the radiosensitivity of HCT116 cells in a COX-2 independent manner by up-regulating BCCIP, Am J Transl Res, 9 (2017) 1088-1100.
[182] J. Kjellstrom, E. Kjellen, A. Johnsson, In vitro radiosensitization by oxaliplatin and 5-fluorouracil in a human colon cancer cell line, Acta Oncol, 44 (2005) 687-693.
[183] A.L. Dunne, C. Mothersill, T. Robson, G.D. Wilson, D.G. Hirst, Radiosensitization of colon cancer cell lines by docetaxel: mechanisms of action, Oncol Res, 14 (2004) 447-454.
[184] E.H. Kim, M.S. Kim, W.G. Jung, The mechanisms responsible for the radiosensitizing effects of sorafenib on colon cancer cells, Oncol Rep, 32 (2014) 2421-2428.
[185] A. Jazayeri, J. Falck, C. Lukas, J. Bartek, G.C. Smith, J. Lukas, S.P. Jackson, ATM- and cell cycle-dependent regulation of ATR in response to DNA double-strand breaks, Nat Cell Biol, 8 (2006) 37-45.
[186] S. Burma, B.P. Chen, M. Murphy, A. Kurimasa, D.J. Chen, ATM phosphorylates histone H2AX in response to DNA double-strand breaks, J Biol Chem, 276 (2001) 42462-42467.
[187] I.M. Ward, J. Chen, Histone H2AX is phosphorylated in an ATR-dependent manner in response to replicational stress, J Biol Chem, 276 (2001) 47759-47762.
[188] C.H. Bassing, F.W. Alt, H2AX may function as an anchor to hold broken chromosomal DNA ends in close proximity, Cell Cycle, 3 (2004) 149-153.
[189] B. Shiotani, L. Zou, Single-stranded DNA orchestrates an ATM-to-ATR switch at DNA breaks, Mol Cell, 33 (2009) 547-558.

[190] R. Okayasu, Repair of DNA damage induced by accelerated heavy ions--a mini review, Int J Cancer, 130 (2012) 991-1000.
[191] K. Camphausen, W. Burgan, M. Cerra, K.A. Oswald, J.B. Trepel, M.J. Lee, P.J. Tofilon, Enhanced radiation-induced cell killing and prolongation of gammaH2AX foci expression by the histone deacetylase inhibitor MS-275, Cancer Res, 64 (2004) 316-321.
[192] E.C. Bourton, P.N. Plowman, D. Smith, C.F. Arlett, C.N. Parris, Prolonged expression of the gamma-H2AX DNA repair biomarker correlates with excess acute and chronic toxicity from radiotherapy treatment, Int J Cancer, 129 (2011) 2928-2934.
[193] S. Kawashima, N. Kawaguchi, K. Taniguchi, K. Tashiro, K. Komura, T. Tanaka, Y. Inomata, Y. Imai, R. Tanaka, M. Yamamoto, Y. Inoue, S.W. Lee, M. Kawai, K. Tanaka, J. Okuda, K. Uchiyama, gamma-H2AX as a potential indicator of radiosensitivity in colorectal cancer cells, Oncol Lett, 20 (2020) 2331-2337.
[194] G. Delaney, S. Jacob, C. Featherstone, M. Barton, The role of radiotherapy in cancer treatment: estimating optimal utilization from a review of evidence-based clinical guidelines, Cancer, 104 (2005) 1129-1137.
[195] S. Jehan, C. Zhong, G. Li, S. Zulqarnain Bakhtiar, D. Li, G. Sui, Thymoquinone Selectively Induces Hepatocellular Carcinoma Cell Apoptosis in Synergism With Clinical Therapeutics and Dependence of p53 Status, Front Pharmacol, 11 (2020) 555283.
[196] R. Gomathinayagam, J.H. Ha, M. Jayaraman, Y.S. Song, C. Isidoro, D.N. Dhanasekaran, Chemopreventive and Anticancer Effects of Thymoquinone: Cellular and Molecular Targets, J Cancer Prev, 25 (2020) 136-151.
[197] P.S. Koka, D. Mondal, M. Schultz, A.B. Abdel-Mageed, K.C. Agrawal, Studies on molecular mechanisms of growth inhibitory effects of thymoquinone against prostate cancer cells: role of reactive oxygen species, Exp Biol Med (Maywood), 235 (2010) 751-760.
[198] T. Konishi, H. Yoshidome, T. Shida, K. Furukawa, T. Takayashiki, S. Kuboki, S. Takano, M. Miyazaki, M. Ohtsuka, Phosphorylated mTOR expression as a predictor of survival after liver resection for colorectal liver metastases, J Surg Oncol, 124 (2021) 598-606.
[199] A. Mardanshahi, N.A. Gharibkandi, S. Vaseghi, S.M. Abedi, S. Molavipordanjani, The PI3K/AKT/mTOR signaling pathway inhibitors enhance radiosensitivity in cancer cell lines, Mol Biol Rep, 48 (2021) 1-14.
[200] L. Chang, P.H. Graham, J. Hao, J. Ni, J. Bucci, P.J. Cozzi, J.H. Kearsley, Y. Li, PI3K/Akt/mTOR pathway inhibitors enhance radiosensitivity in radioresistant prostate cancer cells through inducing apoptosis, reducing autophagy, suppressing NHEJ and HR repair pathways, Cell Death Dis, 5 (2014) e1437.
[201] A.K. Pandurangan, Potential targets for prevention of colorectal cancer: a focus on PI3K/Akt/mTOR and Wnt pathways, Asian Pac J Cancer Prev, 14 (2013) 2201-2205.
[202] A. Spreafico, J.J. Tentler, T.M. Pitts, A.C. Tan, M.A. Gregory, J.J. Arcaroli, P.J. Klauck, M.C. McManus, R.J. Hansen, J. Kim, L.N. Micel, H.M. Selby, T.P. Newton, K.L. McPhillips, D.L. Gustafson, J.V. Degregori, W.A. Messersmith, R.A. Winn, S.G. Eckhardt, Rational combination of a MEK inhibitor, selumetinib, and the Wnt/calcium pathway modulator, cyclosporin A, in preclinical models of colorectal cancer, Clin Cancer Res, 19 (2013) 4149-4162.

[203] Y. Yan, C.P. Black, K.H. Cowan, Irradiation-induced G2/M checkpoint response requires ERK1/2 activation, Oncogene, 26 (2007) 4689-4698.
[204] K.M. Ahmed, J.J. Li, NF-kappa B-mediated adaptive resistance to ionizing radiation, Free Radic Biol Med, 44 (2008) 1-13.
[205] M.A. Hatiboglu, A. Kocyigit, E.M. Guler, K. Akdur, I. Khan, A. Nalli, E. Karatas, S. Tuzgen, Thymoquinone Enhances the Effect of Gamma Knife in B16-F10 Melanoma Through Inhibition of Phosphorylated STAT3, World Neurosurg, 128 (2019) e570-e581.
[206] Z. Fatfat, M. Fatfat, H. Gali-Muhtasib, Therapeutic potential of thymoquinone in combination therapy against cancer and cancer stem cells, World J Clin Oncol, 12 (2021) 522-543.
[207] D.R. Reed, M.I. Friedman, Diet composition alters the acceptance of fat by rats, Appetite, 14 (1990) 219-230.
[208] M. Bhattacharjee, P. Upadhyay, S. Sarker, A. Basu, S. Das, A. Ghosh, S. Ghosh, A. Adhikary, Combinatorial therapy of Thymoquinone and Emodin synergistically enhances apoptosis, attenuates cell migration and reduces stemness efficiently in breast cancer, Biochim Biophys Acta Gen Subj, 1864 (2020) 129695.
[209] K.M. Ibiyeye, A.B.Z. Zuki, Cockle Shell-Derived Aragonite CaCO3 Nanoparticles for Co-Delivery of Doxorubicin and Thymoquinone Eliminates Cancer Stem Cells, Int J Mol Sci, 21 (2020).
[210] K. Anuja, A.R. Chowdhury, A. Saha, S. Roy, A.K. Rath, M. Kar, B. Banerjee, Radiation-induced DNA damage response and resistance in colorectal cancer stem-like cells, Int J Radiat Biol, 95 (2019) 667-679.
[211] Z. Asadzadeh, B. Mansoori, A. Mohammadi, T. Kazemi, A. Mokhtarzadeh, D. Shanehbandi, N. Hemmat, A. Derakhshani, O. Brunetti, S. Safaei, M. Aghajani, S. Najafi, N. Silvestris, B. Baradaran, The combination effect of Prominin1 (CD133) suppression and Oxaliplatin treatment in colorectal cancer therapy, Biomed Pharmacother, 137 (2021) 111364.
[212] K. Kemper, C. Grandela, J.P. Medema, Molecular identification and targeting of colorectal cancer stem cells, Oncotarget, 1 (2010) 387-395.
[213] D. Horst, S.K. Scheel, S. Liebmann, J. Neumann, S. Maatz, T. Kirchner, A. Jung, The cancer stem cell marker CD133 has high prognostic impact but unknown functional relevance for the metastasis of human colon cancer, J Pathol, 219 (2009) 427-434.
[214] M.S. Karetzky, R.R. Jasani, M.A. Zubair, Thallium-201 scintigraphy in the evaluation of graft dysfunction in lung transplantation. Newark Beth Israel Medical Center Lung Transplant Group, Eur Respir J, 9 (1996) 2553-2559.
[215] C. Kantara, M.R. O'Connell, G. Luthra, A. Gajjar, S. Sarkar, R.L. Ullrich, P. Singh, Methods for detecting circulating cancer stem cells (CCSCs) as a novel approach for diagnosis of colon cancer relapse/metastasis, Lab Invest, 95 (2015) 100-112.
[216] R. Moll, R. Krepler, W.W. Franke, Complex cytokeratin polypeptide patterns observed in certain human carcinomas, Differentiation, 23 (1983) 256-269.
[217] Z. Wang, Y. Tang, L. Xie, A. Huang, C. Xue, Z. Gu, K. Wang, S. Zong, The Prognostic and Clinical Value of CD44 in Colorectal Cancer: A Meta-Analysis, Front Oncol, 9 (2019) 309.
[218] M. Lakshman, V. Subramaniam, U. Rubenthiran, S. Jothy, CD44 promotes resistance to apoptosis in human colon cancer cells, Exp Mol Pathol, 77 (2004) 18-25.

[219] L. Li, X. Hao, J. Qin, W. Tang, F. He, A. Smith, M. Zhang, D.M. Simeone, X.T. Qiao, Z.N. Chen, T.S. Lawrence, L. Xu, Antibody against CD44s inhibits pancreatic tumor initiation and postradiation recurrence in mice, Gastroenterology, 146 (2014) 1108-1118.
[220] X. Zhang, P.S. Zheng, [Expression and significance of CK7 and CK19 in colon cancer], Xi Bao Yu Fen Zi Mian Yi Xue Za Zhi, 26 (2010) 157-158.
[221] M. Pastuszak, K. Groszewski, M. Pastuszak, P. Dyrla, S. Wojtun, J. Gil, Cytokeratins in gastroenterology. Systematic review, Prz Gastroenterol, 10 (2015) 61-70.
[222] I.R. Powley, M. Patel, G. Miles, H. Pringle, L. Howells, A. Thomas, C. Kettleborough, J. Bryans, T. Hammonds, M. MacFarlane, C. Pritchard, Patient-derived explants (PDEs) as a powerful preclinical platform for anti-cancer drug and biomarker discovery, Br J Cancer, 122 (2020) 735-744.
[223] J. Kondo, M. Inoue, Application of Cancer Organoid Model for Drug Screening and Personalized Therapy, Cells, 8 (2019).